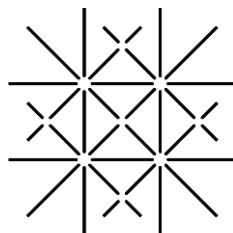


Development in the central nervous system:
studies of activity-dependent plasticity and
synapse refinement



U N I
B A S E L

Inauguraldissertation

zur
Erlangung der Würde eines Doktors der Philosophie
vorgelegt der
Philosophisch-Naturwissenschaftlichen Fakultät
der Universität Basel
von

Julien Gaudias

Aus Strasbourg, Frankreich

Basel, June 2015

Genehmigt von der Philosophisch-Naturwissenschaftlichen Fakultät
auf Antrag von
(Mitglieder des Dissertationskomitees)

Prof. Dr. Kaspar Vogt (Fakultätsverantwortlicher)

Prof. Dr. Heinrich Reichert (Korreferent)

Basel, den 17.09.2013

Prof. Dr. Jörg Schibler
(Dekan)

Summary

The central nervous system (CNS) is a highly specified structure, involved in a large range of function, from sensory processing to motor behavior to cognition. The CNS development is genetically programmed but also heavily dependent on environmental cues. The CNS is a highly plastic structure, most prominently at the synaptic level. Plasticity is a physiological process allowing a rapid change of synaptic strength depending on experience, use and surrounding neuronal activity. It allows the integration of neurons into neuronal networks and is also believed to be the mechanism underlying learning and memory. During development, plasticity underlies the adaptation to the environment, via synapse refinement, and experience-dependent plasticity. Synapse refinement, together with input competition, is marked by synapse pruning and formation, to eliminate early-formed redundant synaptic contacts.

Located in the occipital part of the brain, the cerebellum is involved in motor control and coordination, motor learning and memory, as well as cognition. Endowed with a very peculiar cytoarchitecture, the cerebellar circuitry is centered around Purkinje Cells (PC). PCs integrate inputs arising from the two main afferents to the cerebellum, with a direct connection for climbing fibers (CF), with a relay of the parallel fibers (PF) for the mossy fibers. In the mature cerebellum, each PC is innervated by a unique CF and this strong connection is the result of a very precise developmental process. Early on, PCs are innervated by multiple CFs. This situation evolves to the mature connection profile through a well-characterized four stages process, which is highly dependent on the proper development of other connections to PCs, notably the PF-PC synapse. We studied this process in a model for disturbed cerebellar maturation. Nogo-A is a major neurite outgrowth inhibitor of the CNS. It has been principally studied in CNS injuries, where it restricts the capacity of axons to grow and regenerate. In the cerebellum, the absence of Nogo alters the development of the PF-PC synapse, but does not alter the elimination process of supernumerary CFs. At P14 as well as P28, the proportion of reminiscent supernumerary CF is not affected by the lack of Nogo-A. However, it remains to test how the absence of Nogo-A and its effect of the maturation of PF-PC synapse affect the cerebellar physiology.

Neurodevelopmental disorders have been linked to defects in cellular physiology in numerous areas of the brain. Lately, several studies revealed that autism spectrum disorders (ASD) can be linked to defects in several synaptic proteins, involved in maintaining the structure and anchoring of synaptic contacts. Amongst others, it has been shown that proteins such as neuroligins exhibit genetic alterations in ASD and are responsible for defects in cerebellar physiology. Neuroligin 3 is an adhesion molecule, present at the postsynaptic site, forming a trans-synaptic complex with neurexins, present on the

presynaptic site. This complex is essential for synapse stabilization and function, but not for synapse formation. Defects in cerebellar plasticity have been associated with particular deficits observed in ASD patients. Plasticity in the cerebellum is a developmental process and is inducible by a wide range of protocols. We studied the effect of the absence of neuroligin 3 on long-term depression (LTD) at PF – PC synapses, a well-established model for cerebellar plasticity. In neuroligin 3 KO mice, our stimulation protocol did not produce a decrease of the evoked response in the adult, while a clear reduction was observed in young (P21-30) mice. In WT mice, our stimulation protocol induced a clear decrease of the response in the adult, but not in young mice. Our results suggest that the occlusion of mGluR-LTD observed in adult KO mice is a developmental process. Determining the subtleties underlying this developmental process is a major importance for the development of new treatment strategies in ASD.

The visual cortex is a part of the brain that has been extensively studied, because of the ability to record and image neuronal activation upon presentation of clearly defined sensory inputs, but also because of a peculiar time-window for enhanced experience-dependent plasticity. This critical period is characterized by the ability for monocular deprivation to induce the strengthening of the input from the open eye, at the expense of those from the closed eye. Spike-timing dependent plasticity (STDP) is an activity-dependent plastic process playing an important role in the adaptation of cortical connectivity to the flow of inputs neurons receive. In STDP, the polarity and the amplitude of the response vary according to the relative timing between the presynaptic input and the postsynaptic backpropagating action potential (bAP). We tested if bAPs and STDP were subject to any modifications between several time-points of the critical period. Our results revealed that when pairing a presynaptic spike with the postsynaptic train of bAPs, at a positive timing, the amplitude of the response observed varied throughout the critical period. Our results show that bAPs and STDP are mechanisms of premier importance for the cellular integration of inputs. These two mechanisms participate in sensory input integration, as well as development and refinement of cellular connections during the critical period, in V1 layer 2/3 pyramidal cells.

In summary, my thesis reveals important insights on neuronal physiology and factors implicated in synapse refinement and activity-dependent plasticity, during development.

Table of Contents

1. General introduction	7
2. Chapter 1: Effect of the neurite inhibitor outgrowth Nogo-A on the cerebellar circuit development.	11
2.1. Introduction	11
2.2. Material and methods	18
2.3. Results	19
2.4. Discussion	21
2.5. References	23
3. Chapter 2: Influence of the absence of Neuroligin 3 on the development of mGluR1 LTD in the cerebellum.	27
3.1. Introduction	27
3.2. Material and methods	34
3.3. Results	35
3.4. Discussion	37
3.5. References	41
4. Chapter 3: Variations of action potential backpropagation and spike-timing dependent plasticity in the mouse primary visual cortex, during the critical period.	45
4.1. Introduction	45
4.2. Material and methods	51
4.3. Results	53
4.4. Discussion	56
4.5. References	59
5. Appendix	65
5.1. Petrinovic et al., PNAS 2013; Neuronal Nogo-A negatively regulates dendritic morphology and synaptic transmission in the cerebellum	
5.2. Baudouin et al., Science 2012; Shared synaptic pathophysiology in syndromic and nonsyndromic rodent models for autism.	

6. List of Abbreviations	67
7. Acknowledgements	69
8. Curriculum Vitae	71

Introduction

The central nervous system (CNS) is a highly complex structure responsible for mental function realized by mammals, from motor task to sensory processing to cognition. The CNS can be considered as two groups of structures: the neocortex and subcortical regions. In the brain in general certain regions are devoted to particular functions. These regions are notably defined by their cellular composition, organization, connections and activity. The CNS is mainly constituted of two types of neurons: excitatory/glutamatergic and inhibitory/GABAergic. The ratio between these two neuronal populations varies according to the structure considered and is complemented by multiple neuromodulatory systems. Neuronal progenitors emerge from different regions of the immature CNS and migrate to their predestined localization. Their development and integration in neuronal systems is dictated by genetic cues, depending on the cell type, their architecture, their connections and projections, and their role in the system considered. These neurons are then integrated into defined networks, devoted to a specific purpose..

The development of the vertebrate CNS is genetically programmed but is also adaptive to its environment, to much greater degree compared to other organs of the body. This environmental adaptation is mediated by activity-dependent synaptic maturation and refinement. The CNS has great plastic capabilities, permitting an adequate adjustment of synaptic contact according to activity. Plasticity is a physiological process allowing a rapid change of synaptic strength depending on experience, use and surrounding neuronal activity. It is also believed to be the mechanism underlying learning and memory. Plasticity is present in numerous brain areas, at various synapses and between countless cell types. It allows the integration and adaptation of neurons into brain systems and neuronal networks, via experience-dependent plasticity, input competition and synapse refinement. These processes affect neuronal connectivity at the synaptic level via strengthening and weakening of synapses, as well as synapse formation and pruning, to eliminate early-formed redundant synapses.

Plasticity and synapse refinement are cellular mechanisms that have also been extensively described in the cerebellum, a subcortical structure, involved in motor control and coordination, sensory motor learning and memory, as well as cognition. The cerebellum is constituted by the cerebellar cortex and deep nuclei. Endowed with a very peculiar cellular architecture, the cerebellar cortical circuitry is a repetitive motif found across the ten folia that constitute the cerebellum. This circuitry is centered on Purkinje cell (PC), a GABAergic cell with a large soma and an extensive dendritic tree. This cell integrates inputs coming to the cerebellar cortex via two afferents, climbing fibers (CF) and mossy fibers. The development of the dendritic arborization of PCs follows a very peculiar process and is a perfect

example for synapse refinement (Kano and Hashimoto, 2009). During the early postnatal life, every PC is innervated by multiple CFs and this situation will evolve to the innervation by a unique CF, in a very precise four stages process. This mechanism is dependent on the accurate development of other PC connections, notably parallel fibers – PC synapses. We studied this process in a model of disturbed cerebellar maturation, due to the silencing of Nogo-A, a major inhibitor of neurite outgrowth in the CNS (Schwab, 2010).

Neurodevelopmental disorders have been linked to defect in cellular physiology in numerous areas of the brain. Lately, several studies revealed that autism spectrum disorders (ASD) can be linked to defect in several synaptic proteins, involved in the structure and anchoring of synaptic contacts (Ebert and Greenberg, 2013). Amongst other, it has been shown that proteins such as neuroligins present genetic alterations in ASD and are responsible for defects in cerebellar physiology. Plasticity in the cerebellum is believed to support motor coordination and learning. The inputs arising to the cerebellum and integrated by PCs are also subjected to plasticity. Recently, defects in cerebellar plasticity have been associated with particular deficits observed in ASD patients. Plasticity in the cerebellum is a developmental process and is inducible by a wide range of protocols. We studied the effect of the absence of neuroligin 3 on long-term depression at parallel fiber – PC synapses, a well-established model for cerebellar plasticity (Luscher and Huber, 2010). Determining how a defect in synaptic structure engendered by specific proteins leads to an alteration of cerebellar plasticity hold promise for the development of treatment strategies for ASD.

Similar to the cerebellum, the development of the visual cortex follows a precise protocol with synapse refinement and experience-dependent plasticity. The visual cortex is the part of the brain responsible for the integration of visual inputs arising from the retina, via thalamic lateral geniculate nuclei. In this region, excitatory neuronal activity is driven by sensory inputs. Neurons are responding specifically to visual cues moving with specific orientation and direction. Neurons with similar orientation direction selectivity are associated in subnetworks with reinforced connections. These connections are matured during development in the course of a specific ‘critical period’ with enhanced experience-dependent plasticity (Hensch, 2005). This synapse refinement process allows the creation of these subnetworks with population of cells sharing a similar orientation direction selectivity involved in the integration of sensory inputs. This specification process respects a clearly defined timing and is regulated by several neuronal systems, notably the inhibitory system, whose maturation is tightly linked to the timing and progression of the critical period for experience dependent plasticity. The main purpose of inhibitory neurons, also referred to as interneurons, is to regulate neuronal activity. Interneurons also have a regulatory role towards plasticity processes, notably spike-timing dependent plasticity (STDP). We investigated the variations of STDP, a classical model for activity-dependent plasticity, over the time-course of the critical period.

In summary, my thesis reveals important insights on neuronal physiology and factors implicated in synapse refinement, as well as activity-dependent plasticity.

References:

Ebert DH, Greenberg ME (2013) Activity-dependent neuronal signalling and autism spectrum disorder. *Nature* 493:327-337.

Hensch TK (2005) Critical period plasticity in local cortical circuits. *Nat Rev Neurosci* 6:877-888.

Kano M, Hashimoto K (2009) Synapse elimination in the central nervous system. *Curr Opin Neurobiol* 19:154-161.

Luscher C, Huber KM (2010) Group 1 mGluR-dependent synaptic long-term depression: mechanisms and implications for circuitry and disease. *Neuron* 65:445-459.

Schwab ME (2010) Functions of Nogo proteins and their receptors in the nervous system. *Nat Rev Neurosci* 11:799-811.

Chapter 1: Effect of the neurite inhibitor outgrowth Nogo-A on the cerebellar circuit development.

Introduction

Discovered in the late 80s (Caroni and Schwab, 1988), Nogo-A is a member of the myelin-derived protein Nogo family, known as the most potent inhibitor of neurite outgrowth, axon regeneration and structural plasticity in the adult injured CNS (Pernet and Schwab, 2012). This family contains three isoforms (Nogo-A, B & C), and only the Nogo-A isoform has a long extracellular domain (for a detailed review about Nogo, see Schwab, 2010). These transmembrane proteins are coded by the reticulon 4 (RTN4 also known as NOGO) gene, and they only share the last 188 amino-acids located on the C-terminal, the RTN domain. This domain contains a small loop present in the extracellular space, the Nogo66-loop, which interacts with the two known Nogo-receptors: NgR1 (Nogo Receptor 1, also known as Nogo-66 receptor and reticulon 4 receptor) and PIRB (paired immunoglobulin-like receptor B). While the effects of the activation of the Nogo-A-PIRB complex remain unclear, the binding of Nogo-A to NgR1 leads to the intracellular activation of the RhoA/ROCK/Cofilin pathway that prevents actin cytoskeleton polymerization in the growth cone and therefore inhibits neurite outgrowth (Montani et al., 2009, Nash et al., 2009). Several other proteins can bind to NgR1, such as MAG (myelin-associated glycoprotein) and OMGP (oligodendrocyte myelin glycoprotein), whose also act as neurite outgrowth inhibitors. Because NgR1 has no intracellular domain, it works together with other transmembrane proteins, such as P75, TROY or LINGO1, to induce Nogo signaling. Additionally, Nogo-A contains a small domain (160 aa) called Nogo- Δ 20 fragment on its long extracellular tail. Despite the lack of a known receptor for this

fragment, it has been recently shown to act as a negative regulator of angiogenesis in the mammalian CNS (Walchli et al., 2013), via the RhoA/ROCK pathway.

Over the last 20 years, Nogo has been extensively studied for its role in preventing axonal regrowth and repair after CNS injury (for detailed reviews, see Schwab, 2004, Pernet and Schwab, 2012). The purification and cloning of Nogo-A, in 1998 and 2000 respectively, led to the creation of mouse models and revealed that silencing Nogo-A allows a sprouting of axons after a hemisection of the cortico-spinal tract, a model for lesion in the CNS (Simonen et al., 2003). All these studies generated the corpus of knowledge that allowed the initiation of several clinical trials to test the effect of Nogo-A antibody on injured humans (Zorner and Schwab, 2010).

Studies have focused on Nogo-A because of the lack of specific antibodies for Nogo-B & C. Nogo-A has a non-linear pattern of expression, which also differs among brain regions. During prenatal development, Nogo-A is expressed in migrating neuroblasts and immature neurons, later in many neuron types during the principal outgrowth phase of central and peripheral neurons, especially those with long projecting axons. Whereas the levels of Nogo-A are often undetectable at birth, they are high during development and lower or absent in the adult (Schwab, 2010). In the adult CNS, Nogo-A is found mainly in oligodendrocytes but also in neurons from brain regions with a high level of plasticity, such as the cortex, hippocampus and dorsal root ganglia, as well as in the retina and in the cerebellum (Huber et al., 2002). However, the physiological role of Nogo-A in these regions in the adult has not been fully elucidated. In the hippocampus, several studies pointed out the major role played by Nogo-A for proper hippocampal function and synaptic plasticity. Nogo-A and NgR1 are expressed in hippocampal pyramidal neurons, and their expression is regulated by neuronal activity. Nogo-A has been shown to stabilize and maintain the architecture of hippocampal pyramidal neurons, especially at the level of the spines (Zagrebelsky et al., 2010). Moreover, the absence or silencing of Nogo-A (Delekate et al., 2011) or NgR1 (Lee et al., 2008) is responsible for an increased LTP at the Schaffer collateral-CA1 synapse. In the visual cortex, the absence of NgR1 or Nogo-A/B, as well as PirB, alters the timing of the critical period of ocular dominance plasticity (McGee et al., 2005, Syken et al., 2006). In the adult somatosensory cortex, a recent study discovered that NgR1 is involved in synaptic turnover at the spine level (Akbik et al., 2013). Thus, the Nogo-A-NgR1 complex seems to play an active role in the physiology of several major brain areas in addition to its role in development.

Several pieces of evidence also suggest a role for Nogo-A in the development and the physiology of the cerebellum. Located in the posterior part of the brain, the cerebellum plays a central role in the regulation of motor control, sensory motor learning and memory (Ito, 2006, Sillitoe and Joyner, 2007), cognitive functions and processing of emotions (Strick et al., 2009). The cerebellum can be divided into 3

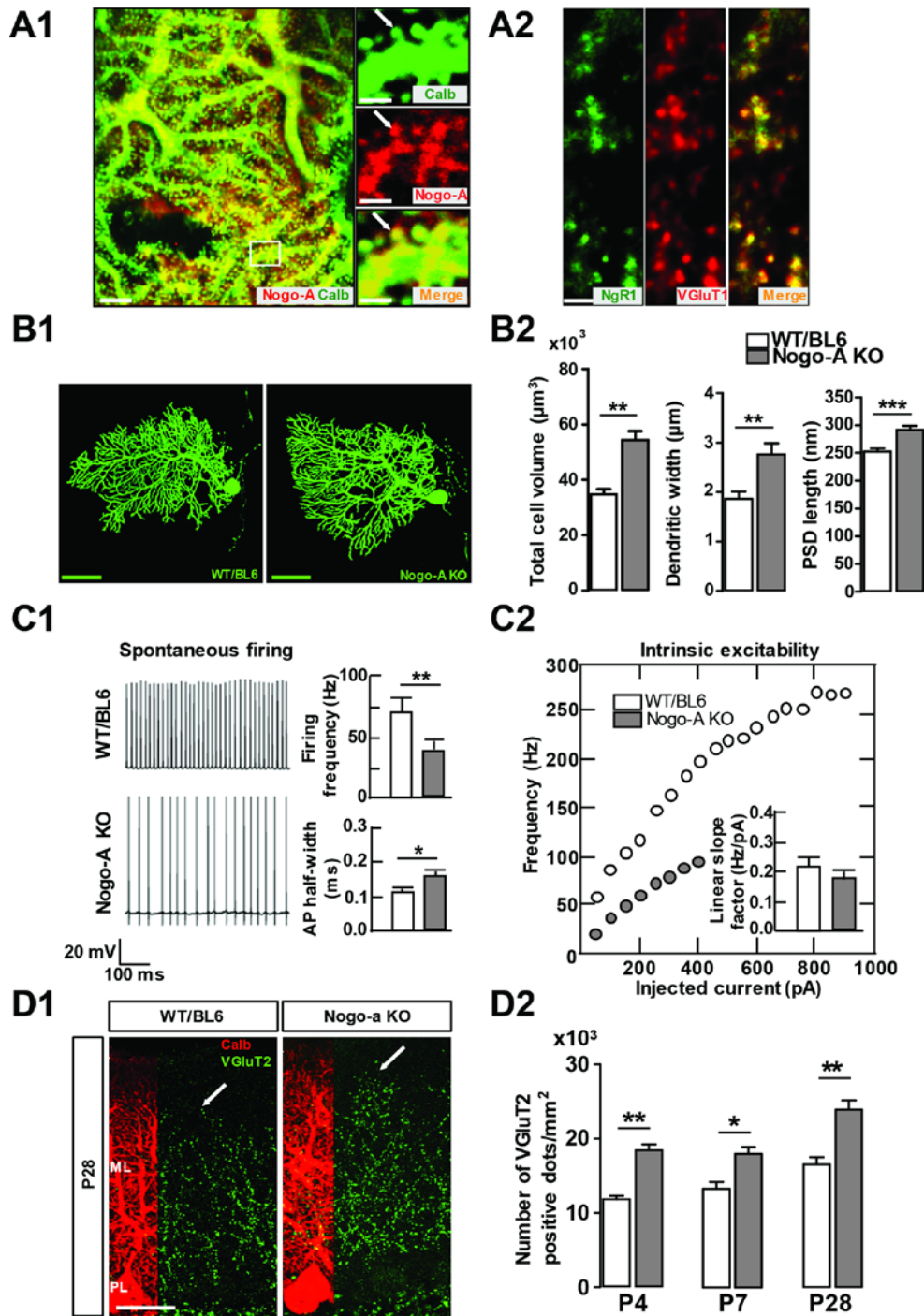
parts: the vestibulocerebellum, the spinocerebellum, and the cerebrocerebellum. Additionally, in the center of the cerebellum, deeply embedded in white matter, four deep nuclei contain the only output of the cerebellum. The cerebellar cortex consists of a repeated and precisely defined cellular architecture that is redundant in a larger structure repeated ten times: the folia. In each of these folia, the cerebral cortex comprises three cellular layers: the granular layer, the Purkinje cell layer and the molecular layer, at the surface of the folia.

The cerebellar circuit is principally organized around Purkinje cells (PC), the major cell of the cerebellar cortex and its only output. With a large cell body and an extensive dendritic tree spreading through the whole molecular layer within a single parasagittal plane, this GABAergic cell projects to the deep cerebellar nuclei. The granule cells, the only excitatory cells of the cerebellar cortex, have their somata located in the granular layer and their axons spread through the dendritic arborization of PCs in the molecular layer, crossing their plane perpendicularly. These axons are referred to as 'parallel fibers' (PF) because they run parallel to each other and to the surface of the cerebellar cortex through the molecular layer. Several types of interneurons are also present in the cerebellum: stellate cells in the molecular layer, basket cells in the Purkinje cell layer and Golgi cells in the granular layer. Their role is to regulate the timing and regularity of PC activity. They have also been implicated in motor coordination and consolidation of learning. Moreover, the cerebellar cortex receives several neuromodulatory afferents that spread through all layers: adrenergic afferents from the locus coeruleus, cholinergic afferents from the pedunculopontine nuclei and serotonergic afferents from the raphe nucleus.

The cerebellar cortex receives two main afferents: the mossy fibers (MF) and the climbing fibers (CF) (for a detailed review, see Apps and Garwicz, 2005). CFs connect PCs directly while the information from MFs reaches PCs via a relay from the granule cells. Both inputs are integrated and processed by PCs. MFs arise from a wide variety of sources, including neurons in the spinal cord, numerous brain stem nuclei (especially the pons) and the cerebellum itself, and they form synapses on proximal dendrites of granule cells. These cells relay the sensory information required for the generation and coordination of movements to the PC via the PFs, which will make hundreds of synaptic contacts on the distal part of the PC's dendritic tree. CFs arise from the contralateral inferior olive, in the ventral part of the caudal brainstem. They split into several branches, spread into the molecular layer and wrap themselves around the dendritic tree of PCs. Each PC receives inputs from a unique CF, which will make numerous synaptic contacts on the proximal part of its dendritic tree. CFs are responsible for the modular organization of the cerebellar cortex along the mediolateral axis, in which the cerebellar cortex can be divided into compartments, PCs in each of these compartments being innervated by CFs emerging from specific subareas of the inferior olive. CFs are thus responsible for the very precise order of the cerebellar cortical organization, comparable to the columnar organization of the cerebral cortex. Overall, the parasagittal

plan of the cerebellum contains a highly complex circuitry, composed of multiple interacting cell types, with the PC as its central element. Within the same sagittal plane, each PC faces the duality of its inputs: CF inputs mainly on the proximal part of the dendritic tree and PFs inputs mostly towards the distal part. Both carry sensory information from the periphery and the cerebral cortex. The input of CFs is multimodal, with a convergence between tactile and nociceptive skin and muscle afferents, and can be considered as an error signal. The potency of their connection to PCs is very strong; a single CF input generates a massive complex spike that elevates the intracellular calcium concentration ($[Ca]_i$) throughout the whole dendritic tree (Davie et al., 2008). The distal part of the dendritic tree receives inputs from numerous PFs, whose activation leads to a brief excitatory post-synaptic potential (EPSC). The PC then transmits the summation of the information from the two main cerebellar afferents to the deep cerebellar nuclei via inhibitory contacts on these nuclei. The PC is a GABAergic cell that is continuously active and has two different firing modes. PCs fire tonically with trains of simple spikes, but they can also produce complex spikes. The oscillation between these two patterns of activity has been described as the so-called phenomenon of bi-stability, where the PCs are in an UP or DOWN state, according to their resting membrane potential (Rokni et al., 2009). Thus, a silent period without any PC inputs sends a powerful signal to the olivo-cerebellar loop. Altogether, the cerebellum and more particularly PCs receive a wide variety of sensory inputs and generate motor-related outputs according to internal rules of computation. As a part of the olivo-cerebellar loop, PCs are major contributors to the fine-tuning of temporal processing from the cerebellum that is important for many functions, from motor coordination to affective control and cognition.

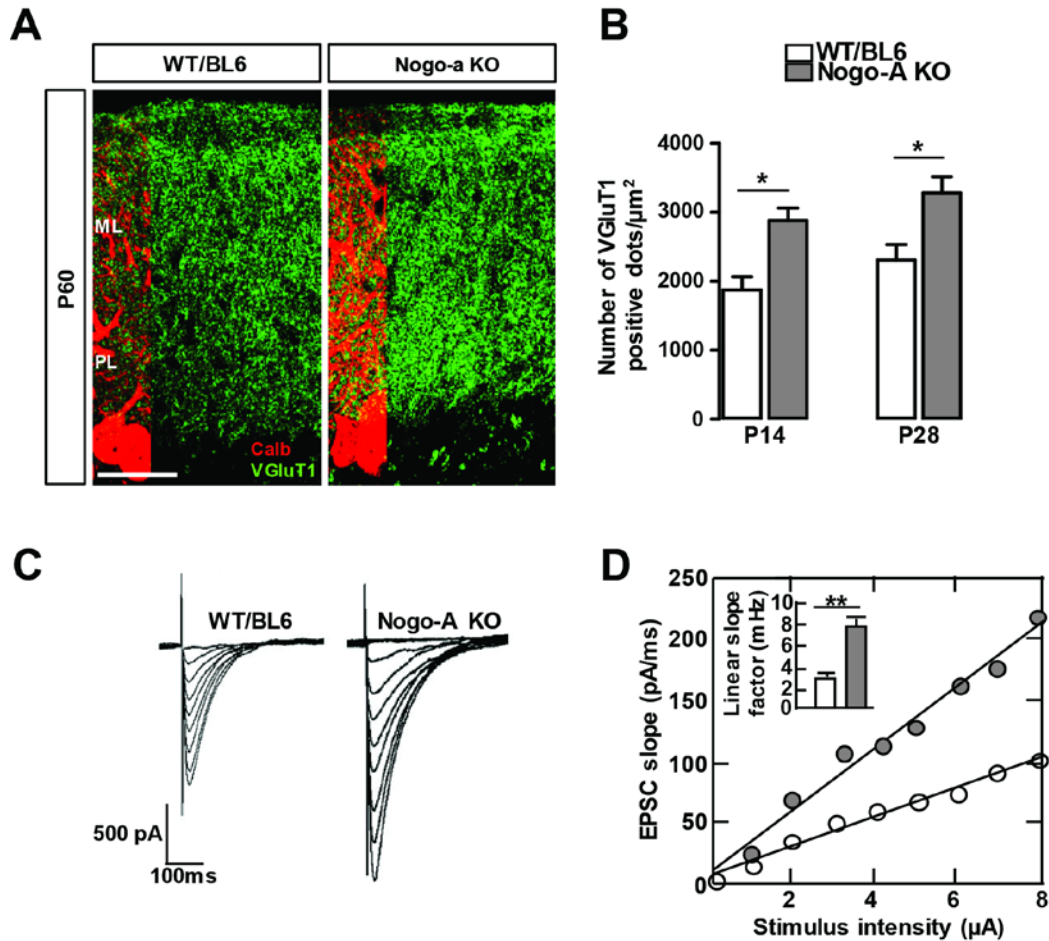
Several studies already highlighted a role for Nogo-A in cerebellar physiology. Nogo-A is present in the dendritic tree of PCs (Box1-A) and also in the presynaptic terminals of PC axons, in the deep cerebellar nuclei (Aloy et al., 2006). NgR1 has been identified in granule cells (Huber et al., 2002), particularly at the pre-synaptic terminals of PFs (Box1-A). Nogo-A KO mice display elevated levels of Nogo-B but still reveal important insights about the physiology of Nogo-A. The size and complexity of PC dendritic trees is negatively modulated by Nogo-A (Box1-B), and PCs in Nogo-A KO mice exhibit a reduced intrinsic excitability (Box1-C). Nogo affects also the two main afferents of PCs: CFs and PFs.



Box1: Cerebellar localization of Nogo-A and its effect on PCs physiology A) Nogo-A and its receptor NgR1 are complementarily expressed at synaptic sites in the cerebellum of P28 WT/BL6 mice. **A1**) Double immunolabeling with anticalbindin (green) and anti-Nogo-A (red) antibodies revealed the presence of Nogo-A in dendrites and spines (arrows) of PCs. Higher magnification micrographs correspond to the boxed region. (Scale bars, 5 μ m; 2 μ m in Insets) **A2**) Double immunolabelling with antibodies against NgR1 (green) and VGluT1 (red) to highlight the strong expression of NgR1 in PF

terminals. **B1)** Confocal images of biocytin-filled PCs from cerebellar slices of P28 Nogo-A KO and the corresponding WT mice. The dendritic tree of Nogo-A Ko PC is larger compared to WT. (Scale bars, 50 μm .) **B2)** The absence of Nogo-A leads to an increase in the total cell volume, in the dendritic width and in the PSD length in PCs, compared to WT. All measurements were done in P28 mice, white bars for WT, grey bars for Nogo-A KO. **C1)** At P28, the lack of Nogo-A leads to a decrease in the PC spontaneous firing accompanied by an increase of the AP half-width. **C2)** The current-frequency plots and the corresponding histogram demonstrate that the lack of Nogo-A has no effect on the intrinsic excitability of PCs at P28. **D)** Effect of the genetic deletion of Nogo-A on the developmental rearrangement of CF terminals onto PC dendrites. **D1)** confocal images of VGluT2+ CF terminals (green) on P28 PCs stained for calbindin (red). The white arrows point to the increased territory of CF synapses on Nogo-A KO mice at P28. Dotted lines indicate the pial surface. ML, molecular layer, PL, PC layer. **D2)** At P4, P7 and P28, Nogo-A KO mice exhibit an increased density of VGluT2+ CF varicosities. Values represent means \pm SEM of 103-116 cells per genotype; * $p < 0.05$, ** $p < 0.01$.

The CF-PC synapse is of major importance to cerebellar physiology and is the result of a very peculiar development. At birth (P0), PCs are innervated by multiple CFs making synaptic contacts onto their somata. Throughout the first 2-3 weeks of life during a process with four distinct stages, this connection will evolve to the adult configuration, in which each PC is innervated by a single CF that makes all its synaptic contacts on the dendritic tree (for detailed reviews, see Kano and Hashimoto, 2009, Watanabe and Kano, 2011). Until P3, PCs are innervated by several CFs with similar connection strengths. From P3 to P9, while the other CFs remain weak, a single CF will strengthen its connection to a PC and shift its connections from the soma to the proximal part of the dendritic tree of the PC. The remaining CFs, which still make a weak somatic connection at this time, will be eliminated in two phases: an early phase, between P7 and P12, independent of PF-PC synapse formation, and a late phase, from P12 to P17, which requires a normal PF-PC synapse formation (Hashimoto et al., 2009). Despite this sophisticated process of synapse elimination and refinement, a remaining secondary weak CF persists in 10% of cases in adult life.



Box2: Influence of Nogo-A on the PF-PC synapse. **A**) Confocal images of VGlut1+ PF terminals (green) on P60 PCs stained for calbindin (red). ML, molecular layer; PL, PC layer. (Scale bar, 50 μm .) **B**) The lack of Nogo-A leads to an increased number of PF terminals making synapse onto PC at P14 as well as at P28 compared to WT. Values represent means \pm SEM of 118–145 cells (six mice) per genotype; * $P < 0.05$. **C-D**) Typical input–output relationships obtained from P28 PCs in response to an increasing stimulation of PFs in Nogo-A KO and the corresponding WT mice. PCs of Nogo-A KO mice exhibit increased response to PF stimulation. Values represent means \pm SEM of 19–25 cells (four to six mice) per genotype; * $p < 0.05$, ** $p < 0.01$.

The developmental up-regulation of Nogo-A coincides with the timing of both somatodendritic translocation and elimination of supernumerary CFs. If the absence of Nogo-A does not lead to an earlier start of synapse elimination, it leads to a precocious somatodendritic translocation of CFs contacts. In adult mice (P28), the absence of Nogo-A leads to a larger spread of CF terminals along the dendritic tree of PCs (Box1, D). Additionally, the absence of Nogo-A affects the PF-PC synapse, with increased levels of proteins involved in the release machinery (VGLUT1 & SNAP25) and a higher synaptic strength

(Box2). All these results lead to the question of whether the absence of Nogo-A interferes with the process of synapse elimination at the CF-PC synapse in young (P14) as well as in old (P28) animals and thus leads to persisting supernumerary CFs.

Materials & Methods

Animals. Nogo-A knockout (KO) [pure C57BL/6 background; postnatal day (P) 14-28] were used in this study. Wild-type (WT) mice of C57BL/6 strain were used as controls. All animal experiments were performed according to the guidelines of the Veterinary Office of the Kanton of Basel-Stadt, Switzerland, and approved by its Commission for Animal Research. All efforts were made to minimize animal suffering and to reduce the number of animals required. Nogo-A KO mice were generated by homologous recombination of exons 2 and 3 in the Nogo-A gene as described previously (Simonen et al., 2003). Animals were backcrossed with C57BL/6 WT mice for more than ten generations resulting in strain purity of > 99.98% (Dimou et al., 2006). Mice had free access to standard laboratory food and water and were maintained on a 12 h light/dark cycle.

Electrophysiology. For the preparation of cerebellar slices, animals were deeply anesthetized by Isoflurane® inhalation and decapitated after loss of the hindpaw withdrawal reflex. The cerebellum was quickly removed and placed in ice-cold ACSF containing (in mM): 125 NaCl, 2.5 KCl, 1 MgCl₂, 2 CaCl₂, 1.25 NaH₂PO₄, 20 glucose, 26 NaHCO₃ and equilibrated with 95% O₂ and 5% CO₂. Parasagittal cerebellar slices, 250 µm thick, were obtained using a vibrating blade microtome (Leica VT1200S, Leica Microsystems Switzerland). Slices were placed in room temperature ACSF to recover for one hour, then placed in an recording chamber of an upright microscope (Olympus BX51WI, Olympus Switzerland) equipped with a 20x lens (Olympus LUMPLAN 20x, Olympus Switzerland) and superfused with room temperature ACSF at a rate of 1 ml/min equilibrated with 95% O₂ and 5% CO₂. Slices were illuminated using a custom-built IR LED system. Purkinje cells were visualized using Nomarski interference contrast, and the image captured with an IR-sensitive video camera (VX55, Till Photonics GmbH, Gräfelfing, Germany). Whole-cell patch-clamp recordings (pipette resistance = 2-4 MΩ) were obtained from PC using a solution containing (in mM): 100 CsCl, 35 Cs-Sulfonate, 11 Tris-Phosphocreatine, 10 HEPES, 4.5 Mg-ATP, 0.3 Tris-GTP, pH 7.25 adjusted with NaOH, Osmolarity: 298 mOsm. The holding potential was set at -10 mV (to inactivate voltage-dependant conductances and to reduce the driving force and current amplitudes). For CF stimulation, a patch pipette (1MΩ) filled with ACSF was placed in the granular cell layer, in the vicinity of the PC, and moved until the climbing fiber response could be elicited with a minimal stimulus intensity. Two current pulses (0.1 ms, paired-pulses interval: 100 ms) were applied

every 20 seconds. These pulses were generated by a stable IS4 stimulator (Sc-Devices, Switzerland). The stimulation intensity was progressively increased (1-10 μ A) until we obtained a large EPSC in an all-or-none manner, indicating that we were stimulating the main climbing fiber. The stimulus intensity was then increased to 200% of the current value eliciting this EPSC.

Statistical Analysis. All data are shown as mean values \pm SEM and considered significant at a level of $P < 0.05$. The significance between the two groups of animals, at P14 and P28, was calculated using an ANOVA-Fisher's test. To compare the Paired-Pulse Ratio values, a Student's t-test was used.

Results

We investigated the CF innervation of PC by electrophysiological measurements on Nogo-A KO mice (P14 and P28) and their WT littermates. PCs were recorded in voltage-clamp configuration, and a stimulus pipette was placed in the granular layer, in the vicinity of the recorded PC (fig. 1A). As the stimulus intensity was increased, a typical large EPSC was elicited in an all-or-none fashion in the majority of PCs which, with a clear paired-pulse depression, demonstrates the CF-mono-innervation of the patched PC. Even in adulthood, in sporadic cases ($\approx 10\%$), PCs' CF-mediated EPSCs had two discrete steps when the stimulus intensity was above the threshold, indicating that these cells had one supernumerary weak CF in addition to the main CF (fig. 1B). At P14, Nogo-A KO mice exhibited a supernumerary CF in 17.24% (5/29 cells) of PCs, while WT cells had a supplementary CF in 23.08% (6/26 cells) (fig. 1C). This difference was however not significant ($p = 0.23$). At P28, 10.71% (3/28 cells) of WT and 3.85% (1/26 cells) of KO PCs ($p = 0.27$) were innervated by more than one CF. Within each genotype, the number of supernumerary CFs decreased with development but not significantly ($p < 0.15$ for WT and Nogo-A KO mice). The CF stimulation consisted of two pulses separated by 100ms. Additionally, the paired-pulse ratio (PPR) was investigated by dividing the amplitude of the second EPSC by the amplitude of the first EPSC. The PPR of CF-mediated EPSCs was different at P14 between WT and Nogo-A KO mice (0.716 ± 0.139 for WT; 0.758 ± 0.008 for Nogo-A KO mice; $p = 0.011$) but not at P28 (0.749 ± 0.001 for WT; 0.768 ± 0.008 for KO; $p = 0.23$) (fig. 1D).

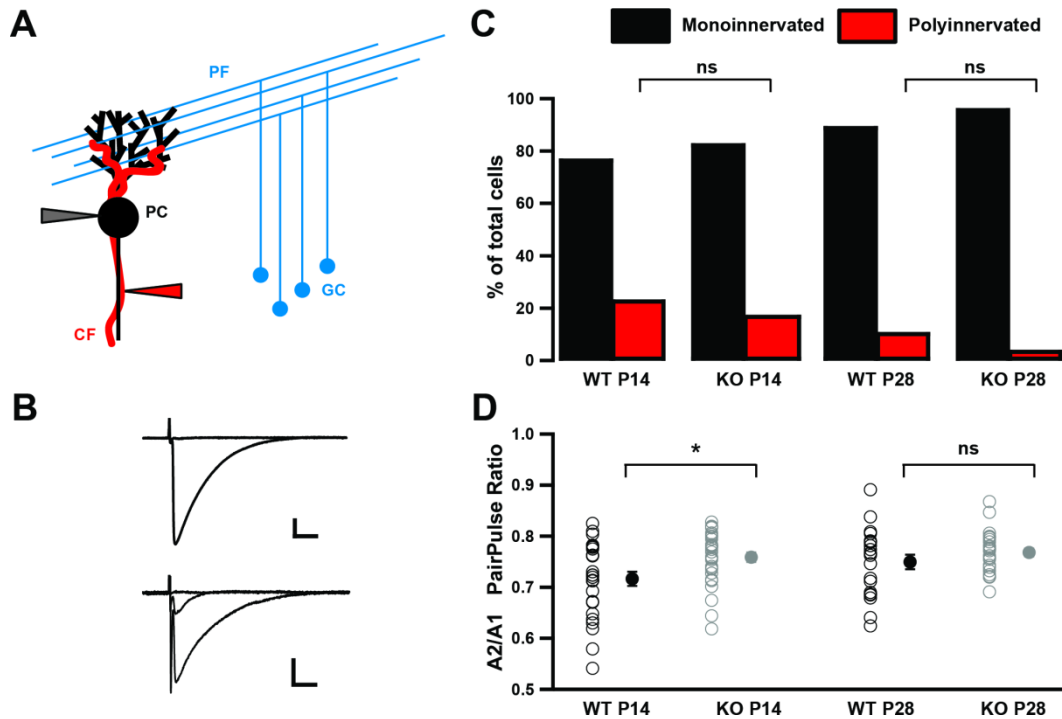


Figure 1: The absence of Nogo-A doesn't lead to an innervation of PCs by multiple climbing fibers. **A)** Classical cerebellar circuitry, organized around the Purkinje cells (PC). Additionally to the pipette for the PC patch (in grey), a stimulus pipette (in red) is placed in the granular layer, in the vicinity of the PC, to stimulate the unique/multiple climbing fiber (CF) (GC: granule cell, PF: parallel fiber). **B)** Representative traces of PCs CF-mediated EPSC, when the PC is innervated by multiple CF (top trace) or a unique CF (bottom trace). **C)** Percentage of PCs innervated by a single (black bars) or multiple (red bars) CF, for WT and Nogo-A KO mice, at P14 and P28 ($p = 0.23$ and 0.27 , respectively). **D)** Pair-Pulse Ratio (amplitude of the second pulse over the amplitude of the first pulse) of the PCs CF-mediated EPSC, for WT (in black) and Nogo-A KO mice (in grey), at P14 and P28 ($*p < 0.05$).

This suggests a difference in the presynaptic level of the CF-PC synapse at P14 which is no longer present in adulthood. Thus, although the lack of Nogo-A affects PCs physiology at several levels, including leading to a precocious translocation of CF contacts from the soma to the dendrites of PCs, the rate of mono-innervated PCs was unchanged in young and adult Nogo-A KO mice compared to WT.

Discussion

Nogo-A has been characterized as a major inhibitor of neurite outgrowth and plays an important role in cerebellar development. We show that the absence of Nogo-A in the mouse cerebellum does not affect the elimination of supernumerary CFs in young (P14) or adult (P28) mice compared to WT mice. We also show that in young mice the absence of Nogo-A leads to a higher PPR, suggesting a difference at the presynaptic level, while the PPR was similar in adult mice regardless of the presence or absence of Nogo-A.

The absence of supernumerary CFs in Nogo-A KO mice is somewhat unexpected due to the strong influence of Nogo-A on cerebellar development. The absence of Nogo-A in the developing cerebellum affects PCs as well as its two main afferents, CF and PF. The study of Nogo-A KO mice reveals the influence of Nogo on the excitability of PCs, as well as on the size of their dendritic trees and somas. Nogo-A also plays a role in several stages of the refinement process of CF-PC synapses: the absence of Nogo-A is responsible for a precocious translocation of the CF contacts from the soma to the dendrites of PCs. In addition, Nogo-A affects the proper development of the PF-PC synapse by acting as a negative regulator of its formation as well as by decreasing its synaptic strength. This synapse and its accurate development are of great importance for a proper maturation of the CF-PC synapse (Hashimoto et al., 2009). Despite the multiple differences in the development of the cerebellar cortex caused by the absence of Nogo-A, the deletion of this protein doesn't lead to any change in the number of CFs innervating PCs: the number of supernumerary CFs persisting in adulthood remains the same compared to WT, regardless of the developmental stage.

The CF-PC synapse is always considered with regard due to the strong potency of connection caused by the multiple contacts a unique CF makes on the dendritic tree of a single PC. It is also of importance because of the sensory feedback, error signal it provides to the brain. Nevertheless, the PF-PC synapse is as crucial to the cerebellar function as the CF-PC connection since both inputs are processed and allow PCs, via an inhibitory connection onto deep cerebellar nuclei, precise control of the motor function as well as a role in other functions such as cognition. The role of Nogo-A in the physiological characteristics of PC and in the proper development of the PF-PC synapse suggest that Nogo-A could play a role in a well-studied yet still complex component of the cerebellar physiology: the PF-PC long-term depression (LTD).

Long-term depression is a major form of synaptic plasticity resulting in a long-lasting decrease in synaptic strength that is thought to have a role in learning and memory, as well as in other physiological processes. LTD in the cerebellum is present at several synapses (Lamont and Weber, 2012) and has been

extensively studied, yet its role as well as some of its mechanistic features still has some grey areas. At the PF-PC synapse, LTD is believed to be the cellular substrate for cerebellar motor learning. LTD can be induced electrically by simultaneously stimulating the PF and PC (Safo and Regehr, 2008), but also chemically with the application of the metabotropic glutamate receptor 1 (mGluR1) agonist 3,5-dihydroxyphenylglycine (DHPG) (Kano et al., 2008). Variations in the intracellular calcium concentration are the main factors responsible for this plastic phenomenon and through a molecular cascade trigger the phosphorylation and internalization of AMPA receptors. Calcium levels have always been linked to plasticity, and their role in these processes follows the so-called 'BCM rule'. Postulated in the late 70s by Elie Bienenstock, Leon Cooper and Paul Munro (Bienenstock et al., 1982, Cooper and Bear, 2012), this theory suggests that the direction of plasticity is linked to the amplitude of the intracellular calcium rise. In the cerebellum, the theory is inverted compared to the cortex and the hippocampus, and a large increase of $[Ca]_i$ is paired with a long-term decrease of the response, while a modest rise of the $[Ca]_i$ leads to an increase of the evoked response.

It would be interesting to investigate if and how the several differences observed in cerebellar circuitry and connectivity due to the absence of Nogo-A would affect such an important trait of the cerebellar physiology. Indeed, several mechanisms of the cerebellar physiology, altered by the absence of Nogo-A, are known to play a role in PF-PC LTD. The purpose of simultaneous stimulation of PF and CF as a pairing protocol is to elicit an increase of $[Ca]_i$, mostly due to the complex spike and its accompanying calcium wave, caused by PC stimulation. Therefore, it would be interesting to investigate if the extension of the CF on the dendritic tree of PCs, causing a hyperinnervation, induces a change in the calcium wave associated with the massive complex spikes created by the discharge of the multiple contacts of the CF onto the PC dendritic tree. It would also be interesting to see if variation in soma size affects the dynamics of intracellular calcium. Furthermore, Nogo-A KO mice exhibit a higher level of the synaptic protein SNAP25 at the presynaptic terminal of the PF-PC synapse. As a part of the SNARE complex, SNAP25 is an essential mediator of vesicle fusion and exocytosis. It is highly expressed in PF-PC terminals (Mandolesi et al., 2009) and known to regulate calcium dynamics and neuronal plasticity. At P28, the levels of SNAP25 in PF terminals are highly elevated in KO mice compared to WT. Levels of VGluT1, the vesicular transporter of glutamate specifically present in the cerebellum at PF-PC synapses, are also elevated in the absence of Nogo-A, at P14 and P28. The synaptic strength of PF-PC synapses for increasing stimulating intensities increased significantly in Nogo-A KO mice. PPR is known to reflect the synaptic release probability, and a higher PPR parallels a lower presynaptic release probability. At P14, the absence of Nogo-A is then responsible for a lower release probability at the PF-PC synapse. All these differences reveal that the PF-PC synapse is altered in Nogo-A KO mice. It would be of importance to see how a modified PF-PC synapse could sustain a plasticity protocol.

All these variations observed in Nogo-A KO mice affect processes important in cerebellar LTD. Testing several different induction protocols might help us to determine which aspects of the deficits due to the absence of Nogo-A could affect the PF-PC LTD, whether it is the changes observed at the PF-PC synapse, at the CF-PC synapse or at the level of the physiology and the architecture of the PC itself.

References

- Akbik FV, Bhagat SM, Patel PR, Cafferty WB, Strittmatter SM (2013) Anatomical plasticity of adult brain is titrated by Nogo Receptor 1. *Neuron* 77:859-866.
- Aloy EM, Weinmann O, Pot C, Kasper H, Dodd DA, Rulicke T, Rossi F, Schwab ME (2006) Synaptic destabilization by neuronal Nogo-A. *Brain Cell Biol* 35:137-156.
- Apps R, Garwicz M (2005) Anatomical and physiological foundations of cerebellar information processing. *Nat Rev Neurosci* 6:297-311.
- Bienenstock EL, Cooper LN, Munro PW (1982) Theory for the development of neuron selectivity: orientation specificity and binocular interaction in visual cortex. *J Neurosci* 2:32-48.
- Caroni P, Schwab ME (1988) Antibody against myelin-associated inhibitor of neurite growth neutralizes nonpermissive substrate properties of CNS white matter. *Neuron* 1:85-96.
- Cooper LN, Bear MF (2012) The BCM theory of synapse modification at 30: interaction of theory with experiment. *Nature Reviews Neuroscience* 13:798-810.
- Davie JT, Clark BA, Hausser M (2008) The origin of the complex spike in cerebellar Purkinje cells. *J Neurosci* 28:7599-7609.
- Delekate A, Zagrebelsky M, Kramer S, Schwab ME, Korte M (2011) NogoA restricts synaptic plasticity in the adult hippocampus on a fast time scale. *Proc Natl Acad Sci U S A* 108:2569-2574.
- Dimou L, Schnell L, Montani L, Duncan C, Simonen M, Schneider R, Liebscher T, Gullo M, Schwab ME (2006) Nogo-A-deficient mice reveal strain-dependent differences in axonal regeneration. *J Neurosci* 26:5591-5603.
- Hashimoto K, Yoshida T, Sakimura K, Mishina M, Watanabe M, Kano M (2009) Influence of parallel fiber-Purkinje cell synapse formation on postnatal development of climbing fiber-Purkinje cell synapses in the cerebellum. *Neuroscience* 162:601-611.
- Huber AB, Weinmann O, Brosamle C, Oertle T, Schwab ME (2002) Patterns of Nogo mRNA and protein expression in the developing and adult rat and after CNS lesions. *J Neurosci* 22:3553-3567.
- Ito M (2006) Cerebellar circuitry as a neuronal machine. *Progress in Neurobiology* 78:272-303.

- Kano M, Hashimoto K (2009) Synapse elimination in the central nervous system. *Curr Opin Neurobiol* 19:154-161.
- Kano M, Hashimoto K, Tabata T (2008) Type-1 metabotropic glutamate receptor in cerebellar Purkinje cells: a key molecule responsible for long-term depression, endocannabinoid signalling and synapse elimination. *Philos Trans R Soc Lond B Biol Sci* 363:2173-2186.
- Lamont MG, Weber JT (2012) The role of calcium in synaptic plasticity and motor learning in the cerebellar cortex. *Neurosci Biobehav Rev* 36:1153-1162.
- Lee H, Raiker SJ, Venkatesh K, Geary R, Robak LA, Zhang Y, Yeh HH, Shrager P, Giger RJ (2008) Synaptic function for the Nogo-66 receptor NgR1: regulation of dendritic spine morphology and activity-dependent synaptic strength. *J Neurosci* 28:2753-2765.
- Mandolesi G, Vanni V, Cesa R, Grasselli G, Puglisi F, Cesare P, Strata P (2009) Distribution of the SNAP25 and SNAP23 synaptosomal-associated protein isoforms in rat cerebellar cortex. *Neuroscience* 164:1084-1096.
- McGee AW, Yang Y, Fischer QS, Daw NW, Strittmatter SM (2005) Experience-driven plasticity of visual cortex limited by myelin and Nogo receptor. *Science* 309:2222-2226.
- Montani L, Gerrits B, Gehrig P, Kempf A, Dimou L, Wollscheid B, Schwab ME (2009) Neuronal Nogo-A modulates growth cone motility via Rho-GTP/LIMK1/cofilin in the unlesioned adult nervous system. *J Biol Chem* 284:10793-10807.
- Nash M, Pribrag H, Fournier AE, Jacobson C (2009) Central nervous system regeneration inhibitors and their intracellular substrates. *Molecular Neurobiology* 40:224-235.
- Pernet V, Schwab ME (2012) The role of Nogo-A in axonal plasticity, regrowth and repair. *Cell Tissue Res* 349:97-104.
- Rokni D, Tal Z, Byk H, Yarom Y (2009) Regularity, variability and bi-stability in the activity of cerebellar purkinje cells. *Front Cell Neurosci* 3:12.
- Safo P, Regehr WG (2008) Timing dependence of the induction of cerebellar LTD. *Neuropharmacology* 54:213-218.
- Schwab ME (2004) Nogo and axon regeneration. *Curr Opin Neurobiol* 14:118-124.
- Schwab ME (2010) Functions of Nogo proteins and their receptors in the nervous system. *Nat Rev Neurosci* 11:799-811.
- Sillitoe RV, Joyner AL (2007) Morphology, molecular codes, and circuitry produce the three-dimensional complexity of the cerebellum. *Annu Rev Cell Dev Biol* 23:549-577.
- Simonen M, Pedersen V, Weinmann O, Schnell L, Buss A, Ledermann B, Christ F, Sansig G, van der Putten H, Schwab ME (2003) Systemic deletion of the myelin-associated outgrowth inhibitor Nogo-A improves regenerative and plastic responses after spinal cord injury. *Neuron* 38:201-211.
- Strick PL, Dum RP, Fiez JA (2009) Cerebellum and nonmotor function. *Annual Review of Neuroscience* 32:413-434.

- Syken J, Grandpre T, Kanold PO, Shatz CJ (2006) PirB restricts ocular-dominance plasticity in visual cortex. *Science* 313:1795-1800.
- Walchli T, Pernet V, Weinmann O, Shiu JY, Guzik-Kornacka A, Decrey G, Yuksel D, Schneider H, Vogel J, Ingber DE, Vogel V, Frei K, Schwab ME (2013) Nogo-A is a negative regulator of CNS angiogenesis. *Proc Natl Acad Sci U S A* 110:E1943-1952.
- Watanabe M, Kano M (2011) Climbing fiber synapse elimination in cerebellar Purkinje cells. *Eur J Neurosci* 34:1697-1710.
- Zagrebelsky M, Schweigreiter R, Bandtlow CE, Schwab ME, Korte M (2010) Nogo-A stabilizes the architecture of hippocampal neurons. *J Neurosci* 30:13220-13234.
- Zorner B, Schwab ME (2010) Anti-Nogo on the go: from animal models to a clinical trial. *Ann N Y Acad Sci* 1198 Suppl 1:E22-34.

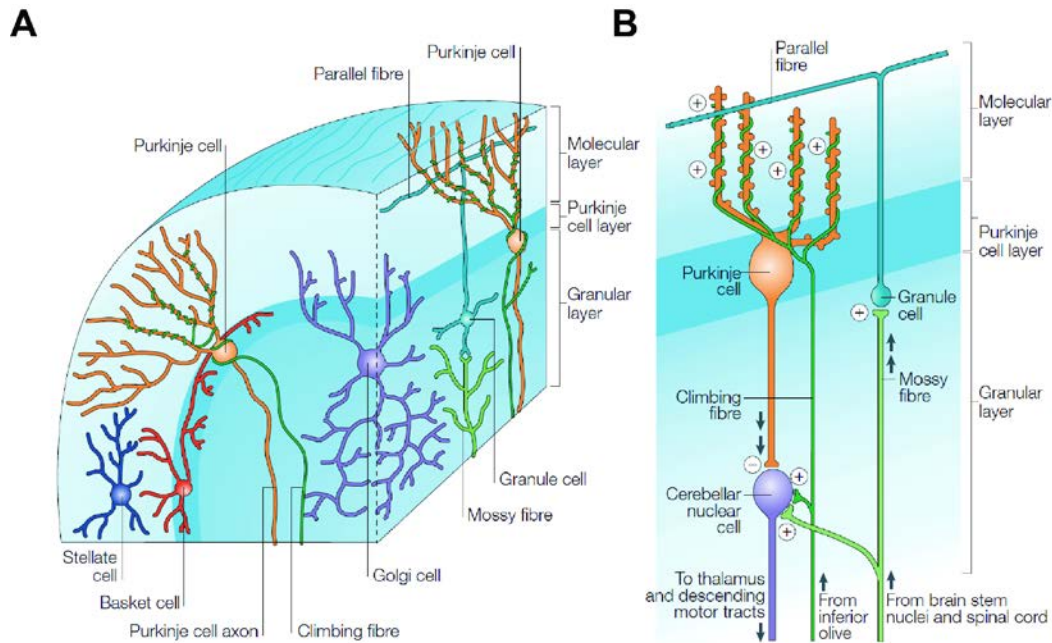
Chapter 2: Influence of the absence of Neuroligin 3 on the development of mGluR1 LTD in the cerebellum

Introduction

The cerebellum is an important actor in the regulation of motor control, sensory motor learning and memory (Ito, 2006, Sillitoe and Joyner, 2007), as well as of cognitive functions and processing of emotions (Strick et al., 2009). Together with the inferior olive, the cerebellum forms a loop of major importance to regulate timing of movements and provides a feed-forward control of muscle contraction. For example, the cerebellum controls the vestibulo-ocular reflex; vestibular stimulation is responsible for reflex movements of the eyes to keep the retinal image stable, preventing degradation of visual processing. Cerebellar dysfunction leads to ataxia, characterized by the inability to perform coordinated smooth movements, visible in gait disturbances, overshooting movements of extremities and imprecise eye movements. Hence the olivo-cerebellar loop is a sophisticated internal feedback circuit that regulates cortical motor programs and plans movements.

The cerebellum has been extensively studied because of its peculiar and stereotypical architecture. The cerebellum can be divided into three anatomical regions: the vestibulocerebellum, the spinocerebellum, and the cerebrocerebellum. The center of the cerebellum contains, profoundly embedded in white matter, four deep nuclei that contain the only output neurons of the cerebellum. The cerebellar cortex is folded into ten folia, which are all composed of three cellular layers: the granular layer, the

Purkinje cell layer and the molecular layer, at the surface of the folia (box 1). The cerebellar circuitry is principally organized around Purkinje cells (PC), the major cell of the cerebellum and the only output neuron of the cerebellar cortex. With a large cell body and an extensive dendritic tree spreading throughout the whole molecular layer, within a single parasagittal plane, this GABAergic cell projects to the deep cerebellar nuclei. The granule cells, the only excitatory cells of the cerebellar cortex, have their somata located in the granular layer, and their axons spread through the dendritic arborization of PCs in the molecular layer, crossing their plane perpendicularly. These axons are referred to as 'parallel fibers' (PF) because they run through the molecular layer, parallel to each other and to the surface of the cerebellar cortex. Several types of interneurons are also present in the cerebellum: stellate cells in the molecular layer, basket cells in the Purkinje cell layer and Golgi cells in the granular layer. Their role is to regulate the timing and the regularity of PC activity, and they have also been implicated in motor coordination and consolidation of learning. The cerebellar cortex receives two main afferents: the mossy fibers and the climbing fibers. Mossy fibers arise from brain stem nuclei and the spinal cord, and form synapses on the terminal portion of the granule cells' short dendrites. They relay sensory information, required for the generation and coordination of movements, to the PC via the PF. The climbing fibers (CF) arise from the inferior olive and transmit cortical information via a relay in the pons. Several axonal branches of one CF will wrap themselves around the proximal dendritic branches of the PC. They convey sensory feedback information, particularly error signals. Moreover, the cerebellar cortex receives several neuromodulatory afferents that spread through all layers: adrenergic afferents from the locus coeruleus, cholinergic afferents from the pedunculopontine nucleus, and serotonergic afferents from the raphe nucleus. Overall, the parasagittal plane of the cerebellum contains a highly complex circuitry, composed of multiple interacting cell types, with the PC as the central element. Within the same sagittal plan, each PC receives hundreds of input from one single CF on the proximal part of its dendritic arbor. The potency of their connection to PC is very strong and a single climbing fiber input generates a complex spike that elevates the intracellular calcium concentration ($[Ca]_i$) in PCs. The distal part of the dendritic tree receives inputs from numerous PFs, whose activation leads to a brief excitatory post-synaptic potential (EPSP). PCs then transmit the summation of the information from the two main cerebellar afferents to the deep cerebellar nuclei via inhibitory contacts on these nuclei. Through the integration and modulation of these afferents, the cerebellum plays the role of a high-level feedback circuit involved in the regulation of motor control, sensory motor learning, memory and perhaps cognition.



Box1: Emblematic structure of the cerebellar cortex (modified from Apps & Garwicz, 2005). **A)** Representation of the diverse cellular types present in a folia of the cerebellum. The two main cells of the typical cerebellar circuitry are the Purkinje and the granule cells. Three types of interneurons control their activity: stellate cells, basket cells and Golgi cells. **B)** Parasagittal plane of the cerebellum: the Purkinje cell receives within the same plane inputs from the climbing fiber and the parallel fiber, the axon of the granule cells which relays the information from the mossy fiber. Mossy fibers and climbing fibers are the two main afferents from the cerebellum, while the Purkinje Cells are the only output of the cerebellar cortex, projecting towards the deep nuclei.

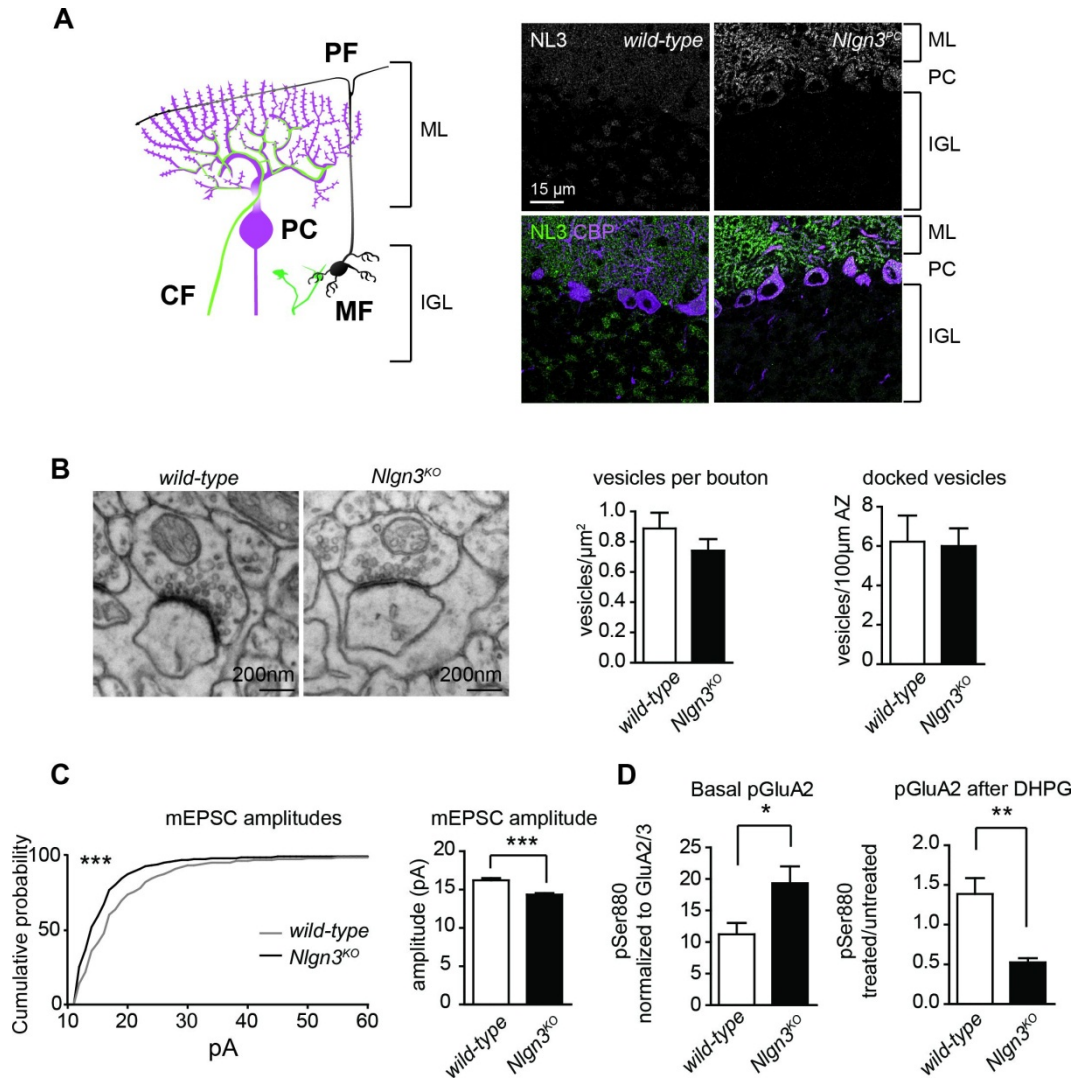
The development and stabilization of this complex circuitry is controlled and realized by numerous cell-adhesion molecules, which structure and anchor synaptic contacts (Missler et al., 2012). Synapses are specialized intercellular junctions dedicated to the transfer of information from a neuron to a target cell. Synapse formation and the specification of synaptic diversity are linked to the actions of synaptic cell-adhesion molecules. Amongst the many actors of this complex structure, neuroligins and neurexins are well characterized (Sudhof, 2008). Neuroligins (nlgn) are an adhesion molecule present at the postsynaptic site forming a trans-synaptic complex with neurexins, present on the presynaptic site, and they interact with intracellular proteins, especially via their PDZ domain. This complex formed by neuroligins and neurexins is essential for synapse stabilization and function but is not involved in synapse formation (Missler et al., 2003, Varoqueaux et al., 2006). The neuroligin family is composed of 4 different proteins: nlgn 1, nlgn 2, nlgn 3 and nlgn 4. While nlgn 1 is exclusively present at excitatory synapses and nlgn 2 is found only at inhibitory contacts, nlgn3 is found at both types (Budreck and Scheiffele, 2007). Since the neurexin-neuroligin complex is of major importance for synaptic function, any alteration of these molecules has dramatic consequences on the proper synaptic function (Sudhof, 2008). The

importance of cell-adhesion molecules for a proper synaptic transmission makes them the ideal link between synaptic function, cognition and cognitive diseases. Indeed, alterations of their functions have been discovered in several cognitive diseases such as schizophrenia and autism spectrum disorder (ASD). Several defects in neuroligin (as well as neurexin) function have been linked to ASD (Sudhof, 2008).

Many recent studies have pointed out that the cerebellum is the most consistent site of structural neural abnormality in ASD (Mostofsky et al., 2009). ASD is a cognitive disorder characterized by impairments in three domains: social interaction, language and range of interests. Several studies have outlined an alteration of physiological function of the cerebellum in ASD patients. Notably, post-mortem analysis of ASD patients' brain has revealed a reduction in the number of PC (Bauman and Kemper, 2005, Amaral et al., 2008). ASD has a strong genetic basis, and recent studies have revealed a large number of mutations that can be linked to ASD (Abrahams and Geschwind, 2008, Caglayan, 2010). There are several forms of autism, and while the details of the classification are still under debate, ASDs can clearly be classified in syndromic and non-syndromic diseases. Autism is considered as "syndromic" when a single, clearly defined, genetic defect is involved, leading to neurodevelopmental defects and a collection of symptoms including autism. Fragile X syndrome (25% of autistic patients), due to the silencing of FMR1 gene, and Rett syndrome, caused by mutations in the MeCP2 gene, affect a large number of patients and are amongst the most studied syndromic forms of ASD. ASD is referred to as "non-syndromic" or "pure autism" when autism is the patient's only deficit. This form of autism is due to mutations or alterations in a single or in multiple genes. Mutations in neuroligins, neurexins, and other proteins of the post-synaptic density such as shank proteins are amongst the most common forms of non-syndromic autism (for detailed reviews, see Zoghbi and Bear, 2012, Ebert and Greenberg, 2013). Many of these mutations affect synaptic proteins playing a role in the process of activity-dependent synapse development and function. For the nlg family, a R451C mutation (arg451→cys451 substitution, altering a conserved residue in the extracellular domain of nlg 3) (Jamain et al., 2003) and deletions of the neuroligin 3 gene (NL3) have been observed in several autistic patients (Gilman et al., 2011). Furthermore, mice carrying this point mutation and NL3-KO mice present an autistic behavior, notably impairments in social interaction and social memory (Tabuchi et al., 2007, Radyushkin et al., 2009). In the cerebellum, NL3 is mainly expressed at the PF-PC synapse (box 2A). The ultrastructural analysis of this synapse on NL3-KO mice didn't reveal any marked differences of the morphological parameters (Box 2B), such as the number of vesicles, but the amplitude of the miniature excitatory post-synaptic currents (mEPSCs) recorded in PC was reduced (Box 2C), pointing towards an alteration of the PF-PC connection.

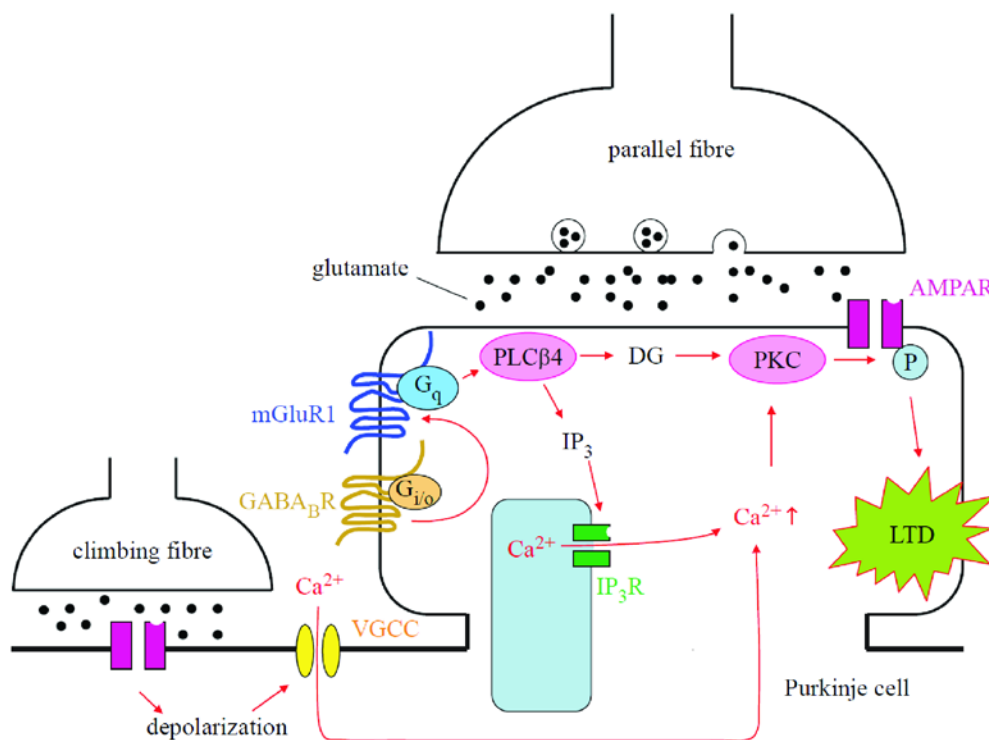
Plasticity is an important process that allows synapse refinement and modulation of synaptic strength in an activity-dependent manner. Amongst the numerous factors involved, AMPA-R trafficking is

a major actor of the variation of synaptic strength observed after the application of various pairing or stimulation protocols (Santos et al., 2009). Calcium is an essential signaling molecule involved in the regulation of many cellular mechanisms, including plasticity phenomena. Plasticity occurs in the cerebellum at several synapses (for a detailed review, see Lamont and Weber, 2012). The development of the CF-PC synapse provides a good example of a particular type of plasticity: synapse elimination and refinement. At birth, PCs are innervated by multiple CFs, making synapses onto their soma. Through a complex but precisely defined process, PCs in adult life will receive a synaptic contact from a single CF, making contact with the proximal part of its dendritic tree (Watanabe and Kano, 2011). Long-term depression (LTD) is a major form of synaptic plasticity resulting in a long-lasting decrease in synaptic response. Like long-term potentiation, it is thought to have a role in learning and memory, along with other physiological processes. LTD in the cerebellum has been extensively characterized at the PF-PC synapse (Hansel et al., 2001). LTD at this synapse can be induced by simultaneous stimulation of PF and CF, with an appropriate timing between both stimulations (Safo and Regehr, 2008). But LTD can also be induced chemically, by application of the metabotropic glutamate receptor 1 (mGluR1) agonist 3,5-dihydroxyphenylglycine (DHPG) (Conquet et al., 1994, reviewed in Kano et al., 2008).



Box2: Importance of neuroligin3 at the PF-PC synapse. **A)** Emblematic circuitry of the cerebellar cortex. In mice overexpressing neuroligin exclusively in Purkinje cells (Nlgn^{PC}), nlg3 immunoreactivity is increased in Purkinje cell dendrites and is abolished in the granular layer (IGL) (PF: parallel fibers; MF: mossy fibers; CF: climbing fibers; ML: molecular layer). **B)** Transmission electron microscopy analysis of PF ultrastructure in absence of nlg3. The number of vesicles per bouton and of docked vesicles doesn't vary significantly in NL3-KO mice. **C)** Cumulative distribution of mEPSCs (***) and mean amplitude (***) and mean amplitude (***) $P < 0.001$, Mann-Whitney test). There is a strong reduction of the amplitude of mEPSCs in NL3-KO mice. **D)** Quantitative Western-Blot analysis of basal and DHPG-induced phospho-GluA2 (normalized to GluA2/3 protein level, * $P < 0.03$, t-test). DHPG-induced phosphorylation is expressed as the ratio of treated to untreated samples (** $P < 0.01$, t-test). If in basal condition, NL3-KO mice have more phospho-GluA2 compared to WT, the application of DHPG causes a decrease in phospho-GluA2, while this level is increased in WT mice.

Calcium role in plasticity has been extensively described in the cerebellum (Lamont and Weber, 2012), where a high increase of $[Ca]_i$ is necessary to produce a LTD. With the electrical pairing protocol, the increase of $[Ca]_i$ is generated by CF stimulation, which will generate a complex spike that elevates the $[Ca]_i$ (Davie et al., 2008). This increase in $[Ca]_i$ will stimulate the PKC which will phosphorylate the GluA2 subunit of AMPA-R at the Ser880 locus, hence inducing internalization of the AMPA-R (Box3) which is necessary for cerebellar LTD (Chung et al., 2003). Upon DHPG stimulation, mGluR1 located on the postsynaptic side triggers the release of calcium from internal stores, via PLC β 4 and IP $_3$. This increase in $[Ca]_i$ will also lead to an activation of the PKC and then internalization of AMPA-R after their phosphorylation on their GluA2 subunit.



Box3: Parallel fiber-Purkinje cell LTD can be induced electrically or chemically (modified from Kano et al., 2008). Increase of internal calcium plays a key role in parallel-fiber-Purkinje cell LTD, by inducing the phosphorylation and then internalization of AMPA receptor via the PKC. This increase can be obtained with the depolarization produced by the climbing fiber, which will open voltage-gated calcium channels (VGCC) and thus increase the internal calcium concentration. Alternatively, activation of mGluR1 receptor via an application of its agonist DHPG will trigger a molecular cascade acting through PLC β 4 that will act on PKC either via DG or through the release of calcium from internal store via IP $_3$ to phosphorylate AMPA receptors.

mGluR LTD is believed to be the cellular substrate for motor learning. In mouse models for fragile-X syndrome, LTD is exaggerated upon DHPG stimulation (Bear et al., 2004). Hence, we decided

to investigate the consequences of the absence of *nlg3* on this important physiological process to determine if a parallel could be established with fragile X syndrome.

Material & Methods

Animals. NL3-KO mice were previously described (Tanaka et al., 2010) and were maintained in C57/B16 background. All mice used for analysis were males between 2-3 months old for the first set of experiments and from P21 to P30 days old for the second set. Mice had free access to standard laboratory food and water and were maintained on a 12h light/dark cycle.

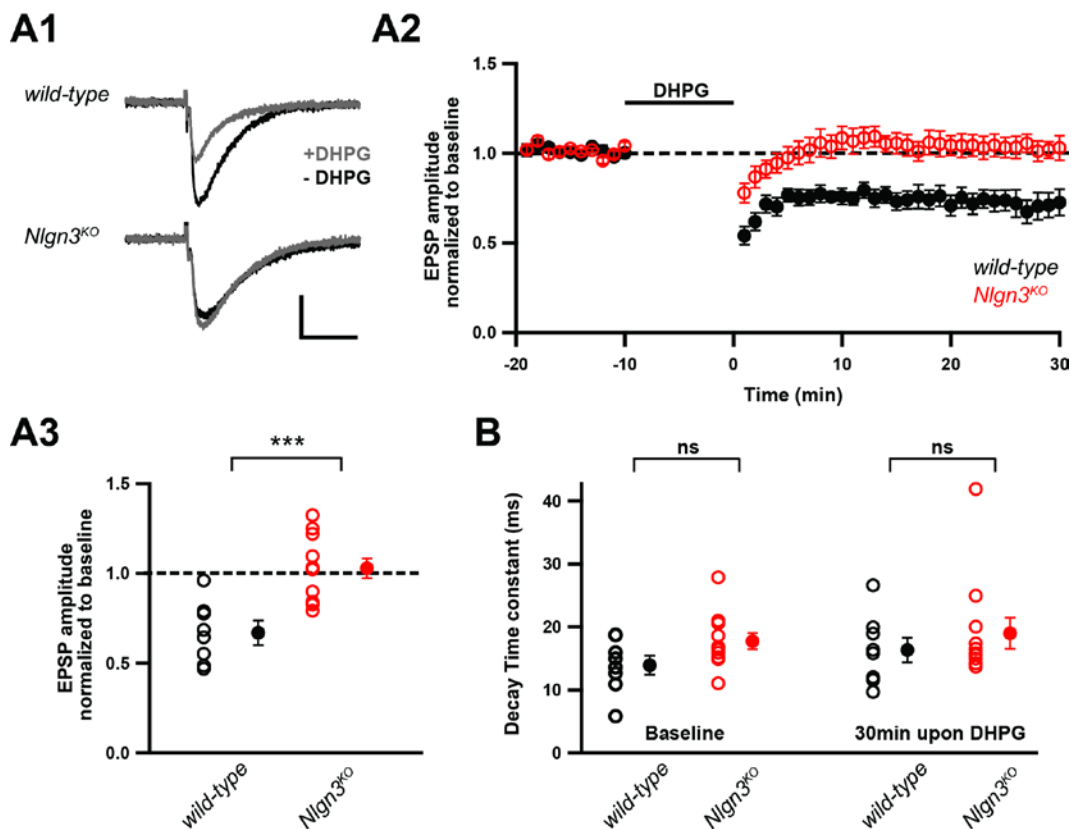
Electrophysiology. For the preparation of cerebellar slices, animals were deeply anesthetized by Isoflurane® inhalation and decapitated after loss of the hindpaw withdrawal reflex. The cerebellum was quickly removed and placed in ice-cold ACSF containing (in mM): 125 NaCl, 2.5 KCl, 1 MgCl₂, 2 CaCl₂, 1.25 NaH₂PO₄, 20 Glc, 26 NaHCO₃, and equilibrated with 95% O₂ and 5% CO₂. Parasagittal cerebellar slices, 250µm thick, were obtained using a vibrating blade microtome (Leica VT1200S, Leica Microsystems Switzerland). Slices were placed in room temperature ACSF to recover for one hour, then placed in the recording chamber of an upright microscope (Olympus BX51WI, Olympus Switzerland) equipped with a 20x lens (Olympus LUMPLAN 20x, Olympus Switzerland) and superfused with room temperature ACSF at a rate of 1 ml/min, equilibrated with 95% O₂ and 5% CO₂. Slices were illuminated using a custom-built IR LED system. PCs were visualized using Nomarski interference contrast, and the image captured with an IR-sensitive video camera (VX55, Till Photonics GmbH, Gräfelfing, Germany). Whole-cell patch-clamp recordings (pipette resistance=2-4MΩ) were obtained from PC using K-based internal solution containing (in mM) 120 K-Gluconate, 5 KCl, 11 tris-Phosphocreatine, 20 HEPES, 4.5 Mg-ATP, 0.3 Tris-GTP, 1 EGTA, pH=7.3, 291mOsm. Signals were recorded using a dual voltage- and current-clamp amplifier (Multiclamp 700B, Molecular Devices, Sunnyvale, USA). Data were filtered at 10 kHz and digitized at 20 kHz using an A/D board (National Instruments Switzerland) using custom written macros in IGOR (Wavemetrics, Lake Oswego, USA). PCs were held at -60 mV and a patch pipette (1MΩ) filled with ACSF was placed in the molecular layer, in the vicinity of the PC, and moved until the PF response could be elicited with a minimal stimulus intensity. Two current pulses (0.2ms, paired-pulses interval: 100ms) were applied every 20 seconds, generated by a stable IS4 stimulator (Sc-Devices, Switzerland). The stimulation intensity was chosen to obtain an evoked excitatory post-synaptic current (eEPSC) with an amplitude of approximately 200pA. A baseline was recorded for at least 10 min and when judged stable, the cell was switched to current-clamp mode (with no holding current applied) for

the application of 10ml (*RS*)-3,5-Dihydroxyphenylglycine (DHPG) 50 μ M. The cell was then switch back to voltage-clamp and the response to pair-pulse stimulation was recorded for at least 30min.

Statistical Analysis. Data points were reduced to one point per minute, and normalized to the average value of the baseline over 10 minutes. For the analysis of the cell response to the application of DHPG and to compare the response between the different genotypes, we averaged the value of the response over 5 minutes, 30 minutes after the end of the perfusion of DHPG. Pairwise comparisons were performed using Student's t test. Data are represented as the mean \pm standard error of the mean (SEM).

Results

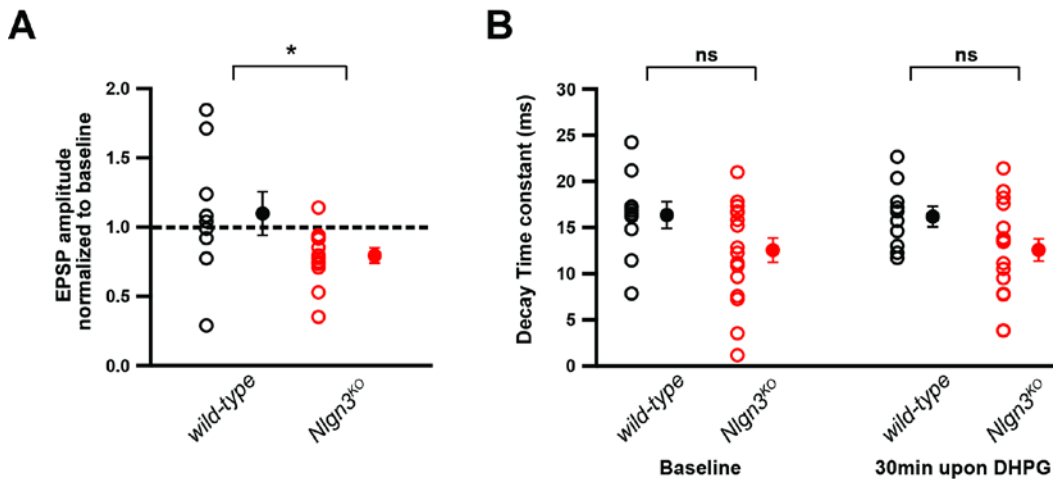
mGluR-LTD in the cerebellum, on the PF-PC synapse is a well-defined physiological process that has been extensively studied (for detailed reviews, see Kano et al., 2008, Luscher and Huber, 2010).



mGluR-LTD at the PF-PC synapse in 2-3 months old NL3-KO mice. **A1)** representatives traces of the EPSC recorded in Purkinje cells evoked by PF stimulation, at the basal level (black traces) and 30min after application of 50 μ M DHPG (grey traces) to WT and NL3-KO mice. **A2)** Average EPSC amplitude (normalized to baseline) evoked by PF stimulation, before and after perfusion of 50 μ M DHPG. **A3)** EPSC amplitude, normalized to baseline, 30min after perfusion of 50 μ M DHPG (***)P<0.001, t-test). WT in

black, KO in red (averages: filled circles). **B**) Decay time constant of the EPSC, evoked by PF stimulation, at the basal level and 30min after application of 50 μ M DHPG (P=0.076 at the basal level, and P=0.41 at 30min, t-test). WT in black, KO in red.

On cerebellar slices from 2-3 months old wild-type mice (WT), the perfusion of 50 μ M DHPG for 10 min induced a strong decrease in the amplitude of eEPSCs recorded in the PC, evoked by PF stimulation ($66.9 \pm 6.9\%$, N = 8 cells, normalized to baseline, measured 30 minutes after the end of the perfusion, Fig. 1, A1-3). In contrast, with NL3-KO cerebellar slices, the perfusion of DHPG did not produce any reduction of the evoked response in the PC ($102.9 \pm 5.4\%$, N = 11 cells, $p < 0.001$, Fig. 1, A1-3). The decay time constant of the eEPSCs varied under control conditions between WT ($\tau = 13.9 \pm 1.5$ ms) and KO ($\tau = 17.7 \pm 1.3$ ms) but not significantly ($p = 0.0761$, Student's t-test) and didn't have any differences after the induction of LTD ($\tau = 16.3 \pm 1.9$ and 19.0 ± 2.5 for WT and NL3-KO respectively, $p = 0.413$, Student's t-test, Fig. 1, B).



mGluR-LTD at the PF-PC synapse in P21-P30 NL3-KO mice. **A**) EPSC amplitude, normalized to baseline, 30min after perfusion of 50 μ M DHPG (*P<0.05, t-test). WT in black, KO in red (averages: filled circles). **B**) Decay time constant of the EPSC, evoked by PF stimulation, at the basal level and 30min after application of 50 μ M DHPG (P=0.074 at the basal level, and P=0.055 at 30min, t-test). WT in black, KO in red.

Cerebellar architecture is the result of a peculiar and clearly defined developmental process. We thus investigated the efficiency of our protocol with younger mice (P21-30). Using the same induction protocol, the perfusion of DHPG did not produce LTD at WT PF-PC synapses ($110 \pm 16\%$, N = 9 cells, Fig. 2, A). On the other hand, KO PF-PC synapses exhibited a distinct reduction of the evoked response ($79 \pm 5\%$, N = 13 cells, $p < 0.05$, Fig. 2, A), in clear opposition to the results obtained with older animals.

Additionally, the analysis of the decay time constant on this second set of experiments revealed a strong but yet not significant difference between the two genotypes ($p = 0.074$ during the baseline and $p = 0.055$, 30 minutes after the perfusion of DHPG, Student's t-test, Fig. 2, B).

Discussion

Our study reveals that in NL3-KO adult mice (2-3 months old), DHPG stimulation doesn't induce a persistent reduction of EPSC amplitude at the PF-PC synapse in the cerebellum, while a clear LTD is observed in WT mice. However, the same experimental protocol produces a clear reduction of the response in NL3 KO young mice (P21-30) but does not affect EPSC amplitude in young WT mice.

Synaptic plasticity is a process described extensively in numerous parts of the brain. It is widely used to probe the role of many proteins in specific neuronal circuitry. Alterations of synaptic plasticity can be due to subtle synaptic disturbances that can occur at several levels. The absence of modulation of the synaptic strength after a stimulation protocol can be due to a blockade of the mechanisms responsible for the modification at the postsynaptic side. Abundant studies prove that any genetic variation affecting one of the main proteins involved in the synaptic machinery (at the structural level and at the level of the molecular cascade triggered by synaptic activity) can affect the physiology of this synapse and thus alter its plastic potential. For the PF-PC synapse, any defect at the level of the post-synaptic molecular cascade involved, as well as at the architectural level, can alter the plastic capabilities of this synapse. If the maturation of the CF is altered, the complex spike (produced by CF stimulation during the pairing protocol) and its accompanying calcium wave can be affected and the variation of internal calcium cannot be sufficient to induce a depression of the synaptic response (Bienenstock et al., 1982, Cooper, 2012). At the molecular level, anything affecting the molecular cascade leading to the phosphorylation and internalization of AMPA-R can disturb the possibilities of synaptic plasticity. Plastic phenomena, notably LTD, can also be occluded when the system is already depressed in its basal state and doesn't allow further reduction of the response.

In the molecular layer of the cerebellum, *nlg3* is present exclusively at the post-synaptic side of the PF-PC synapse. Therefore any mutation or silencing of this protein can alter the physiological properties of this synapse. *mGluR1 α* and *GluA2* are important actors of the PF-PC LTD. The phosphorylation of the *GluA2* subunit of AMPA-R is necessary for their internalization and the reduction of eEPSC at the PF-PC synapse (Chung et al., 2003). In NL3-KO mice, basal levels of Phospho-GluA2

are largely higher than in WT, but upon DHPG stimulation Phospho-GluA2 levels are decreased in KO mice while increased in WT. Also, basal levels of mGluR1 α are increased in NL3-KO mice. Altogether, these findings point out that in NL3-KO mice the PF-PC synapse is already in a depressed state compared to WT synapses, thus limiting the possibility of downward plasticity. Additionally, the inability to induce a decrease of the eEPSC after DHPG stimulation confirms that in NL3-KO adult mice mGluR LTD is occluded.

It is interesting to notice that while DHPG stimulation fails to induce a reduction of the evoked response to PF stimulation in PC of 2-3 months old NL3-KO mice, the same protocol produces a clear decrease of the response in young (three weeks) NL3-KO mice but not in WT mice. These results are unexpected because plasticity is a phenomenon described mostly in young animals and is known to be generally severely reduced in adult life. Calcium is a major actor in any plasticity processes, and its role in these phenomena has been theorized through the so called 'BCM rule'. The BCM theory was developed during the late 1970's by Elie Bienenstock, Leon Cooper and Paul Munro (Bienenstock et al., 1982, Cooper, 2012) and postulates that the direction of plasticity is directed by the amplitude of the intracellular calcium increase. According to this paradigm, a small rise in $[Ca]_i$ will accompany a long-lasting decrease of the response, while a large increase in $[Ca]_i$ will be responsible for a long-term potentiation of the response. This theory has been validated in the cortex and the hippocampus, but it is also known to be inverted in the cerebellum, where a large calcium increase gives rise to an LTD and a small rise leads to an LTP (Jorntell and Hansel, 2006). In 2-3 month old NL3-KO mice, DHPG stimulation tends to increase eEPSC. This reveals that the absence of nlg3 leads to synaptic defects that don't allow a sufficient rise in $[Ca]_i$ to produce a LTD. In young mice, the stimulation with DHPG is powerful enough to induce an LTD in NL3-KO mice but not in WT mice. This indicates that NL3-KO PF-PC synapses are weaker than in WT and that DHPG is capable of inducing an increase in $[Ca]_i$ strong enough to induce LTD in young KO mice. Altogether, these experiments allow us to suggest that in KO mice the synapses are weaker than in WT, regardless of the age, and that WT synapses at 2-3 months are weaker than the same synapse at three weeks.

Put together, our results support that nlg3 has a strong developmental effect on the maturation of the PF-PC synapse. The absence of nlg3 is responsible for the alteration of PF-PC synapses, a process that is developmentally dependent and complete only in adulthood. Furthermore, the altered mGluR1 function in the adult NL3-KO mice, responsible of the occluded mGluR-LTD, is a developmental process not complete until adulthood.

PF-PC LTD is a well-defined and extensively studied plasticity protocol that can also be induced electrically by a pairing PF and CF stimulation (Ito, 2001; but see Safo and Regehr, 2008). The purpose of

this pairing protocol is to produce a large depolarization in the PC due to the CF stimulation. This depolarization and the simultaneous PF stimulation will produce a massive complex spike, a sign that the cell is full of calcium with all the voltage-gated calcium channels open due to the depolarization. The elevated $[Ca]_i$ will stimulate the PKC and then promote the phosphorylation and internalization of AMPA R, leading to a decrease of the eEPSC. The rise in $[Ca]_i$ can also be induced by injecting a depolarizing current pulse into the PC. These protocols are well established and lead to numerous publications. However, certain traits of these protocols are not clear. The timing between the two stimuli, the intensity of stimulation, the age of the animals are amongst the points that are not always clearly specified and make these experiments delicate to reproduce. When pairing a depolarizing pulse and PF stimulation, obtaining a complex spike accompanying the increase in $[Ca]_i$ is not a reliable process, therefore altering the capacity to judge the proper efficacy of the protocol. Defining a reliable electrical LTD protocol, robust enough to induce an LTD in young WT mice, could then allow us to investigate the alteration of the PF-PC synapse on young mice in the absence of *nlg3*. We could thus determine if the occlusion of cerebellar PF-LTD is a feature of *NL3-KO* mice or a developmental process.

During the last year, numerous studies have enlightened the genetic map responsible for ASD. Several studies in major scientific journals have focused on specific genes whose mutations are found in ASDs patients. The study of specific animal models revealed that most of these genes encode for proteins or molecules playing a role at the synaptic level and, more precisely, at the level of the postsynaptic density (Zoghbi and Bear, 2012, Ebert and Greenberg, 2013). Shank proteins are multi-domain scaffolding proteins present at the postsynaptic density and important regulators of the structure and function of excitatory synapses (Kreienkamp, 2008, Hayashi et al., 2009). Rare mutations in *SHANK2* and *SHANK3* genes have been associated with non-syndromic forms of ASD (Berkel et al., 2010). Moreover, a recent study by Won and colleagues (Won et al., 2012) showed that *shank2*-mutant mice exhibit autistic-like behavior and have decreased NMDA function, resulting in impaired long-term plasticity in the hippocampus. Tuberous sclerosis complex (TSC) is one of the main forms of syndromic ASD. It is a genetic disorder due to mutations of either *TSC1* or *TSC2* genes, which negatively regulate mammalian target of rapamycin (mTOR) signaling. The pathway TSC-mTOR plays an important role in neuronal morphology and function and is known to regulate dendritic spine numbers; and it has already been reported that *Tsc 1* protein loss is responsible for altered synaptic properties such as defects in mGluR-LTD in the hippocampus (Tavazoie et al., 2005, Bateup et al., 2011). In addition to social impairment and restrictive behavior, *Tsc 1* mutant mice also have a reduced number of PC in the cerebellum and the excitability of these cells is reduced (Tsai et al., 2012). Taken together amongst other recently published scientific reports, these data highlight that similar deficits can be observed in syndromic and non-

syndromic forms of ASD. They also emphasize the fact that ASD is a multi-gene disease and many factors are responsible for the symptoms observed in the cerebellum and in other brain areas.

Most, if not all, of the proteins that have been linked to ASD play an active role in the formation and/or the maintenance of synapses, therefore being responsible for proper synaptic transmission and maintaining the excitatory/inhibitory balance (E/I) at the network level. It has been hypothesized that some forms of autism are due to an alteration of the E/I ratio in local circuits involved in sensory, social and emotional processing. The resulting hyperexcitability could alter the normal formation of cortical maps of sensory representation, leading to a relatively unstable state (Rubenstein and Merzenich, 2003). This hypothesis is supported by the fact that one third of ASD patients suffer from epileptic seizures (notably those with fragile-X syndrome), a clear sign of a disturbed E/I ratio. The so-called “mini-column” is a typical feature of the cerebral cortical architecture where all the cells within this column (functionally related glutamatergic & gabaergic neurons that together process thalamic inputs) are dedicated to one specific function, such as the barrel cortex where each unit represents the activity of a single whisker. Postmortem analysis of autistic patients’ brains revealed several defects of these micro-columns (Casanova et al., 2002), along with an altered GABAergic function: parietal and cerebellar cortices of autistic patients have a 50% reduction in protein levels of GAD 65 & 67, the enzymes synthesizing GABA (Fatemi et al., 2002). The changes of the GABAergic system observed in ASD patients or in animal models for ASDs point toward a disruption of the E/I equilibrium, which can be responsible for altered cognitive function. Cognitive functions are supported by gamma oscillations (30-80Hz) and are generated by network of parvalbumin-positive (PV) interneurons in the cortex and the hippocampus (Bartos et al., 2007). They provide a temporal structure for information processing in the brain. A study from the laboratory of Takao Hensch (Gogolla et al., 2009) has shown a reduction of PV cells in several ASD mouse models, thus supporting the hypothesis of a disrupted E/I in ASD patients. Moreover, PV cells are responsible for the proper timing of the critical period in sensory development in the different sensory cortices (Hensch, 2005). Any defect of these cells, such as a reduction of GAD enzymes, can lead to an alteration of the correct development of neuronal connections shaped by sensory experience, a phenomenon present in the etiology of cognitive developmental disorders such as ASD. Therefore any deficit in GABAergic function can have a strong impact on sensory processing and cognition (Uhlhaas and Singer, 2007).

Taken together, all the studies published within the last years revealed that ASD is a complex disease with a very strong genetic basis, altering synaptic function at various levels and leading to numerous disabilities for ASD patients. Nonetheless, the identification of the factors responsible for these defects opens the way for targeted therapeutic strategies to counteract and thus rescue the altered physiological function.

References:

- Abrahams BS, Geschwind DH (2008) Advances in autism genetics: on the threshold of a new neurobiology. *Nat Rev Genet* 9:341-355.
- Amaral DG, Schumann CM, Nordahl CW (2008) Neuroanatomy of autism. *Trends Neurosci* 31:137-145.
- Bartos M, Vida I, Jonas P (2007) Synaptic mechanisms of synchronized gamma oscillations in inhibitory interneuron networks. *Nat Rev Neurosci* 8:45-56.
- Bateup HS, Takasaki KT, Saulnier JL, Deneffrio CL, Sabatini BL (2011) Loss of *Tsc1* in vivo impairs hippocampal mGluR-LTD and increases excitatory synaptic function. *J Neurosci* 31:8862-8869.
- Bauman ML, Kemper TL (2005) Neuroanatomic observations of the brain in autism: a review and future directions. *Int J Dev Neurosci* 23:183-187.
- Bear MF, Huber KM, Warren ST (2004) The mGluR theory of fragile X mental retardation. *Trends Neurosci* 27:370-377.
- Berkel S, Marshall CR, Weiss B, Howe J, Roeth R, Moog U, Endris V, Roberts W, Szatmari P, Pinto D, Bonin M, Riess A, Engels H, Sprengel R, Scherer SW, Rappold GA (2010) Mutations in the *SHANK2* synaptic scaffolding gene in autism spectrum disorder and mental retardation. *Nat Genet* 42:489-491.
- Bienenstock EL, Cooper LN, Munro PW (1982) Theory for the development of neuron selectivity: orientation specificity and binocular interaction in visual cortex. *J Neurosci* 2:32-48.
- Budreck EC, Scheiffele P (2007) Neuroligin-3 is a neuronal adhesion protein at GABAergic and glutamatergic synapses. *Eur J Neurosci* 26:1738-1748.
- Caglayan AO (2010) Genetic causes of syndromic and non-syndromic autism. *Dev Med Child Neurol* 52:130-138.
- Casanova MF, Buxhoeveden DP, Switala AE, Roy E (2002) Minicolumnar pathology in autism. *Neurology* 58:428-432.
- Chung HJ, Steinberg JP, Haganir RL, Linden DJ (2003) Requirement of AMPA receptor GluR2 phosphorylation for cerebellar long-term depression. *Science* 300:1751-1755.
- Conquet F, Bashir ZI, Davies CH, Daniel H, Ferraguti F, Bordi F, Franz-Bacon K, Reggiani A, Matarese V, Conde F, et al. (1994) Motor deficit and impairment of synaptic plasticity in mice lacking mGluR1. *Nature* 372:237-243.
- Cooper LNB, M. F. (2012) The BCM theory of synapse modification at 30: interaction of theory with experiment. *Nature Reviews Neuroscience* 13:798-810.
- Ebert DH, Greenberg ME (2013) Activity-dependent neuronal signalling and autism spectrum disorder. *Nature* 493:327-337.

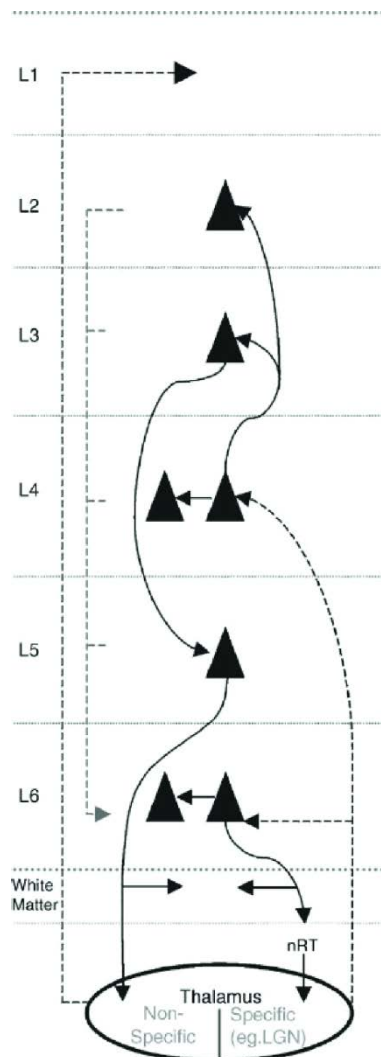
- Fatemi SH, Halt AR, Stary JM, Kanodia R, Schulz SC, Realmuto GR (2002) Glutamic acid decarboxylase 65 and 67 kDa proteins are reduced in autistic parietal and cerebellar cortices. *Biol Psychiatry* 52:805-810.
- Gilman SR, Iossifov I, Levy D, Ronemus M, Wigler M, Vitkup D (2011) Rare de novo variants associated with autism implicate a large functional network of genes involved in formation and function of synapses. *Neuron* 70:898-907.
- Gogolla N, Leblanc JJ, Quast KB, Sudhof TC, Fagiolini M, Hensch TK (2009) Common circuit defect of excitatory-inhibitory balance in mouse models of autism. *J Neurodev Disord* 1:172-181.
- Hansel C, Linden DJ, D'Angelo E (2001) Beyond parallel fiber LTD: the diversity of synaptic and non-synaptic plasticity in the cerebellum. *Nat Neurosci* 4:467-475.
- Hayashi MK, Tang C, Verpelli C, Narayanan R, Stearns MH, Xu RM, Li H, Sala C, Hayashi Y (2009) The postsynaptic density proteins Homer and Shank form a polymeric network structure. *Cell* 137:159-171.
- Hensch TK (2005) Critical period plasticity in local cortical circuits. *Nat Rev Neurosci* 6:877-888.
- Ito M (2001) Cerebellar long-term depression: characterization, signal transduction, and functional roles. *Physiol Rev* 81:1143-1195.
- Ito M (2006) Cerebellar circuitry as a neuronal machine. *Progress in Neurobiology* 78:272-303.
- Jorntell H, Hansel C (2006) Synaptic memories upside down: bidirectional plasticity at cerebellar parallel fiber-Purkinje cell synapses. *Neuron* 52:227-238.
- Kano M, Hashimoto K, Tabata T (2008) Type-1 metabotropic glutamate receptor in cerebellar Purkinje cells: a key molecule responsible for long-term depression, endocannabinoid signalling and synapse elimination. *Philos Trans R Soc Lond B Biol Sci* 363:2173-2186.
- Kreienkamp HJ (2008) Scaffolding proteins at the postsynaptic density: shank as the architectural framework. *Handbook of Experimental Pharmacology* 186:365-380.
- Lamont MG, Weber JT (2012) The role of calcium in synaptic plasticity and motor learning in the cerebellar cortex. *Neurosci Biobehav Rev* 36:1153-1162.
- Luscher C, Huber KM (2010) Group 1 mGluR-dependent synaptic long-term depression: mechanisms and implications for circuitry and disease. *Neuron* 65:445-459.
- Missler M, Sudhof TC, Biederer T (2012) Synaptic cell adhesion. *Cold Spring Harb Perspect Biol* 4:a005694.
- Missler M, Zhang W, Rohlmann A, Kattenstroth G, Hammer RE, Gottmann K, Sudhof TC (2003) Alpha-neurexins couple Ca²⁺ channels to synaptic vesicle exocytosis. *Nature* 423:939-948.
- Mostofsky SH, Powell SK, Simmonds DJ, Goldberg MC, Caffo B, Pekar JJ (2009) Decreased connectivity and cerebellar activity in autism during motor task performance. *Brain* 132:2413-2425.

- Radyushkin K, Hammerschmidt K, Boretius S, Varoquaux F, El-Kordi A, Ronnenberg A, Winter D, Frahm J, Fischer J, Brose N, Ehrenreich H (2009) Neuroligin-3-deficient mice: model of a monogenic heritable form of autism with an olfactory deficit. *Genes Brain Behav* 8:416-425.
- Rubenstein JL, Merzenich MM (2003) Model of autism: increased ratio of excitation/inhibition in key neural systems. *Genes Brain Behav* 2:255-267.
- Safo P, Regehr WG (2008) Timing dependence of the induction of cerebellar LTD. *Neuropharmacology* 54:213-218.
- Santos SD, Carvalho AL, Caldeira MV, Duarte CB (2009) Regulation of AMPA receptors and synaptic plasticity. *Neuroscience* 158:105-125.
- Sillitoe RV, Joyner AL (2007) Morphology, molecular codes, and circuitry produce the three-dimensional complexity of the cerebellum. *Annu Rev Cell Dev Biol* 23:549-577.
- Strick PL, Dum RP, Fiez JA (2009) Cerebellum and nonmotor function. *Annual Review of Neuroscience* 32:413-434.
- Sudhof TC (2008) Neuroligins and neurexins link synaptic function to cognitive disease. *Nature* 455:903-911.
- Tabuchi K, Blundell J, Etherton MR, Hammer RE, Liu X, Powell CM, Sudhof TC (2007) A neuroligin-3 mutation implicated in autism increases inhibitory synaptic transmission in mice. *Science* 318:71-76.
- Tanaka KF, Ahmari SE, Leonardo ED, Richardson-Jones JW, Budreck EC, Scheiffele P, Sugio S, Inamura N, Ikenaka K, Hen R (2010) Flexible Accelerated STOP Tetracycline Operator-knockin (FAST): a versatile and efficient new gene modulating system. *Biol Psychiatry* 67:770-773.
- Tavazoie SF, Alvarez VA, Ridenour DA, Kwiatkowski DJ, Sabatini BL (2005) Regulation of neuronal morphology and function by the tumor suppressors Tsc1 and Tsc2. *Nat Neurosci* 8:1727-1734.
- Tsai PT, Hull C, Chu Y, Greene-Colozzi E, Sadowski AR, Leech JM, Steinberg J, Crawley JN, Regehr WG, Sahin M (2012) Autistic-like behaviour and cerebellar dysfunction in Purkinje cell Tsc1 mutant mice. *Nature* 488:647-651.
- Uhlhaas PJ, Singer W (2007) What do disturbances in neural synchrony tell us about autism. *Biol Psychiatry* 62:190-191.
- Varoquaux F, Aramuni G, Rawson RL, Mohrmann R, Missler M, Gottmann K, Zhang W, Sudhof TC, Brose N (2006) Neuroligins determine synapse maturation and function. *Neuron* 51:741-754.
- Watanabe M, Kano M (2011) Climbing fiber synapse elimination in cerebellar Purkinje cells. *Eur J Neurosci* 34:1697-1710.
- Won H, Lee HR, Gee HY, Mah W, Kim JI, Lee J, Ha S, Chung C, Jung ES, Cho YS, Park SG, Lee JS, Lee K, Kim D, Bae YC, Kaang BK, Lee MG, Kim E (2012) Autistic-like social behaviour in Shank2-mutant mice improved by restoring NMDA receptor function. *Nature* 486:261-265.
- Zoghbi HY, Bear MF (2012) Synaptic dysfunction in neurodevelopmental disorders associated with autism and intellectual disabilities. *Cold Spring Harb Perspect Biol* 4.

Chapter 3: Variations of action potential backpropagation and spike-timing dependent plasticity in the mouse primary visual cortex, during the critical period.

Intro

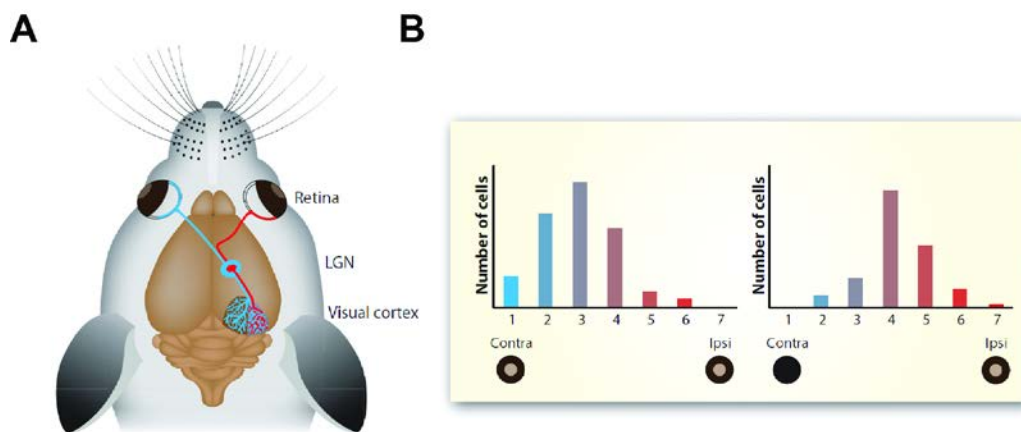
Divided into numerous areas according to their function, the neocortex is the largest part of the brain, and its cytoarchitecture is highly preserved amongst mammals. The cerebral cortex is mainly composed of two types of neurons: glutamatergic/excitatory neurons ($\approx 80\%$) and GABAergic/inhibitory neurons ($\approx 20\%$), organized in 6 different layers according to their morphology, connections and functions. This laminar architecture is found in all neocortical areas and is also responsible for a perfectly defined pattern of connections between cells from the same and from different layers. For sensory cortices, inputs arise from the corresponding thalamic nuclei and make connections on excitatory neurons in layer 4. The information is then relayed forward to layer 2/3, which is more superficial, for the second stage of cortical processing and afterwards sent to the deeper layers 5 and 6 from where the information will be sent to other cortical or subcortical structures (Gilbert, 1993, Bannister, 2005, detailed in box 1). For the visual system, inputs from the retina are relayed in the thalamic lateral geniculate nuclei and then forwarded to the primary visual cortex (V1), located in the occipital part of the brain, where they exhibit a retinotopic organization as well as a variable binocularity, depending on the species considered. Information is then processed and further transferred to several higher visual areas, such as the secondary visual cortex and the posteromedial cortex.



Box 1: Classical pattern of cellular connections in sensory cortices (adapted from Bannister, Neuroscience Research 2005). Inputs arising from thalamic nuclei are integrated in layer 4 and then forwarded to layer 2/3 for integration. The information is then transmitted to layer 5, which will send it to subcortical structures, as well as other cortical areas.

In sensory cortices, sensory inputs drive neuronal activity. In the barrel cortex of rodents, activity is triggered by whisker deflection. In V1, neurons are tuned to respond to specific features of a visual scene, such as the position, orientation or direction of motion of a given stimulus (Wiesel and Hubel, 1963, Rochefort et al., 2011). Under experimental conditions, cell firing can be activated by the presentation of a drifting grating with specific orientation and direction. In the neocortex, cells processing similar or related stimuli are highly interconnected. In non-rodent mammals, cells sharing similar orientation direction selectivity are localized in a columnar organization through the different layers (Ohki et al., 2005). Found across species in sensory cortices, the columnar organization is an important feature

of the cerebral cortex, both at the architectural and at the functional level (Defelipe et al., 2012). This emblematic structure has been studied at length in the barrel field of the primary somatosensory cortex (S1) of rodents. This highly specified cortical area presents a precise somatotopic map where inputs from a single whisker activate cells in a precisely defined columnar structure: the barrel (Petersen, 2007). In the rodent visual system, cells with similar orientation direction selectivity don't exhibit columnar organization but are spread, in a "salt-and-pepper" manner (Ohki et al., 2005, Ohki and Reid, 2007). Nevertheless, several studies revealed that cells with similar orientation direction selectivity have a higher probability of connection (Ko et al., 2011) and form subnetworks devoted to the processing of related sensory information.



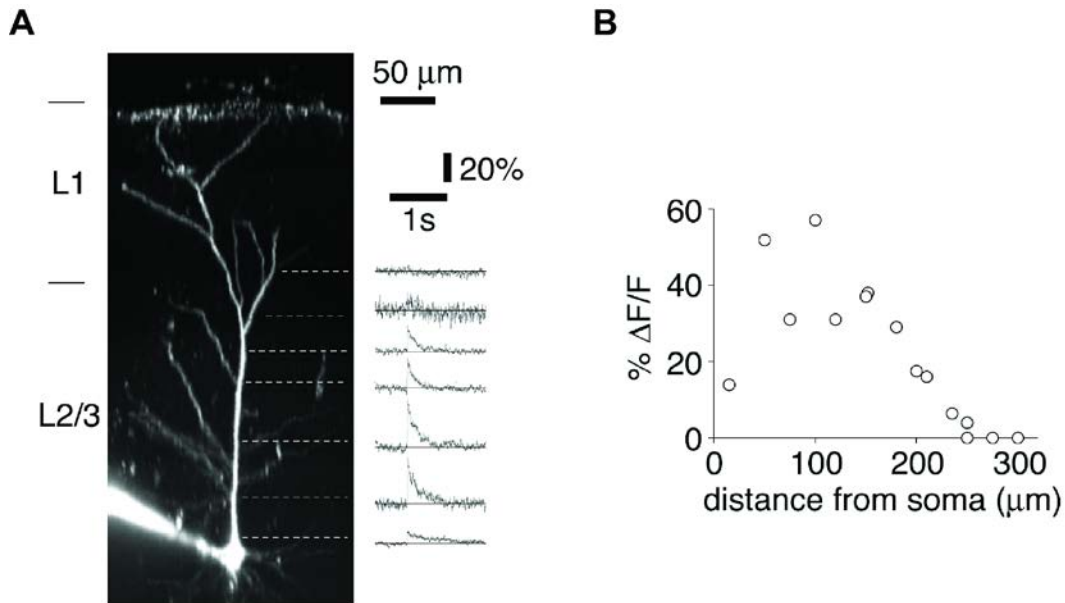
Box 2: Ocular Dominance (OD) plasticity in the mouse visual cortex (adapted from Levelt & Hubener, AnnuReviewNeurosci 2012). A) Schematic of the mouse visual system. The primary visual cortex receives inputs from both eyes via a relay in the thalamic lateral geniculate nuclei (LGN). B) Typical example of OD plasticity occurring during the critical period: due to the visual deprivation of the contralateral eye, inputs arising from this eye are progressively replaced by inputs coming from the ipsilateral eye.

During development, the bulk of the refinement of neuronal connections occurs during a special period of enhanced experience-dependent plasticity. This 'critical period of plasticity' occurs in all sensory cortices but has been extensively studied in V1, notably because of its precisely defined timing (P19 to P32 in mice, Gordon and Stryker, 1996). In V1, this period is also defined by ocular dominance plasticity, described as the ability of monocular deprivation to induce a shift in ocular dominance. Therefore during the critical period, a brief (few days) period of monocular deprivation will cause a rapid loss of response to the deprived eye, accompanied by a gain in response by the open eye (Box 2, for detailed reviews, see Hensch, 2005, Levelt and Hubener, 2012). The monocular deprivation period is then responsible for strengthening the inputs from the open eye at the expense of those from the deprived eye. Numerous factors are involved in this complex plastic process and in its precise timing. The timing of the critical period is highly correlated with the development of the network of GABAergic parvalbumin

positive interneurons (Hensch et al., 1998, reviewed in Sale et al., 2010) and with the developmental change in GABA_AR subunit composition to mostly $\alpha 1$ subunit containing GABA_AR. In addition, the timing of the critical period is sensitive to changes in the inhibitory system, and these changes are exclusively mediated by $\alpha 1$ subunit containing GABA_AR (Fagiolini et al., 2004). Thus any alteration of the maturation of the inhibitory transmission will most likely disturb the timing of the critical period in consequence. Appropriate levels of BDNF (Huang et al., 1999) and normal development of perineuronal nets (Beurdeley et al., 2012), dense structures of the extracellular matrix, are also essential elements for establishing the correct time-window of the critical period. During development, V1 is thus a highly plastic structure allowing a precise refinement of the connection for a proper processing of the visual information.

Presented as the substrate of learning and memory, plasticity is a physiological process that allows a rapid change in synapse strength in response to experience and use. Plasticity is present in the brain in many forms and at numerous synapses. In V1, long-term potentiation (LTP) and depression (LTD) have been proposed to underlie the modifications in ocular dominance observed during the critical period (Smith et al., 2009). Amongst the multiple forms of plasticity observed in the cortex, spike-timing dependent plasticity (STDP) has been thought to play an important role in the adaptation of cortical connectivity to the flow of inputs neurons receive. STDP relies on the coincidence detection of backpropagating action potentials (bAP) and synaptic inputs. Initiated at the axon initial segment, action potentials (AP) propagate through the axon but also backpropagate into the dendritic arborization (Box 3). Dendrites are the main recipients for synaptic inputs. Their compartmentalization and their thin and complex architecture allow and support dendritic signal integration that is crucial for information processing in the brain (Larkum and Nevian, 2008, Major et al., 2013). Dendrites are active compartments that contain many voltage-gated conductances, notably Na⁺ and Ca²⁺ channels. These conductances support action potentials, generated at the axon initial segment, in backpropagating through basal and apical dendrites. The bAP is thus a retrograde signaling mechanism that reports spike output to dendrites, promotes dendritic Ca²⁺ influx, and thereby enables plasticity based on the coincidence of APs and synaptic inputs (Sjostrom and Nelson, 2002). bAPs have been extensively studied in layer 5 cortical pyramidal cells, along their extensive apical dendrites. These studies revealed that APs can propagate back into the dendritic tree, supported by Na⁺ conductances, and generate a concomitant Ca²⁺ wave via voltage gated calcium channels (VGCC) and NMDA receptors. bAPs characteristics vary according to the dendritic architecture, ion channel distribution and type of the cell studied. The study of bAPs in layer 5 pyramidal cells allowed the identification of dendritic “hotspots” containing a large number of VGCCs and located on the apical dendrite at the level of the tuft (Larkum et al., 2009), highlighting another

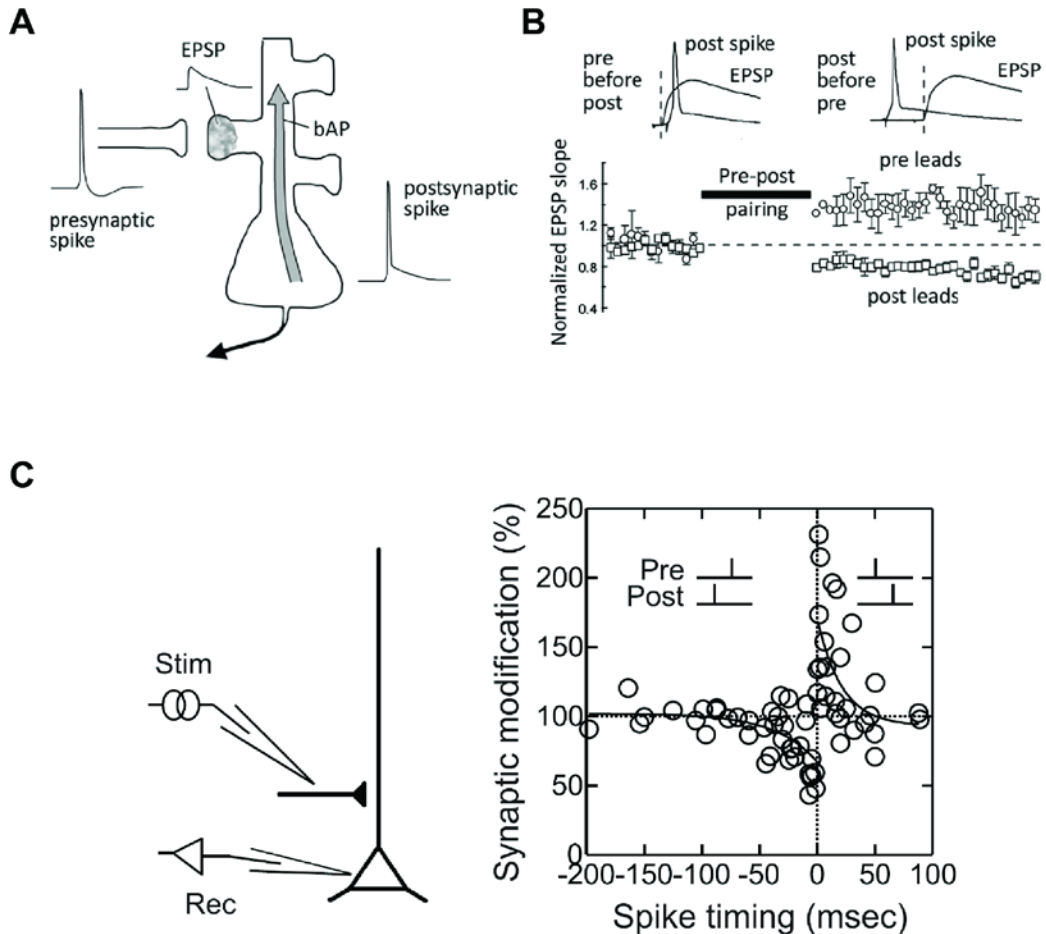
important role for Ca^{2+} signaling in neuronal physiology. bAPs have been identified in vitro and in vivo and serve as an input/output coincidence detector for the cell.



Box 3: Back-propagating Action Potentials in layer 2/3 of the somatosensory cortex. (Adapted from Waters et al JNeuroscience 2003). **A)** Examples of calcium transients evoked by a somatic AP, at different level of the apical dendrite, measured in vivo. **B)** Average values of the fluorescence of the calcium transient evoked by a somatic AP compared to the measured site along the apical dendrite. The fluorescence associated with the calcium transient increases to a peak at around 100 μm from the soma, then slowly decreases towards the tuft of the apical dendrite.

bAPs are also of crucial importance for STDP. In 1949, Donald Hebb postulated that persistent activation of a postsynaptic neuron by a presynaptic input should lead to a strengthening of the connection between these two cells: “what fires together wires together” (Hebb, 1949). It has since been demonstrated that the timing between the presynaptic EPSP and the postsynaptic spike determines the direction of the long-term change induced by the pairing (Markram et al., 1997, detailed in box 4). It’s a synaptic learning rule for encoding learning and memory that relies on the relative timing of neuronal activity on either side of the synapse (for a detailed review, see Feldman, 2012). STDP is a powerful means of forming and modifying neuronal circuits and has been found at many synapses throughout the brain. The magnitude and the temporal efficacy of the pairing protocol also depends on the frequency of the bAPs (Froemke and Dan, 2002) and varies along the apical dendrite (Froemke et al., 2005). NMDA receptors play a key role in the induction of many forms of synaptic plasticity. In STDP, it has been shown that the slow Mg^{2+} unblock of NMDAR channels by bAPs makes the time-window more precise (Kampa et al., 2004).

Furthermore, STDP is regulated by inhibition (reviewed in Lamsa et al., 2010) and neuromodulators (Pawlak et al., 2010).



Box 4: bAP and STDP are tightly linked together (Adapted from Feldman, Neuron 2012, and Froemke et al., Frontiers in Synaptic Neuroscience 2010). **A**) Schematic representation of the STDP protocol, in which a presynaptic EPSP is paired with a postsynaptic spike, backpropagating through the apical dendrite. **B**) Typical experiment of STDP. The timing between the presynaptic EPSP and the postsynaptic spike, during the pairing, determines the direction and the magnitude of the long-term change induced by the pairing. **C**) Average values of the long-term change induced by the pairing protocol, according to the timing between the presynaptic EPSP and the postsynaptic spike. This is a classic example of Hebbian plasticity, where a positive timing, between the pre- and the postsynaptic spike respectively, leads to a long-term increase of the response, and a negative timing leads to a long-term decrease of the response.

bAP and STDP are two tightly linked phenomena that have been identified *in vivo* and *in vitro*. They have mostly been studied in layer 5 pyramidal cells because their long apical dendrites are

particularly suited to investigating the influence of dendrites and their active conductances on these processes. However several studies have also emphasized STDP in layer 2/3 pyramidal cells. These cells are known as the second stage of cortical processing and play an important role in cortico-cortical connections (Petersen and Crochet, 2013). In the mouse V1, their spiking activity and concomitant Ca^{2+} signal are driven by visual inputs. They display precise orientation selectivity and form strongly connected subnetworks according to their orientation preferences. We therefore decided to investigate bAPs and STDP in V1 layer 2/3 pyramidal cells during the critical period. We wanted to determine if these two cellular processes were subject to any modifications between several time points of the critical period: at P19 just before the start; at P25, at the ‘peak’ of plasticity; and at P32, at the end of the critical period.

Materials & Methods

Animals. Wild-Type mice [pure C57BL/6 background], of postnatal day (P) 19-32 were used in this study. All animal experiments were performed according to the guidelines of the Veterinary Office of the Kanton of Basel-Stadt, Switzerland, and approved by its Commission for Animal Research. All efforts were made to minimize animal suffering and to reduce the number of animals required. Mice had free access to a standard laboratory diet and water and were maintained on a 12 h light/dark cycle.

Electrophysiology. For the preparation of visual cortex slices, animals were deeply anesthetized by Isoflurane® inhalation and decapitated after loss of the hindpaw withdrawal reflex. The brain was quickly removed and placed in ice-cold ACSF containing (in mM): 125 NaCl, 2.5 KCl, 1 MgCl_2 , 2 CaCl_2 , 1 NaH_2PO_4 , 20 glucose, 26 NaHCO_3 , equilibrated with 95% O_2 and 5% CO_2 . Frontal slices, 250 μm thick, were obtained using a vibrating blade microtome (Leica VT1200S, Leica Microsystems Switzerland). Slices were placed in room temperature ACSF to recover for one hour, then placed in the recording chamber of an upright microscope (Olympus BX51WI, Olympus Switzerland) equipped with a 20x lens (Olympus LUMPLAN 20x, Olympus Switzerland) and superfused with room temperature ACSF at a rate of 1 ml/min, equilibrated with 95% O_2 and 5% CO_2 . Slices were illuminated using a custom-built IR LED system. Neurons in the primary visual cortex were visualized using Nomarski interference contrast and the images captured with an IR-sensitive video camera (VX55, Till Photonics GmbH, Gräfelfing, Germany). Layer 2/3 pyramidal cells were identified by their position in the slice and their pyramidal somata. Whole-cell patch-clamp recordings (pipette resistance = 3-5 $\text{M}\Omega$) were performed using a solution containing (in mM): 130 K-Gluconate, 10 Tris-Phosphocreatine, 30 HEPES, 4 Mg-ATP, 0.3 Na-GTP, 5 KCl, pH 7.28 adjusted with NaOH, Osmolarity: 296 mOsm.

Back-propagating Action Potential. 100 μM of Oregon Green 488 BAPTA-1 (Invitrogen, Carlsbad, CA) was added to the internal solution for Ca^{2+} imaging of the bAP. 25 μM of Alexa 594 (Invitrogen, Carlsbad, CA) was also added to the internal solution for visualization of the dendritic tree. Dyes were allowed to fill the neurons for at least 15-20 min before Ca^{2+} signals were measured. Dendritic Ca^{2+} transients were induced by bAPs evoked with somatic current injections: 4 square pulses (2 nA, 2 ms long) at 125 Hz. Ca^{2+} transients were recorded with a two-photon scanning system ($\lambda = 845 \text{ nm}$) in a line-scan mode with a temporal resolution of 800 Hz. A delay of 1.5-2 min was observed between each trial. Ca^{2+} transients were recorded at several levels of the dendritic tree. Ca^{2+} transients are reported as relative changes in OGB-1 fluorescence and were calculated as $F(t)=F(t)/F_0$, where F_0 is the baseline fluorescence, measured within 200 ms before the stimulation. Cells were excluded when the resting membrane potential changed $> 10\%$ over the entire protocol. Data points were reduced to 100 Hz and analyzed offline using Igor Pro and ImageJ. Fluorescence traces are averages of three to five trials and group data are presented as means \pm SEM. The peak of the Ca^{2+} /spike was analyzed as an average of the fluorescence intensity between 30 and 50 ms after the bAP induction. At the end of each experiment, the cell was imaged for a 3D reconstruction and to verify its localization and the intactness of the dendritic tree.

Spike-Timing Dependent Plasticity. 50 μM of Alexa 594 (Invitrogen, Carlsbad, CA) was added to the internal solution to allow a 3D reconstruction and to verify the cell's localization and the intactness of its dendritic tree. A stimulus pipette (resistance = 1 $\text{M}\Omega$), filled with ACSF, was placed in the vicinity of the apical dendrite, at 50-70 μm from the soma. Extracellular stimuli (100 μs , 10-20 μA) were generated by a stable IS4 stimulator (Sc-Devices, Switzerland) and were adjusted to evoke baseline single-component EPSPs with an amplitude between 3 and 5 mV. Baseline EPSPs were recorded for 10 min at 0.05 Hz. EPSPs were then paired with a train of three APs (evoked by somatic square pulses of 1.5-2 nA) at 50 Hz, 60 times at 0.1 Hz, starting at 10 ms after the onset of the EPSPs. The change in EPSP amplitude was evaluated 30 min after the end of the pairing period and normalized to the baseline EPSP amplitude. Cells were excluded if the input resistance changed $> 20\%$ over the entire experiment.

Statistical Analysis. All data are shown as mean \pm SEM. One-way ANOVA was used when comparing three different conditions, with a Tukey multiple comparison Post Hoc test. Student's paired t test was used when comparing two data sets. Statistical significance was reached at $p < 0.05$.

Results

We examined the effect of bAPs on Ca^{2+} signals in the apical dendrites of layer 2/3 pyramidal cells in the mouse V1. Morphologically identified layer 2/3 pyramidal cells were patched and kept in current clamp mode throughout the protocol. We induced a train of 4 APs at 125 Hz at the soma and used two-photon dendritic calcium imaging techniques to measure the Ca^{2+} transients accompanying the bAPs at several key spots of the dendritic tree: at the start of the apical dendrite, before the split of the apical dendrite into two main branches (the dendritic “hot-spot”), and occasionally further away in the distal branches of the apical dendrite (fig 1A). We performed these experiments on WT mice at several time-points of the critical period: P19, P25 and P32. At the start of the apical dendrite, the average fluorescence signal observed at the three different ages did not reveal any significant differences (fig 1B1-2; $p > 0.5$): the amplitude of the Ca^{2+} signal induced by bAPs did not vary across the critical period. At the level of the split of the apical dendrites into two main branches, generally located 50 to 100 μm from the soma, the Ca^{2+} signal accompanying bAPs was higher at P32 (2.74 ± 0.24 , $n = 6$; fig 1,C1-2) than at P19 and P25 (2.3 ± 0.24 , $n = 8$; and 2.33 ± 0.17 , $n = 10$, respectively), but this marked trend was not statistically significant ($p < 0.5$). Also, the increase in Ca^{2+} transients observed between the start of the apical dendrite and the dendritic bifurcation didn't show any significant differences (P19, $p = 0.49$; P25, $p = 0.74$; fig 1,D) despite a trend of increase at P32 ($p < 0.15$). Altogether, our results revealed that the Ca^{2+} signal induced by a train of bAPs in the apical dendrite does not vary significantly across the critical period.

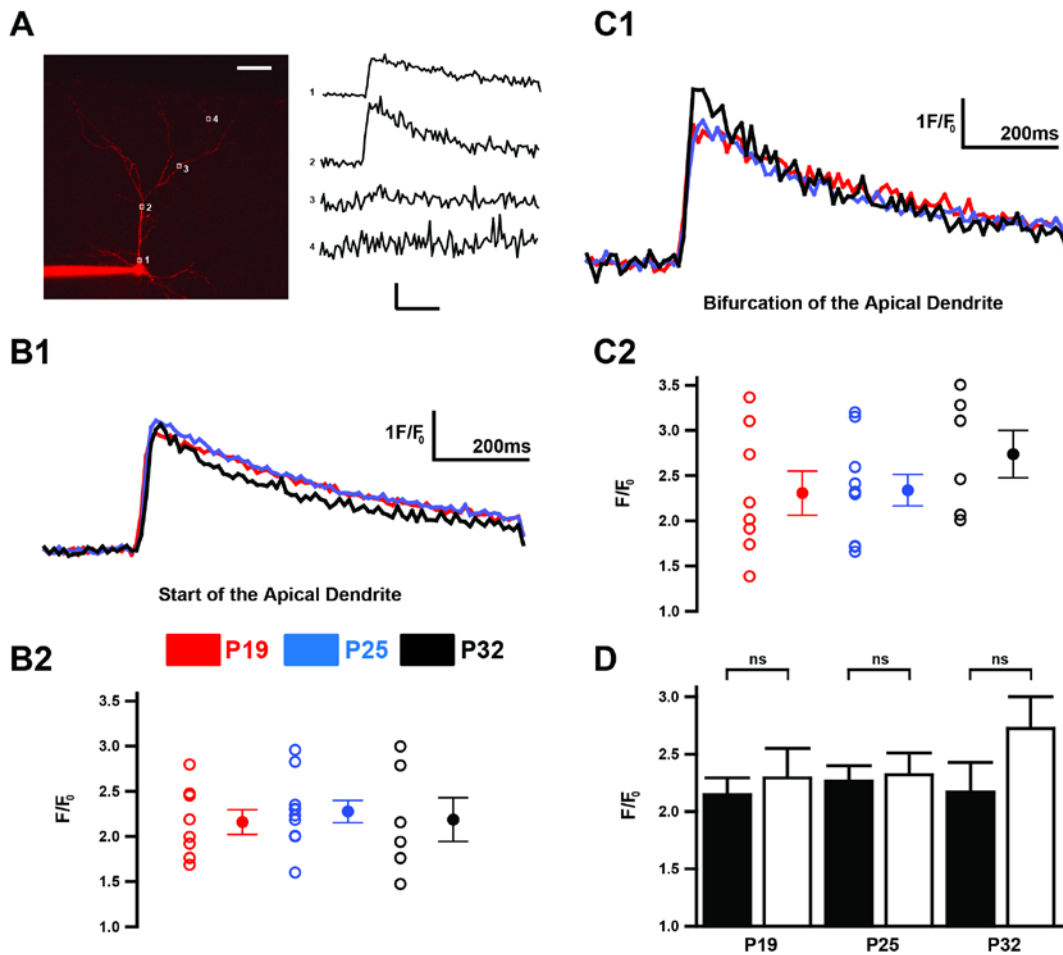


Figure 1: Variations of the calcium signal concomitant to bAPs in layer 2/3 pyramidal cells in the mouse primary visual cortex. **A)** Confocal image of a Layer 2/3 pyramidal cell, filled with 100 μ M OGB1 + 25 μ M red Alexa 594. A train of 4 APs at 125 Hz is evoked at the soma, and the calcium signal accompanying the bAPs is measured at four levels on the dendritic tree, indicated by the four small white boxes. **B1)** Average calcium signal at the start of the apical dendrite, at three different time points of the critical period: P19 (in red), P25 (in blue) and P32 (in black). **B2)** Average and individual values for the peak calcium signal at the start of the apical dendrite, at three different time points of the critical period. $p = 0.84$. **C1)** Average calcium signal at the bifurcation of the apical dendrite, at three different time points of the critical period. **C2)** Average and individual values for the peak calcium signal at the bifurcation of the apical dendrite. $p = 0.38$. **D)** Comparison of the peak calcium signals at the start of the apical dendrite and at its bifurcation, at three different time points of the critical period (at P19, $p = 0.49$; at P25, $p = 0.74$; at P32, $p = 0.14$).

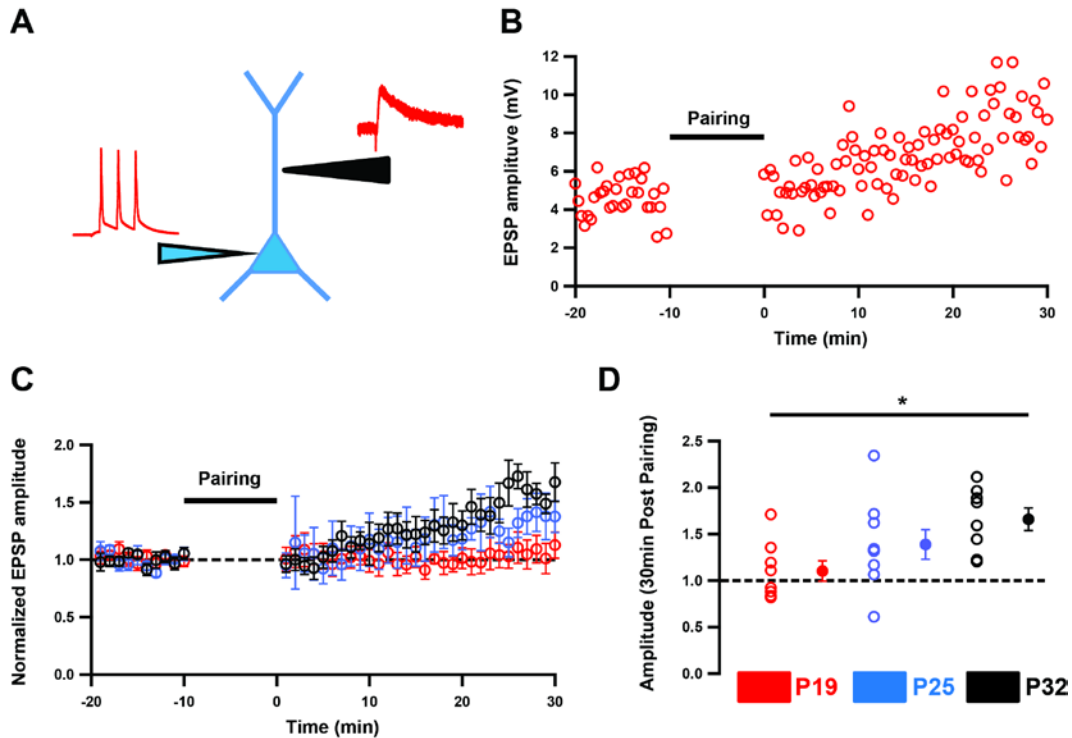


Figure 2: Variation of the STDP in layer 2/3 pyramidal cells of the mouse visual cortex during the critical period. **A)** Schematic representation of the pipettes disposition for the STDP pairing protocol. The blue pipette records the presynaptic spike, evoked by the stimulation pipette (in black). **B)** Representative experiment. An EPSP is produced by extracellular stimulation. For the pairing protocol, the EPSP is paired with a train of three APs at 50 Hz, at +10ms. Values are normalized to baseline. **C)** Average EPSP amplitude before and after the pairing protocol, at three different time points of the critical period: P19 (red), P25 (blue) and P32 (black). Data are normalized to baseline. **D)** Average values of EPSP amplitude 30 min after the pairing protocol, at 3 different time points of the critical period. $p = 0.032$.

We then focused on the STDP in layer 2/3 pyramidal cells: we wanted to test if there was a timing dependence for pairing a single EPSP that was elicited by extracellular stimulation with a somatic burst of three APs. The stimulus electrode was placed $\approx 50 \mu\text{m}$ from the soma, near the apical dendrite (fig 2, A). During the pairing, a train of three APs at 50 Hz was paired at +10 ms with the EPSP. This experiment was performed at the same three time-points of the critical period, P19, P25 and P32. This specific pairing protocol induced significantly different responses at the three different ages (fig 2, C, D; measured 30 min after the pairing: $p < 0.05$). At P19, the pairing protocol barely changed the amplitude of the response to the extracellular stimulation (1.1 ± 0.11 , $n = 8$, at 30 min, normalized to baseline), while the pairing protocol was responsible for a small, but clearly detectable, increase and a large increase in the EPSP at P25 and P32, respectively, (P25: 1.39 ± 0.16 , $n = 9$; P32: 1.66 ± 0.12 , $n = 8$). Therefore, we concluded that this specific pairing protocol, performed on the apical dendrite of V1 layer 2/3 pyramidal cells in the vicinity of the soma, produced a varying response according to the time-point of the critical period at which the experiments was performed.

Discussion

The visual cortex is a part of the brain that has been extensively studied both because of its ability to record and image neuronal activation upon clearly defined sensory inputs but also because of its peculiar plastic time-window. In the present study, we show that Ca^{2+} transients induced by bAPs in the apical dendrite of layer 2/3 pyramidal cells don't vary significantly during the critical period, despite a trend pointing towards an increase at the end of the critical period. In addition, we show that when a presynaptic EPSP and a postsynaptic burst are paired with a positive timing, the amplitude of the response observed in the postsynaptic neuron increases along with the animals' progress through the critical period.

bAPs are of major importance for the physiology of the cell and the postsynaptic element of neuronal coincidence detection, at the level of the dendritic tree. In layer 2/3 pyramidal cells, backpropagation of APs is actively supported by Na^+ channels and produces a concomitant Ca^{2+} influx (Waters et al., 2003). This increase in Ca^{2+} is supported by VGCCs and by NMDA receptors, whose Mg^{2+} block is removed by the backpropagating depolarization. The increased amplitude of the Ca^{2+} spike at the bifurcation of the apical dendrite, compared to that at the start of the apical dendrite, suggests the existence of a dendritic "hotspot" with a high density of VGCC, similar to what has been demonstrated in layer 5 pyramidal neurons (Larkum et al., 2009). The presence and distribution of VGCCs over the dendritic tree vary during development. In S1 layer 5 pyramidal neurons, Ca^{2+} evoked by Na^+ spikes can only be recorded in the apical tuft after P28 (Zhu, 2000). Despite the lack of statistically significant differences, our study reveals a manifest trend towards an increase in the Ca^{2+} transients associated with bAPs as we progress through the timing of the critical period. A developmental change in Ca^{2+} channel subtypes has been observed in the apical dendrite of CA1 pyramidal neurons (Magee and Johnston, 1995). It would thus be of major interest to pharmacologically determine the presence, possible variations and implication of diverse VGCCs, notably L- and T-type VGCCs, in AP back-propagation during the critical period.

The amplitude of the dendritic Ca^{2+} spike induced by bAPs strongly depends on the internal frequency of the train of APs and the number of APs present in the train evoked at the soma. A recent study by Grewe and colleagues (Grewe et al., 2010) in rat S1 layer 5A pyramidal cells revealed that both the critical frequency (Cf) enabling dendritic spikes and the concomitant dendritic Ca^{2+} influx vary during development. In rat S1 layer 2/3 pyramidal cells, the critical frequency is $\approx 130\text{Hz}$ (Larkum et al., 2007). In our experimental paradigm, we somatically evoke a train of 4 APs at 125Hz, which is above the Cf for layer 2/3 pyramidal neurons in V1 (data not shown). A precise investigation of the Cfs in layer 2/3

pyramidal cells across the critical period would be important to determine the optimal frequency to induce dendritic spikes and reveal if this parameter is subject to modifications as the visual cortex matures.

The maturation of the inhibitory system, notably parvalbumin positive interneurons, exerts a fundamental control over the timing of the critical period and the regulation of experience-dependent plasticity (Hensch et al., 1998). Interneurons regulate neuronal activity and can thus impact the backpropagation of APs into the dendritic arborization. In CA1 pyramidal neurons, inhibition reduces the amplitude of Na^+ and CA^{2+} spikes in distal dendrites (Tsubokawa and Ross, 1996). Several factors, such as the level of BDNF and the development of perineuronal nets, control the proper development of the inhibitory network. Parvalbumin positive interneurons make synaptic contacts on the somata and proximal dendrites of pyramidal neurons and can therefore affect the initiation of bAPs. During the critical period, the maturation of GABAergic transmission is accompanied by a shift in the subunit composition of $\text{GABA}_{\text{A}}\text{R}$, from $\alpha 2$ to $\alpha 1$ subunit, which is responsible for a faster GABAergic transmission (Chen et al., 2001). It would be of major interest to test how the maturation of the inhibitory system, and especially the evolution of transmission kinetics, can affect bAPs initiation and propagation in layer 2/3 pyramidal neurons.

Endocannabinoids are important modulators of synaptic transmission and synaptic plasticity. In the cortex, the highest levels of type 1 cannabinoid receptor (CB1) are found in layer 2/3, where their main effect is to suppress GABA release. In S1 layer 2/3 pyramidal cells, the activation of CB1 receptors induces an increase of the calcium transients associated with bAPs via suppression of GABAergic transmission (Hsieh and Levine, 2013). It would be interesting to test how endocannabinoids affect bAPs in V1 during the critical period and if this effect is dependent on the maturation of the inhibitory network.

bAP is thus a complex phenomenon of major importance to the cell physiology, where it plays a crucial role in plasticity, dendritic integration and neuronal output. bAP is also tightly linked to STDP, where its relative timing, paired with the presynaptic EPSP, will determine the direction and magnitude of the postsynaptic change. STDP has been extensively studied in sensory systems (reviewed in Larsen et al., 2010). These studies revealed that the internal frequency of the train of APs is as important as the timing between the pre- and the postsynaptic spike for the direction and the magnitude of the change of the postsynaptic response. The pairing protocol we chose has been used to evoke STDP at basal dendrites of S1 layer 2/3 pyramidal cells in very young (P13-15) rats (Nevian and Sakmann, 2006). It allows us to obtain a reliable increase in the evoked EPSP at all three ages of the critical period. It remains to test if other pairing protocols, with a different timing and/or the elicitation of a different train of APs, would result in a more pronounced difference across the three ages of the critical period. STDP is considered as “Hebbian plasticity” when LTP is induced by a presynaptic spike preceding the postsynaptic spike, and

LTD is induced by a postsynaptic spike preceding the presynaptic spike. Nonetheless, this model can be biased or subject to variations during development. In S1 layer 2/3 pyramidal cells, STDP properties shift towards a more classical bidirectional “Hebbian” plasticity after P13-15 (Itami and Kimura, 2012), a time when whisker response is established. This timing is classically considered as the critical period in S1. In this study, the authors pair the presynaptic spike with a single postsynaptic spike, as opposed to our protocol. It would thus be of major interest to test if a clear bidirectional “Hebbian” plasticity can be obtained at different timings of the critical period or if, early on during this period, we would observe LTP regardless of the order of the pre- and postsynaptic spike, similar to what is observed in S1 before P13-15. We would also need to test if the same results can be obtained with either a single postsynaptic spike or a postsynaptic burst.

Inhibition plays a major role in the experience-dependent plasticity observed in the visual cortex and has also been shown to regulate bAPs and spike output. A recent study also revealed that in the striatum, GABAergic circuits exert an important control over STDP polarity. In V1, interneurons are broadly tuned for orientation selectivity (Jia et al., 2010). This suggests that they receive numerous contacts from pyramidal cells presenting various orientation direction selectivity, thus belonging to several specific subnetworks (Ko et al., 2011). The link provided by interneurons between these subnetworks could allow a fine control of the integration of sensory inputs from different orientations, notably via a temporal control over STDP on these cells. During the critical period, the changes that can be observed during the maturation of the inhibitory network, as well as the stabilization of this network by perineuronal nets, allow a complete refinement and stabilization of neuronal connections. These improvements in connectivity are responsible for the appropriate regulation of neurons’ output processing, observed at the end of the critical period.

In addition to the control from the GABAergic network, STDP is also under the control of several neuromodulatory systems (for a detailed review, see Pawlak et al., 2010). In V1 layer 2/3 pyramidal cells, the activation of neuromodulator receptors coupled to adenylate cyclase and phospholipase C influence the polarity of STDP (Seol et al., 2007). BDNF is a growth factor involved in neuronal development as well as plasticity (reviewed in Gottmann et al., 2009). BDNF is released in an activity-dependent manner and affects GABAergic maturation, notably the establishment of the dendrites (Rauskolb et al., 2010). Early postnatal overexpression of BDNF leads to an early time-course for the critical period (Hanover et al., 1999). BDNF thus appears as an important factor supporting the complex phenomena occurring during the critical period. Its implication in synaptic scaling and its activity-dependent release suggest a role in the regulation of STDP.

Altogether, bAPs and STDP are mechanisms of premier importance for the cellular integration of inputs. Under the control of several neuronal systems, these two mechanisms participate in sensory input integration, as well as development and refinement of cellular connections during the critical period, in V1 layer 2/3 pyramidal cells.

References:

- Bannister AP (2005) Inter- and intra-laminar connections of pyramidal cells in the neocortex. *Neurosci Res* 53:95-103.
- Beurdeley M, Spatazza J, Lee HH, Sugiyama S, Bernard C, Di Nardo AA, Hensch TK, Prochiantz A (2012) Otx2 binding to perineuronal nets persistently regulates plasticity in the mature visual cortex. *J Neurosci* 32:9429-9437.
- Chen L, Yang C, Mower GD (2001) Developmental changes in the expression of GABA(A) receptor subunits (alpha(1), alpha(2), alpha(3)) in the cat visual cortex and the effects of dark rearing. *Brain Res Mol Brain Res* 88:135-143.
- Defelipe J, Markram H, Rockland KS (2012) The neocortical column. *Front Neuroanat* 6:22.
- Fagiolini M, Fritschy JM, Low K, Mohler H, Rudolph U, Hensch TK (2004) Specific GABAA circuits for visual cortical plasticity. *Science* 303:1681-1683.
- Feldman DE (2012) The spike-timing dependence of plasticity. *Neuron* 75:556-571.
- Froemke RC, Dan Y (2002) Spike-timing-dependent synaptic modification induced by natural spike trains. *Nature* 416:433-438.
- Froemke RC, Poo MM, Dan Y (2005) Spike-timing-dependent synaptic plasticity depends on dendritic location. *Nature* 434:221-225.
- Gilbert CD (1993) Circuitry, architecture, and functional dynamics of visual cortex. *Cereb Cortex* 3:373-386.
- Gordon JA, Stryker MP (1996) Experience-dependent plasticity of binocular responses in the primary visual cortex of the mouse. *J Neurosci* 16:3274-3286.
- Gottmann K, Mittmann T, Lessmann V (2009) BDNF signaling in the formation, maturation and plasticity of glutamatergic and GABAergic synapses. *Exp Brain Res* 199:203-234.
- Grewe BF, Bonnan A, Frick A (2010) Back-Propagation of Physiological Action Potential Output in Dendrites of Slender-Tufted L5A Pyramidal Neurons. *Front Cell Neurosci* 4:13.
- Hanover JL, Huang ZJ, Tonegawa S, Stryker MP (1999) Brain-derived neurotrophic factor overexpression induces precocious critical period in mouse visual cortex. *J Neurosci* 19:RC40.
- Hebb DO (1949) *The Organization of Behavior*. New York: Wiley.

- Hensch TK (2005) Critical period plasticity in local cortical circuits. *Nat Rev Neurosci* 6:877-888.
- Hensch TK, Fagiolini M, Mataga N, Stryker MP, Baekkeskov S, Kash SF (1998) Local GABA circuit control of experience-dependent plasticity in developing visual cortex. *Science* 282:1504-1508.
- Hsieh LS, Levine ES (2013) Cannabinoid modulation of backpropagating action potential-induced calcium transients in layer 2/3 pyramidal neurons. *Cereb Cortex* 23:1731-1741.
- Huang ZJ, Kirkwood A, Pizzorusso T, Porciatti V, Morales B, Bear MF, Maffei L, Tonegawa S (1999) BDNF regulates the maturation of inhibition and the critical period of plasticity in mouse visual cortex. *Cell* 98:739-755.
- Itami C, Kimura F (2012) Developmental switch in spike timing-dependent plasticity at layers 4-2/3 in the rodent barrel cortex. *J Neurosci* 32:15000-15011.
- Jia H, Rochefort NL, Chen X, Konnerth A (2010) Dendritic organization of sensory input to cortical neurons in vivo. *Nature* 464:1307-1312.
- Kampa BM, Clements J, Jonas P, Stuart GJ (2004) Kinetics of Mg²⁺ unblock of NMDA receptors: implications for spike-timing dependent synaptic plasticity. *J Physiol* 556:337-345.
- Ko H, Hofer SB, Pichler B, Buchanan KA, Sjöstrom PJ, Mrsic-Flogel TD (2011) Functional specificity of local synaptic connections in neocortical networks. *Nature* 473:87-91.
- Lamsa KP, Kullmann DM, Woodin MA (2010) Spike-timing dependent plasticity in inhibitory circuits. *Front Synaptic Neurosci* 2:8.
- Larkum ME, Nevian T (2008) Synaptic clustering by dendritic signalling mechanisms. *Curr Opin Neurobiol* 18:321-331.
- Larkum ME, Nevian T, Sandler M, Polsky A, Schiller J (2009) Synaptic integration in tuft dendrites of layer 5 pyramidal neurons: a new unifying principle. *Science* 325:756-760.
- Larkum ME, Waters J, Sakmann B, Helmchen F (2007) Dendritic spikes in apical dendrites of neocortical layer 2/3 pyramidal neurons. *J Neurosci* 27:8999-9008.
- Larsen RS, Rao D, Manis PB, Philpot BD (2010) STDP in the Developing Sensory Neocortex. *Front Synaptic Neurosci* 2:9.
- Levelt CN, Hubener M (2012) Critical-period plasticity in the visual cortex. *Annual Review of Neuroscience* 35:309-330.
- Magee JC, Johnston D (1995) Characterization of single voltage-gated Na⁺ and Ca²⁺ channels in apical dendrites of rat CA1 pyramidal neurons. *J Physiol* 487 (Pt 1):67-90.
- Major G, Larkum ME, Schiller J (2013) Active Properties of Neocortical Pyramidal Neuron Dendrites. *Annual Review of Neuroscience* 36:1-24.
- Markram H, Lubke J, Frotscher M, Sakmann B (1997) Regulation of synaptic efficacy by coincidence of postsynaptic APs and EPSPs. *Science* 275:213-215.

- Nevian T, Sakmann B (2006) Spine Ca²⁺ signaling in spike-timing-dependent plasticity. *J Neurosci* 26:11001-11013.
- Ohki K, Chung S, Ch'ng YH, Kara P, Reid RC (2005) Functional imaging with cellular resolution reveals precise micro-architecture in visual cortex. *Nature* 433:597-603.
- Ohki K, Reid RC (2007) Specificity and randomness in the visual cortex. *Curr Opin Neurobiol* 17:401-407.
- Pawlak V, Wickens JR, Kirkwood A, Kerr JN (2010) Timing is not Everything: Neuromodulation Opens the STDP Gate. *Front Synaptic Neurosci* 2:146.
- Petersen CC (2007) The functional organization of the barrel cortex. *Neuron* 56:339-355.
- Petersen CC, Crochet S (2013) Synaptic computation and sensory processing in neocortical layer 2/3. *Neuron* 78:28-48.
- Rauskolb S, Zagrebelsky M, Dreznjak A, Deogracias R, Matsumoto T, Wiese S, Erne B, Sendtner M, Schaeren-Wiemers N, Korte M, Barde YA (2010) Global deprivation of brain-derived neurotrophic factor in the CNS reveals an area-specific requirement for dendritic growth. *J Neurosci* 30:1739-1749.
- Rocheffort NL, Narushima M, Grienberger C, Marandi N, Hill DN, Konnerth A (2011) Development of direction selectivity in mouse cortical neurons. *Neuron* 71:425-432.
- Sale A, Berardi N, Spolidoro M, Baroncelli L, Maffei L (2010) GABAergic inhibition in visual cortical plasticity. *Front Cell Neurosci* 4:10.
- Seol GH, Ziburkus J, Huang S, Song L, Kim IT, Takamiya K, Huganir RL, Lee HK, Kirkwood A (2007) Neuromodulators control the polarity of spike-timing-dependent synaptic plasticity. *Neuron* 55:919-929.
- Sjostrom PJ, Nelson SB (2002) Spike timing, calcium signals and synaptic plasticity. *Curr Opin Neurobiol* 12:305-314.
- Smith GB, Heynen AJ, Bear MF (2009) Bidirectional synaptic mechanisms of ocular dominance plasticity in visual cortex. *Philos Trans R Soc Lond B Biol Sci* 364:357-367.
- Tsubokawa H, Ross WN (1996) IPSPs modulate spike backpropagation and associated [Ca²⁺]_i changes in the dendrites of hippocampal CA1 pyramidal neurons. *J Neurophysiol* 76:2896-2906.
- Waters J, Larkum M, Sakmann B, Helmchen F (2003) Supralinear Ca²⁺ influx into dendritic tufts of layer 2/3 neocortical pyramidal neurons in vitro and in vivo. *J Neurosci* 23:8558-8567.
- Wiesel TN, Hubel DH (1963) Single-Cell Responses in Striate Cortex of Kittens Deprived of Vision in One Eye. *J Neurophysiol* 26:1003-1017.
- Zhu JJ (2000) Maturation of layer 5 neocortical pyramidal neurons: amplifying salient layer 1 and layer 4 inputs by Ca²⁺ action potentials in adult rat tuft dendrites. *J Physiol* 526 Pt 3:571-587.

Appendix

Appendix #1 : Original manuscript : Petrinovic et al., PNAS 2013. Neuronal Nogo-A negatively regulates dendritic morphology and synaptic transmission in the cerebellum.

Appendix #2 : Original manuscript : Baudouin et al., Science 2012. Shared synaptic pathophysiology in syndromic and nonsyndromic rodents models of autism.

Neuronal Nogo-A negatively regulates dendritic morphology and synaptic transmission in the cerebellum

Marija M. Petrinovic^{a,b,1,2}, Raphael Hourez^c, Elisabeth M. Aloy^{a,b}, Gregoire Dewarrat^{a,b}, David Gall^c, Oliver Weinmann^{a,b}, Julien Gaudias^d, Lukas C. Bachmann^{a,b}, Serge N. Schiffmann^c, Kaspar E. Vogt^d, and Martin E. Schwab^{a,b,2}

^aBrain Research Institute, University of Zürich, 8057 Zürich, Switzerland; ^bDepartment of Health Sciences and Technology, ETH Zürich, 8057 Zürich, Switzerland; ^cLaboratoire de Neurophysiologie, Université Libre de Bruxelles, 1070 Brussels, Belgium; and ^dDivision of Pharmacology and Neurobiology, Biozentrum, University of Basel, 4056 Basel, Switzerland

Edited by Masao Ito, RIKEN Brain Science Institute, Wako, Japan, and approved November 27, 2012 (received for review August 29, 2012)

Neuronal signal integration as well as synaptic transmission and plasticity highly depend on the morphology of dendrites and their spines. Nogo-A is a membrane protein enriched in the adult central nervous system (CNS) myelin, where it restricts the capacity of axons to grow and regenerate after injury. Nogo-A is also expressed by certain neurons, in particular during development, but its physiological function in this cell type is less well understood. We addressed this question in the cerebellum, where Nogo-A is transiently highly expressed in the Purkinje cells (PCs) during early postnatal development. We used general genetic ablation (KO) as well as selective overexpression of Nogo-A in PCs to analyze its effect on dendritogenesis and on the formation of their main input synapses from parallel (PFs) and climbing fibers (CFs). PC dendritic trees were larger and more complex in Nogo-A KO mice and smaller than in wild-type in Nogo-A overexpressing PCs. Nogo-A KO resulted in premature soma-to-dendrite translocation of CFs and an enlargement of the CF territory in the molecular layer during development. Although spine density was not influenced by Nogo-A, the size of postsynaptic densities of PF–PC synapses was negatively correlated with the Nogo-A expression level. Electrophysiological studies revealed that Nogo-A negatively regulates the strength of synaptic transmission at the PF–PC synapse. Thus, Nogo-A appears as a negative regulator of PC input synapses, which orchestrates cerebellar connectivity through regulation of synapse morphology and the size of the PC dendritic tree.

The ability of a neuron to integrate into neuronal networks and process information is determined by the size and shape of its dendritic arbor. Dendritic spines contribute importantly to synaptic function and plasticity (1). The molecular mechanisms controlling these parameters are not fully understood. In addition to neurotransmitters and activity-related signaling systems, classes of molecules that are known to regulate neurite outgrowth and their receptors have been implicated in dendritic and/or spine growth and plasticity (2).

An important negative regulator of neurite outgrowth is the membrane protein Nogo-A (3). Whereas the growth inhibitory function of Nogo-A in the injured central nervous system (CNS) is well documented (4, 5), only few studies have addressed its physiological roles (3, 6, 7). Recent observations also point to functions of Nogo-A at synapses: overexpression of Nogo-A in adult Purkinje cells (PCs) induces synapse disassembly (8), whereas the overexpression of its receptor NgR1 leads to impairments in long-term memory (3). Nogo-A and both known Nogo receptors, NgR1 and paired immunoglobulin-like receptor B (PirB), negatively modulate hippocampal long-term potentiation (LTP) (9–11). NgR1 and PirB are also involved in the restriction of developmental, activity-driven plasticity in the visual cortex (3).

In addition to its mainly glial expression in the adult CNS (12, 13), Nogo-A is expressed by many central and peripheral neurons where its levels are high during development but lower or undetectable in the adult (3). In rodent cerebellum Nogo-A and

NgR1 are expressed in a complementary manner: Nogo-A is mainly present in PCs, whereas the granule cells (GCs) are a main site of NgR1 expression (14–16). The time course of high Nogo-A expression in PCs correlates with the time of PC dendritogenesis, climbing fiber (CF)–PC synapse refinement and parallel fiber (PF)–PC synapse development (6, 8, 14). These findings suggest that Nogo-A could play a role in the regulation of PC connectivity.

Nogo-A knockout (KO) mice and transgenic mice (TG) overexpressing Nogo-A exclusively in PCs under the L7 promoter (L7–Nogo-A TG), revealed in the present study that Nogo-A acts as a negative regulator of the size and complexity of the PC dendritic arbor as well as of the size and strength of the PF synapses. In addition, genetic ablation of Nogo-A influences the establishment of CF innervation on the PC dendrites. These results identify a distinct biological function for Nogo-A expressed by neurons for the development of synaptic connections in the cerebellum.

Results

Four types of mice were used in this study: Nogo-A KO and wild-type (WT) mice of C57BL/6 background and L7–Nogo-A TG mice, which overexpress Nogo-A only in PCs (8), and their corresponding WT controls of FVB/N background. To account for strain differences (17) we always compared mutant animals with the WT mice of the corresponding strain. As the cerebellar lobules, and even different regions of the same lobule, mature at different time points (18, 19), we always analyzed the bank and gyrus subdivisions of the lobules IV/V, VI/VII, and IX.

Nissl staining showed no differences between the mutants and the WT animals with regard to the size, foliation, laminar organization, and histology of the cerebellum (Fig. S1A). No obvious differences in PC arrangement and their calbindin immunoreactivity were noted between the four lines of mice (Fig. S1B). Western blot (WB) analysis of cerebella at postnatal day (P) 28 revealed comparable Nogo-A and -B expression in WT mice of both strains (Fig. S2A). Nogo-A KO mice had elevated levels of Nogo-B as described earlier (20) (Fig. S2A). WB with the antibody 3D11, which is specific for the Nogo-A transgene of rat origin (21), confirmed the overexpression of Nogo-A in cerebellar

Author contributions: M.M.P., E.M.A., S.N.S., and M.E.S. designed research; M.M.P., R.H., E.M.A., G.D., D.G., O.W., J.G., and L.C.B. performed research; M.M.P., R.H., E.M.A., G.D., D.G., O.W., J.G., and K.E.V. analyzed data; and M.M.P., S.N.S., and M.E.S. wrote the paper.

The authors declare no conflict of interest.

This article is a PNAS Direct Submission.

¹Present address: F. Hoffmann-La Roche AG, pRED, Pharma Research and Early Development, DTA Neuroscience, 4070 Basel, Switzerland.

²To whom correspondence may be addressed. E-mail: marija-magdalena.petrinovic@roche.com or schwab@hifo.uzh.ch.

This article contains supporting information online at www.pnas.org/lookup/suppl/doi:10.1073/pnas.1214255110/-DCSupplemental.

lysates of P28 L7-Nogo-A TG mice (Fig. S2B). Protein levels of NgR1 were equal in all four groups of mice (Fig. S2C).

Distribution of Nogo-A and NgR1 in the Cerebellum. At P28, Nogo-A was found only in PC bodies, dendrites, and their spines (Fig. 1A). Double labeling with anti-NgR1 and anti-vesicular glutamate transporter 1 (anti-VGluT1) antibodies demonstrated a strong expression of NgR1 in PF terminals (Fig. 1B), whereas colabeling with antibodies against calbindin and NgR1 revealed very weak expression of NgR1 in PC bodies (Fig. S2D). The presence of Nogo-A in the postsynaptic PC spines and of NgR1 in the presynaptic PF terminals was confirmed by immunoelectron microscopy (Fig. S3A and B).

Nogo-A expression in the PCs is developmentally regulated (6, 14). Our WB analysis confirmed a weak expression of Nogo-A in the cerebellum of WT mice during the first postnatal week, followed by a fivefold up-regulation by P14 (Fig. S3C). Similar pattern of Nogo-A expression was observed in L7-Nogo-A TG mice, in line with the notion that the L7 promoter is fully activated only in the second postnatal week (22) (Fig. S3D). With the progression of development, the Nogo-A gets down-regulated in WT mice to ~25% of the level at P14 (Fig. S3C). No down-regulation occurred in L7-Nogo-A TG mice (Fig. S3D). Developmental regulation of Nogo-A expression in PCs was confirmed by immunohistochemistry (IHC) (Figs. S1B and S3E).

Nogo-A Negatively Regulates PC Dendritic Tree Morphology and Input Synapses. For a morphometric analysis, P28 PCs were filled with biocytin. The overall cellular volume was increased in Nogo-A KO PCs (Fig. 2A and B), with both an increase in size (μm^3) of the somatic (WT/B: $5,288 \pm 298$ and KO: $6,629 \pm 368$; $P < 0.01$) and the dendritic (WT/B: $32,956 \pm 2,994$ and KO: $47,996 \pm 4,317$; $P < 0.01$) compartment. Overexpression of Nogo-A in PCs led to a decrease in their cellular volume (μm^3) (Fig. 2A and B); both the somatic (WT/F: $6,265 \pm 316$ and TG: $5,237 \pm 261$; $P < 0.05$) and the dendritic (WT/F: $45,754 \pm 4,418$ and TG: $31,890 \pm 2,219$; $P < 0.05$) compartments were affected. The observed modifications of the dendritic tree volume could be a consequence of changes in the thickness, length, and/or complexity of dendrites. The average width of distal dendritic segments was enlarged in the Nogo-A KO and reduced in the L7-Nogo-A TG PCs (Fig. 2B). The length (μm) of the primary dendrites (the main, central dendrites, directly connected to the cell body of PCs) was also negatively influenced by Nogo-A (WT/B: 140.32 ± 7.63 and KO: 167.69 ± 9.86 ; $P < 0.05$; WT/F: 132.32 ± 8.93 and TG: 106.84 ± 12.97 ; $P < 0.05$). To assess the complexity of the

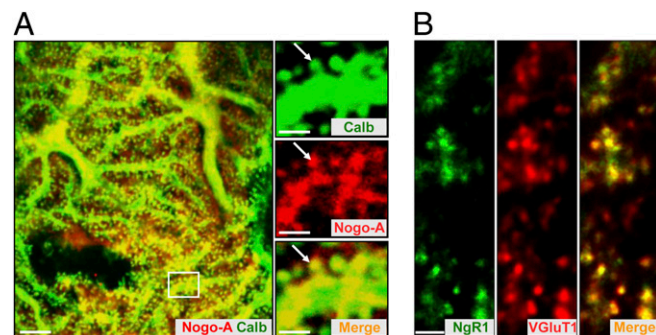


Fig. 1. Distribution of Nogo-A and NgR1 in the cerebellum. (A and B) Nogo-A and its receptor NgR1 are complementarily expressed at synaptic sites in the cerebellum of P28 WT/BL6 mice. (A) Double immunolabeling with anti-calbindin (green) and anti-Nogo-A (red) antibodies revealed the presence of Nogo-A in dendrites and spines (arrows) of PCs. Higher power micrographs correspond to the boxed region. (Scale bars, 5 μm ; 2 μm in *Insets*.) (B) Colabeling with antibodies against NgR1 (green) and VGluT1 (red) demonstrates the strong expression of NgR1 in the presynaptic, VGluT1⁺ PF terminals. (Scale bar, 2 μm .)

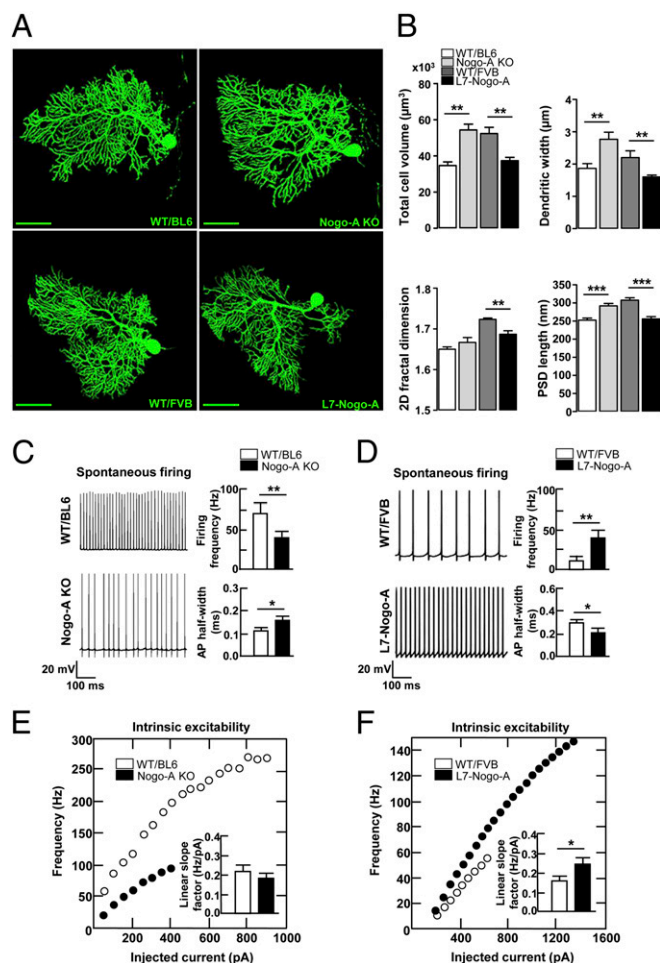


Fig. 2. Nogo-A negatively regulates PC dendritic tree morphology and affects electrophysiological properties of PCs. (A) Confocal images of biocytin-filled PCs from cerebellar slices of P28 Nogo-A KO, L7-Nogo-A TG and the corresponding WT mice. Note the larger dendritic arbor of the Nogo-A KO PC compared with its WT/BL6 control and the less complex arbor and a smaller cell body of the Nogo-A overexpressing PCs compared with strain-matched WT controls. (Scale bars, 50 μm .) (B) Nogo-A negatively regulates the total cell volume, width of distal dendritic segments, and the length of PSDs. Whereas Nogo-A KO exerts no effect on the 2D fractal dimension, overexpression of Nogo-A reduces the complexity of PC dendritic arbors (B). (C and D) Nogo-A regulates the spontaneous firing activity of P28 PCs, as well as the action potential half-width. (E and F) Current-frequency plots and corresponding histograms demonstrate that Nogo-A KO has no effect on PC intrinsic excitability (E), whereas its overexpression leads to an increase of the intrinsic neuronal excitability compared with WT controls (F). Values represent means \pm SEM of 11–26 cells (three to six mice) per genotype; * $P < 0.05$, ** $P < 0.01$, *** $P < 0.001$, Student *t* test.

PC dendritic tree, we used a 2D fractal analysis. Whereas Nogo-A KO PCs were not significantly different from WT controls, those overexpressing Nogo-A demonstrated a significant decrease in 2D fractal dimension (Fig. 2B). PKC γ , which has been suggested to play a role in dendritic growth and differentiation of PCs (23), was down-regulated in the Nogo-A KO and doubled in the L7-Nogo-A TG mice (Fig. S4A and B). These results suggest that Nogo-A negatively modulates PC size and the complexity of its dendritic tree.

Spine density showed no abnormalities in PCs either lacking (WT/B: 2.90 ± 0.20 and KO: 2.30 ± 0.70 ; $P = 0.58$) or overexpressing (WT/F: 1.73 ± 0.09 and TG: 1.74 ± 0.24 ; $P = 1.00$) Nogo-A. This absence of change in spine density, combined with the differing size of the dendritic tree, points to a negative

regulation of the total spine number by Nogo-A. To analyze a key functional component of spine synapses, the postsynaptic density (PSD), we used electron microscopy (EM). At P28, the average length of the PSD, a measure that is well correlated with the spine head volume and the strength of synaptic transmission (1), was increased in Nogo-A KO and reduced in L7–Nogo-A TG compared with WT PCs (Fig. 2B). Similar changes in the PSD length (nm) were also observed in 5-mo-old mutant mice (WT/B: 275.60 ± 4.95 and KO: 321.41 ± 5.43 ; $P < 0.001$; WT/F: 346.91 ± 7.12 and TG: 269.20 ± 6.38 ; $P < 0.001$). Biochemically, glutamate receptors, CamKII, PSD95 and Homer, are major constituents of PSDs (24). WB and IHC evaluation demonstrated negative correlation between these PSD components and the expression level of Nogo-A in the molecular layer (ML) of P28 mice (Figs. S4 A and B and S5 A and B).

Electrophysiological Properties of PCs Are Affected by Nogo-A. Alterations in Nogo-A content affected neither the resting membrane resistance (M Ω) (WT/B: 146 ± 19 and KO: 170 ± 22 ; $P = 0.47$; WT/F: 218 ± 31 and TG: 232 ± 54 ; $P = 0.76$) nor the minimal membrane potential (mV) measured during spontaneous activity (WT/B: -54.5 ± 1.7 and KO: -56.4 ± 1.0 ; $P = 0.38$; WT/F: -63.9 ± 1.6 and TG: -67.6 ± 1.6 ; $P = 0.63$). The spontaneous firing rate was positively correlated with Nogo-A level (Fig. 2 C and D). In addition, Nogo-A KO PCs showed a $\sim 30\%$ increase in the action potential half-width evaluated at the threshold potential where fast repetitive spiking is obtained (Fig. 2C), whereas a commensurate $\sim 30\%$ decrease of action potential half-width was observed in L7–Nogo-A TG PCs (Fig. 2D).

Intrinsic neuronal excitability, which is well correlated with the spontaneous firing frequency, was investigated by holding the membrane potential at -80 mV and injecting steps of depolarizing current from 0 to 2.5 nA with 50-pA increments. Whereas intrinsic excitability was slightly, although not significantly reduced in Nogo-A KO PCs (Fig. 2E), it was significantly enhanced in L7–Nogo-A TG PCs compared with WT cells (Fig. 2F).

Genetic Ablation of Nogo-A Affects the Developmental Rearrangement of CF Terminals on PCs. The reduction of poly- to single CF innervation of PCs has long been a model for developmental synapse elimination (25). In mice, pruning of surplus CF connections finishes by the end of the third postnatal week, leaving $\sim 90\%$ of the PCs innervated by only one CF (26). Simultaneously, the CF terminals translocate from the PC somata to the proximal dendrites (25, 27). Developmental up-regulation of Nogo-A coincides with the time of both somatodendritic translocation and elimination of supernumerary CFs, suggesting its possible involvement in the regulation of the synapse refinement processes in the cerebellum.

Quantification of VGluT2⁺ CF terminals at early developmental stages (P4–P7), i.e., before the onset of synapse elimination, revealed a higher density of CF terminals in the ML of Nogo-A KOs, whereas no difference was observed between L7–Nogo-A TG mice and their WT controls (Fig. 3 B and C). At P14, a stage when $\sim 50\%$ of WT PCs bear only one CF, the average density (terminals per mm²) of VGluT2⁺ puncta in the ML was again higher in the Nogo-A KO mice (WT/B: $14,320 \pm 831.9$ and KO: $18,960 \pm 622.0$; $P < 0.001$), whereas the overexpression of Nogo-A showed no effect (WT/F: $14,940 \pm 310.1$ and TG: $15,250 \pm 411.7$; $P = 0.34$). At 4 wk, when the synaptic rearrangement should be finished, the density of VGluT2⁺ terminals in Nogo-A KOs was $\sim 50\%$ higher than in WT mice, whereas no abnormalities were observed in L7–Nogo-A TG mice (Fig. 3 A and D). A WB analysis confirmed the increase in the amount of VGluT2 protein in the ML of P28 Nogo-A KOs, and no detectable change in its expression in the cerebella of L7–Nogo-A TGs compared with WT controls (Fig. S4 A and B). In adult (P60) mice the VGluT2 immunostaining pattern showed a comparable density of CF terminals in mutant mice and their WT controls (Fig. 3E).

We further analyzed the CF innervation patterns in P28 Nogo-A KO mice by labeling a small fraction of CFs with biotinylated dextran amine (BDA) and counterstaining the sections for VGluT2 and calbindin. In both WT and Nogo-A KO mice, all PC bodies contacted by BDA⁺ CF showed a complete overlap of BDA and VGluT2 staining and an absence of BDA⁻ CF terminals, which would have originated from additional, non-BDA-labeled CFs (Fig. S6A). Thus, multiply innervated PCs were not detectable by this method. CF innervation of PCs was also analyzed by electrophysiological measurements: CFs were stimulated in the GC layer of sagittal cerebellar slices from P28 Nogo-A KO mice and their WT littermates. As the stimulus intensity was gradually increased, a typical large excitatory postsynaptic current (EPSC) was elicited in an all-or-none fashion in the majority of the PCs, indicating that these PCs are innervated by a single CF in WT and Nogo-A KO PCs (Fig. S6 B and C). In $\sim 11\%$ of WT and $\sim 4\%$ of Nogo-A KO PCs CF-mediated EPSCs had two discrete steps when the stimulus intensity was above the threshold, suggesting that these cells had one supernumerary CF in addition to the main CF (Fig. S6 B and C). Thus, the higher density of VGluT2⁺ CF terminals observed in P28 Nogo-A KO PCs points to a hyperinnervation emerging from a single inferior olive axon.

During normal cerebellar maturation, CF contacts shift from the soma to the dendrites as PCs elaborate their dendritic arbor. Whereas the somatodendritic translocation of CF contacts occurred to an equivalent extent in the WT and the L7–Nogo-A TG cerebella, significant differences were found between WT and Nogo-A KO mice (Fig. S7 A and B). At P14 Nogo-A KO mice had more PCs without any VGluT2⁺ dots on their soma (Fig. S7B), but fewer PCs with more than six VGluT2⁺ dots on their soma than their WT littermates (Fig. S7B), indicating either precocious somatodendritic translocation or, alternatively, an earlier start of CF–PC synapse refinement. To distinguish these possibilities, we performed anterograde labeling of CFs with BDA combined with immunofluorescence for VGluT2 and calbindin in addition to electrophysiological recordings of CF EPSCs. All polyinnervated Nogo-A KO and WT PCs had comparable numbers of BDA⁺/VGluT2⁺ and BDA⁻/VGluT2⁺ CF terminals on their somata (BDA⁺/VGluT2⁺: WT/B, 3.21 ± 0.38 and KO, 4.32 ± 0.27 ; $P = 0.89$; BDA⁻/VGluT2⁺: WT/B, 3.60 ± 0.22 and KO, 2.8 ± 0.19 ; $P = 0.74$) (Fig. S7C). Similarly, electrophysiological measurements showed that the percentage of P14 PCs displaying either single or dual CF innervation was comparable between WT (23% dually innervated PCs; $n = 6/26$) and Nogo-A KO mice (17% dually innervated PCs, $n = 5/29$) (Fig. S7 D and E). Thus, both approaches excluded the possibility of an earlier start of synapse elimination in the absence of Nogo-A.

Precocious translocation of CF contacts from the soma to the dendrites of PCs was further confirmed by an increase in the extent (%) of the CF innervation territory in Nogo-A KO mice (P14: WT/B, 59.03 ± 2.11 and KO, 74.12 ± 1.42 ; $P < 0.05$; P28: WT/B, 79.09 ± 1.19 and KO, 92.24 ± 1.15 ; $P < 0.05$) (Fig. 3A and Fig. S6A, arrows). No genotypic differences were observed with regard to the total thickness (μ m) of the ML at P28 (WT/B, 178.21 ± 8.92 and KO, 183.65 ± 12.14 ; $P = 0.46$; WT/F, 167.18 ± 10.67 and TG, 172.49 ± 9.84 ; $P = 0.72$). In the adult (P60) Nogo-A KO (WT/B, 88.40 ± 1.73 and KO, 90.28 ± 1.06 ; $P = 0.74$) as well as in the developing and adult L7–Nogo-A TG mice, the CF innervation territory (%) was comparable with that of WT controls (P14: WT/F, 58.21 ± 1.42 and TG, 61.64 ± 1.53 ; $P = 0.36$; P28: WT/F, 84.38 ± 1.33 and TG, 82.85 ± 1.78 ; $P = 0.63$; and P60: WT/F, 91.12 ± 1.12 and TG, 90.75 ± 1.13 ; $P = 0.75$) (Fig. 3A). Thus, deletion of Nogo-A enhances the translocation and spread of CF terminals along the dendritic tree and leads to a temporary hyperinnervation of the PCs.

Nogo-A Affects the PF–PC Synapse Number and Synaptic Transmission. The density of the VGluT1⁺ PF terminals was determined in the ML of P14, P28, and P60 mice; it was negatively correlated with Nogo-A expression level at all three developmental stages

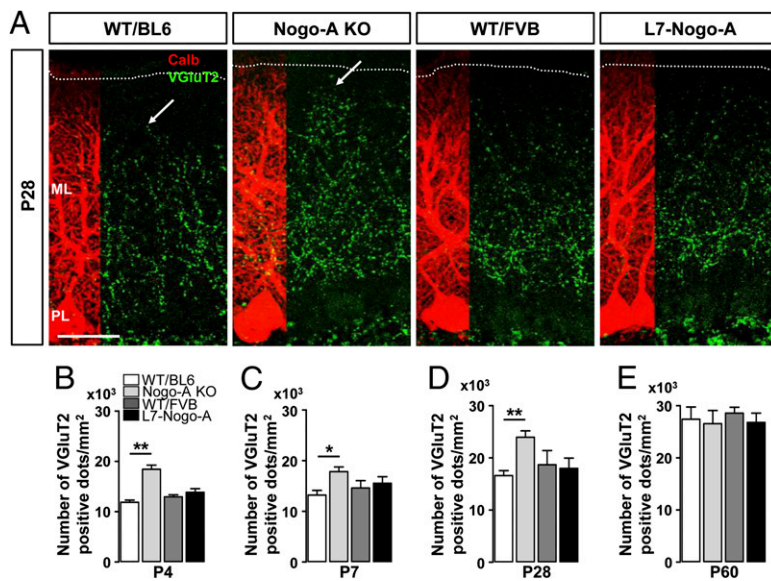


Fig. 3. Genetic deletion of Nogo-A affects the developmental rearrangement of CF terminals on PC dendrites. (A) Confocal images of VGlut2⁺ CF terminals (green) on P28 PCs stained for calbindin (red). Note the increased territory of CF synapses in Nogo-A KO mice at P28 (arrows). Dotted lines indicate the pial surface. ML, molecular layer; PL, PC layer. (Scale bar, 50 μ m.) An increase in the density of VGlut2⁺ CF varicosities was found in Nogo-A KO mice at P4 (B), P7 (C), and P28 (A and D). This effect of Nogo-A KO on the CF innervation pattern was no longer visible at P60 (E). Overexpression of Nogo-A had no effect on either the density or the position of CF terminals (A–E). Values represent means \pm SEM of 103–116 cells (six mice) per genotype; * P < 0.05, ** P < 0.01, Student t test.

(Fig. 4 A–D). WB analysis of P28 mutant and WT mouse cerebellar lysates confirmed the negative correlation between the VGlut1 and Nogo-A expression levels (Fig. S4 A and B). Similarly to VGlut1, SNAP25, which is highly expressed in PF terminals (28), was up-regulated in Nogo-A KO and down-regulated in L7-Nogo-A TG mice (Fig. S4 A and B).

To test whether Nogo-A expression affects excitatory PF transmission, we measured EPSCs in the PCs in response to the electrical stimulation of a beam of PFs in P28 acute cerebellar slices of mutant and WT mice. Input–output relations measuring EPSC initial slope as a function of PF stimulus intensity were established for each recorded neuron. Because this relation is linear, we used the mean linear slope factor to compare the synaptic strength of the PF–PC synapses in mutant vs. WT mice. The synaptic strength for increasing PF stimulation was significantly increased in Nogo-A KO (Fig. 4 E and G) and decreased in L7-Nogo-A TG PCs compared with WT controls (Fig. 4 F and H). These results suggest an involvement of Nogo-A in the regulation of synaptic strength of the PF–PC synapses.

To determine whether Nogo-A acts pre- and/or postsynaptically we studied paired-pulse facilitation (PPF), a form of short-term synaptic plasticity associated with a change in the probability of glutamate release from the presynaptic PFs during a second stimulation that closely follows the first. PPF was elicited by twin pulses at different time intervals (5–245 ms in 2-ms increments) in L7-Nogo-A TG and control WT cells. The absence of a significant difference between mutant and WT cells (Fig. S8 A and B) suggests that the observed effects of Nogo-A on the synaptic strength are not likely due to regulations of glutamate release.

Discussion

Nogo-A expression in PCs reaches its peak during the second postnatal week and is afterward down-regulated to the low adult levels (8, 14). This time window correlates with the dendritic outgrowth of PCs, synapse formation, and refinement. The signaling pathways that regulate PC dendritic growth and complexity are poorly understood. Our morphological analysis showed that Nogo-A has a negative influence on the size of the PC bodies as well as the thickness, length, and complexity of PC dendrites. These results are well in line with previous studies in adult animals showing that Nogo-A is a negative regulator of the neuronal growth program (3, 29), as well as with the recent findings showing negative regulation of dendritic length and complexity by Nogo-A and NgR1 in hippocampal neurons (7, 30). PC dendrites are tightly packed and intermingled in the developing ML, and they were suggested to express NgR1 (31,

32). We speculate that they repulse each other mutually in a process of territorial sorting, whereby one repulsive/growth-restricting cue would be Nogo-A. Presence of NgR1 in the PC (31, 32) raises the possibility of its *cis*-interaction with Nogo-A in PC membrane, although such a mechanism has not been described for Nogo-A so far. Nevertheless, by binding to NgR1 or another yet unidentified receptor, Nogo-A activates the small GTPase RhoA (33), which has been shown to slow dendritic branch formation, yielding smaller and fewer branched dendritic arbors in various types of neurons (34). Notably, activation of RhoA has been recently identified as a mechanism by which NgR1 restricts dendritic growth and synapse formation in hippocampal neurons (30). Additionally, several studies have demonstrated that synaptic activity affects the dendritic arbor development (35, 36), thus opening the possibility that by negatively regulating synaptic transmission at PF–PC synapses, Nogo-A in turn negatively regulates dendritic growth.

Electrophysiological Properties of PCs Are Influenced by Nogo-A. The membrane resistance and the minimal membrane potential of PCs were not affected by Nogo-A. Alterations in excitability can be caused by a modification of cell volume/area as the cell capacitance will vary accordingly. Spontaneous firing rate was correlated with Nogo-A expression. In addition to the possible role of the Nogo-A-induced changes in the cell size, changes in the excitability and spontaneous firing rate of a neuron can be caused by the alteration in ionic conductances in the cell membrane (37). Previous studies (38, 39) suggested possible roles of Nogo-A for the regulation of Ca²⁺ and K⁺ channels, which, in turn, have been considered to play a role in spontaneous firing of a neuron (37). All these results suggest that neuronal Nogo-A helps to maintain the PC output within a proper dynamic range, either by a regulatory influence on ion channels or indirectly through the modifications of the PC size and morphology. As neurons can increase their excitability to maintain a fixed level of firing output (40), the decrease in PF synaptic transmission in L7-Nogo-A TG mice may be compensated by the observed increase in intrinsic excitability of the PCs.

Nogo-A Influences the Maturation of the CF–PC Innervation. In the Nogo-A KO mice, the development of the CF input to PCs was disturbed: From P4 to P28 the number of CF terminals was increased by ~35–55%, and they were distributed over larger areas of the ML. The disturbance seemed transitory, however, and no remaining polyinnervation of PCs could be detected. The absence

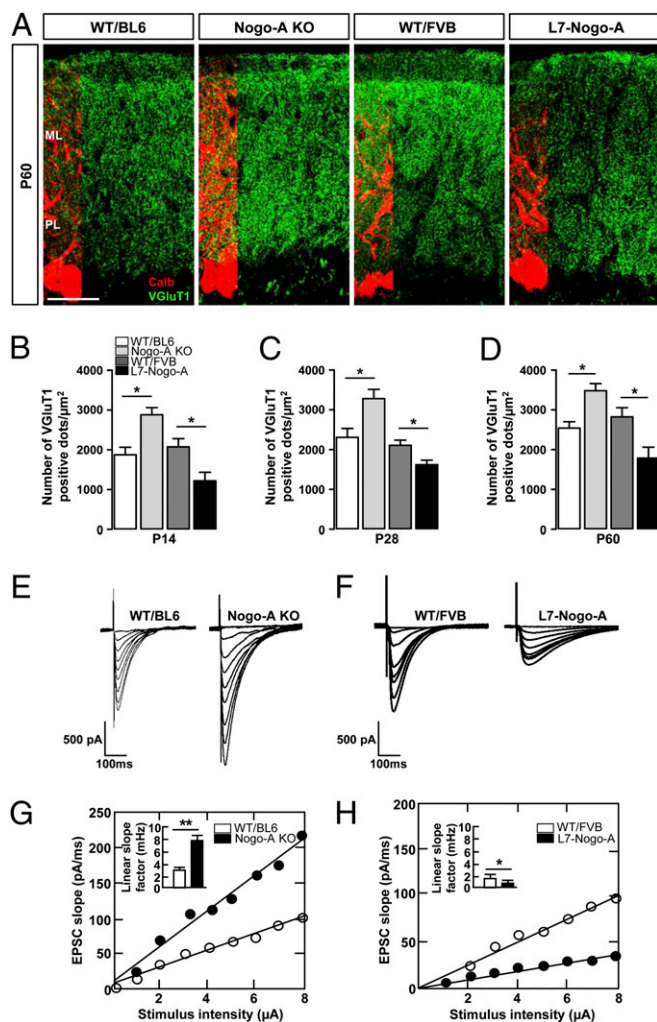


Fig. 4. Nogo-A negatively regulates the density and synaptic strength of the PF–PC synapses. (A) Confocal images of VGLUT1⁺ PF terminals (green) on P60 PCs stained for calbindin (red). ML, molecular layer; PL, PC layer. (Scale bar, 50 μm .) Nogo-A KO leads to an increase in the number of PF terminals synapsing onto PC dendrites during development (B and C) as well as in the adult (A and D). Conversely, overexpression of Nogo-A in PCs resulted in a decrease in the number of PF terminations both during development (B and C) and in the adult (A and D). Values represent means \pm SEM of 118–145 cells (six mice) per genotype; * $P < 0.05$, ** $P < 0.01$, Student *t* test. (E and F) Typical input–output relationships obtained from P28 PCs in response to an increasing stimulation of PFs in Nogo-A KO (E), L7-Nogo-TG (F), and the corresponding WT mice. PCs of Nogo-A KO mice exhibit increased response to PF stimulation (G), whereas Nogo-A overexpression leads to a decrease in PC response to the same stimulus (H). Values represent means \pm SEM of 19–25 cells (four to six mice) per genotype; * $P < 0.05$, ** $P < 0.01$, Student *t* test.

of detectable effects of Nogo-A overexpression may be due to the late onset of the promoter used (22).

The molecular mechanisms that regulate CF synaptogenesis and fine tuning are not well understood. The GluR82, which probably acts as an adhesion molecule (41, 42), P/Q-type voltage-dependent Ca^{2+} channels, insulin-like growth factor (IGF), focal adhesion kinase (FAK), tyrosine-related kinase B (TrkB), myosinVa, glutamate transporter GLAST, a novel brain specific receptor-like protein family BSRP, mGluR1, the α subunit of the Gq subtype of GTP-binding protein, phospholipase C β 4, and PKC γ were shown to play roles for the development of CF and PC connectivity (42–46). PKC γ , which has been shown to be activated by Nogo-A (47) was down-regulated in Nogo-A KO

and doubled in L7–Nogo-A TG mice, but its role in PC dendritic tree development seems rather complex (23, 48) and a possible role of this pathway for the observed effects of Nogo-A remains to be studied in detail. Importantly, several repulsive factors have also been identified to contribute to the synaptic specificity and synapse elimination in different CNS regions (49–52). In the maturing cerebellum, the mostly repulsive ephrin–Eph ligand–receptor family has been shown to guide olivo–cerebellar CF axons and influence their synapse and spine formation (53, 54). The present results show that the repulsive cell surface molecule Nogo-A influences CF synapse numbers, possibly by effects on synaptic pruning, and somatodendritic migration of the CF synapses. In light of the findings that functional differentiation of multiple CF inputs at P4–P7 is mainly based on an increase in the number of synaptic terminals supplied by each CF to the PC soma (55) it is tempting to speculate that the increase in the number of CF terminals observed in Nogo-A KO mice during the same time span contributes to the earlier establishment of the winning CF and thus its earlier translocation to PC dendrites. An increase in the number of the VGLUT2⁺ CF terminals in P14–P28 Nogo-A KO mice could then be explained by the higher number of branches of the winning CF in Nogo-A KO mice and the longer time needed for their elimination.

Nogo-A Is a Negative Regulator of PF Synaptogenesis and Synaptic Transmission. The density of VGLUT1⁺ PF terminals was increased in Nogo-A KO and decreased in L7–Nogo-A TG mice at P14–P60 compared with the WT controls. The results suggest that Nogo-A acts as a negative factor also for the formation of PF synapses, which starts in the second postnatal week, i.e., during the transient Nogo-A up-regulation in PCs. Importantly, this effect persisted into adulthood. Previous studies have shown the critical role for GluR82 and Cbln1 for selective strengthening of PF–PC synapses (45, 56). We also saw a significant increase in the PSD length in the P28 as well as in 5-mo-old Nogo-A KO mice and a decrease in the L7–Nogo-A TG animals. Several synaptic markers including GluR1, GluR2/3, Homer, PSD95, and CamKII showed corresponding changes.

Nogo-A is a potent repulsive molecule with destabilizing effects on the cytoskeleton of growth cones mediated by its downstream effectors RhoA/LIM Kinase (LIMK)/cofilin (3, 29). Actin and RhoA are enriched in presynaptic endings and in dendritic spines (57) and may link synaptic plasticity to actin and synaptic cytoskeleton remodeling (58). The negative correlation observed in the present study between the PF–PC synaptic length, the PF terminal number, and the expression level of Nogo-A may be due to such mechanisms. Alternatively, the changes in the PSD length observed after manipulation of the Nogo-A levels may be primarily a reflection of altered synaptic strength and activity, which leads to alterations in spine structure (35). The increase in the PSD length generally leads to spine stabilization, which may explain the enhanced motor learning observed in the Nogo-A KO mice (59). Conversely, in addition to the progressive loss of the inhibitory PC terminals, decreased length of the PSD and the consequent spine destabilization may be contributing to observed deficits in motor learning and coordination in the adult L7–Nogo-A TG mice (8).

The increased synaptic strength observed at the PF synapses of Nogo-A KO mice and the decreased transmission in the Nogo-A overexpressors at P28 are in line with the morphological and biochemical observations. The absence of a significant difference between WT and mutant animals in PPF suggests that the effects of Nogo-A on EPSC are not due to changes in pre-synaptic release mechanisms but are rather caused by the change in synapse number and/or size. Interestingly, it has been suggested that NgR1 restricts the synapse number in the developing hippocampus (30) and the enhancement of the hippocampal LTP was observed after Nogo-A neutralization or KO and in NgR1 KO mice (9–11). Whether acute suppression of Nogo-A or NgR1 in the adult cerebellum would also induce

changes in PF function remains to be analyzed. The present results corroborate the role of Nogo-A as a negative controller of synaptic development, strength, and structure in several brain regions. In conclusion, the present results show that Nogo-A expressed by cerebellar PCs plays important roles for the development of these neurons and their input. Neuronal Nogo-A also influences, as a negative regulator, development, structure, and function of cerebellar synapses.

Materials and Methods

Nogo-A KO (pure C57BL/6 background) and L7-Nogo-A TG (in FVB/N background) mice of various developmental stages (P4-P60) were used in this

study. WT mice of both C57BL/6 and FVB/N strains were used as respective controls. Detailed information on mutant animals, histology, IHC, electrophysiology, morphometric analysis of PCs and EM is provided in *SI Materials and Methods*.

ACKNOWLEDGMENTS. We thank C. Orlando for help with confocal microscopy. This work was supported by the Swiss National Science Foundation (SNSF) (3100A0-122527/1), the National Center of Competence in Research (NCCR) "Neural Plasticity and Repair," the Christopher and Dana Reeve Foundation, the European Union Sixth Framework Programme Network of Excellence NeuroNE, the Queen Elisabeth Medical Foundation (Belgium), Fonds National de la Recherche Scientifique (FNS-FNRS) (Belgium), and Action de Recherche Concertée from the Communauté Française de Belgique (CFWB).

- Nimchinsky EA, Sabatini BL, Svoboda K (2002) Structure and function of dendritic spines. *Annu Rev Physiol* 64:313–353.
- Jan YN, Jan LY (2003) The control of dendrite development. *Neuron* 40(2):229–242.
- Schwab ME (2010) Functions of Nogo proteins and their receptors in the nervous system. *Nat Rev Neurosci* 11(12):799–811.
- Schwab ME (2004) Nogo and axon regeneration. *Curr Opin Neurobiol* 14(1):118–124.
- Yiu G, He Z (2006) Glial inhibition of CNS axon regeneration. *Nat Rev Neurosci* 7(8):617–627.
- Gianola S, Savio T, Schwab ME, Rossi F (2003) Cell-autonomous mechanisms and myelin-associated factors contribute to the development of Purkinje axon intracortical plexus in the rat cerebellum. *J Neurosci* 23(11):4613–4624.
- Zagrebel'sky M, Schweigreiter R, Bandtlow CE, Schwab ME, Korte M (2010) Nogo-A stabilizes the architecture of hippocampal neurons. *J Neurosci* 30(40):13220–13234.
- Aloy EM, et al. (2006) Synaptic destabilization by neuronal Nogo-A. *Brain Cell Biol* 35(2–3):137–156.
- Delekaté A, Zagrebel'sky M, Kramer S, Schwab ME, Korte M (2011) NogoA restricts synaptic plasticity in the adult hippocampus on a fast time scale. *Proc Natl Acad Sci USA* 108(6):2569–2574.
- Lee H, et al. (2008) Synaptic function for the Nogo-66 receptor NgR1: Regulation of dendritic spine morphology and activity-dependent synaptic strength. *J Neurosci* 28(11):2753–2765.
- Raiker SJ, et al. (2010) Oligodendrocyte-myelin glycoprotein and Nogo negatively regulate activity-dependent synaptic plasticity. *J Neurosci* 30(37):12432–12445.
- Caroni P, Schwab ME (1988) Antibody against myelin-associated inhibitor of neurite growth neutralizes nonpermissive substrate properties of CNS white matter. *Neuron* 1(1):85–96.
- Chen MS, et al. (2000) Nogo-A is a myelin-associated neurite outgrowth inhibitor and an antigen for monoclonal antibody IN-1. *Nature* 403(6768):434–439.
- Huber AB, Weinmann O, Brösamle C, Oertle T, Schwab ME (2002) Patterns of Nogo mRNA and protein expression in the developing and adult rat and after CNS lesions. *J Neurosci* 22(9):3553–3567.
- Hunt D, Coffin RS, Pridjha RK, Campbell G, Anderson PN (2003) Nogo-A expression in the intact and injured nervous system. *Mol Cell Neurosci* 24(4):1083–1102.
- Josephson A, et al. (2002) Nogo-receptor gene activity: Cellular localization and developmental regulation of mRNA in mice and humans. *J Comp Neurol* 453(3):292–304.
- Sillitoe RV, Joyner AL (2007) Morphology, molecular codes, and circuitry produce the three-dimensional complexity of the cerebellum. *Annu Rev Cell Dev Biol* 23:549–577.
- Altman J (1972) Postnatal development of the cerebellar cortex in the rat. I. The external germinal layer and the transitional molecular layer. *J Comp Neurol* 145(3):353–397.
- Nishiyama H, Linden DJ (2004) Differential maturation of climbing fiber innervation in cerebellar vermis. *J Neurosci* 24(16):3926–3932.
- Simonen M, et al. (2003) Systemic deletion of the myelin-associated outgrowth inhibitor Nogo-A improves regenerative and plastic responses after spinal cord injury. *Neuron* 38(2):201–211.
- Oertle T, et al. (2003) Nogo-A inhibits neurite outgrowth and cell spreading with three discrete regions. *J Neurosci* 23(13):5393–5406.
- Smeyne RJ, et al. (1991) Dynamic organization of developing Purkinje cells revealed by transgene expression. *Science* 254(5032):719–721.
- Metzger F, Kapfhammer JP (2000) Protein kinase C activity modulates dendritic differentiation of rat Purkinje cells in cerebellar slice cultures. *Eur J Neurosci* 12(6):1993–2005.
- Lin YC, Koleske AJ (2010) Mechanisms of synapse and dendrite maintenance and their disruption in psychiatric and neurodegenerative disorders. *Annu Rev Neurosci* 33:349–378.
- Kano M, Hashimoto K (2009) Synapse elimination in the central nervous system. *Curr Opin Neurobiol* 19(2):154–161.
- Hashimoto K, Kano M (2003) Functional differentiation of multiple climbing fiber inputs during synapse elimination in the developing cerebellum. *Neuron* 38(5):785–796.
- Chedotal A, Sotelo C (1992) Early development of olivocerebellar projections in the fetal rat using CGRP immunocytochemistry. *Eur J Neurosci* 4(11):1159–1179.
- Mandolesi G, et al. (2009) Distribution of the SNAP25 and SNAP23 synaptosomal-associated protein isoforms in rat cerebellar cortex. *Neuroscience* 164(3):1084–1096.
- Montani L, et al. (2009) Neuronal Nogo-A modulates growth cone motility via RhoGTPase/LIMK1/cofilin in the unlesioned adult nervous system. *J Biol Chem* 284(16):10793–10807.
- Wills ZP, et al. (2012) The nogo receptor family restricts synapse number in the developing hippocampus. *Neuron* 73(3):466–481.
- Foscarin S, et al. (2009) Overexpression of GAP-43 modifies the distribution of the receptors for myelin-associated growth-inhibitory proteins in injured Purkinje axons. *Eur J Neurosci* 30(10):1837–1848.
- Wang X, et al. (2002) Localization of Nogo-A and Nogo-66 receptor proteins at sites of axon-myelin and synaptic contact. *J Neurosci* 22(13):5505–5515.
- Niederöst B, Oertle T, Fritsche J, McKinney RA, Bandtlow CE (2002) Nogo-A and myelin-associated glycoprotein mediate neurite growth inhibition by antagonistic regulation of RhoA and Rac1. *J Neurosci* 22(23):10368–10376.
- Li Z, Aizenman CD, Cline HT (2002) Regulation of rho GTPases by crosstalk and neuronal activity in vivo. *Neuron* 33(5):741–750.
- Engert F, Bonhoeffer T (1999) Dendritic spine changes associated with hippocampal long-term synaptic plasticity. *Nature* 399(6731):66–70.
- Maletic-Savatic M, Malinow R, Svoboda K (1999) Rapid dendritic morphogenesis in CA1 hippocampal dendrites induced by synaptic activity. *Science* 283(5409):1923–1927.
- Smith SL, Otis TS (2003) Persistent changes in spontaneous firing of Purkinje neurons triggered by the nitric oxide signaling cascade. *J Neurosci* 23(2):367–372.
- Dodd DA, et al. (2005) Nogo-A, -B, and -C are found on the cell surface and interact together in many different cell types. *J Biol Chem* 280(13):12494–12502.
- Nie DY, et al. (2003) Nogo-A at CNS paranodes is a ligand of Caspr: Possible regulation of K(+) channel localization. *EMBO J* 22(21):5666–5678.
- Schulz DJ (2006) Plasticity and stability in neuronal output via changes in intrinsic excitability: It's what's inside that counts. *J Exp Biol* 209(Pt 24):4821–4827.
- Mandolesi G, et al. (2009) GluRdelta2 expression in the mature cerebellum of hotfoot mice promotes parallel fiber synaptogenesis and axonal competition. *PLoS ONE* 4(4):e5243.
- Hashimoto K, et al. (2001) Roles of glutamate receptor delta 2 subunit (GluRdelta 2) and metabotropic glutamate receptor subtype 1 (mGluR1) in climbing fiber synapse elimination during postnatal cerebellar development. *J Neurosci* 21(24):9701–9712.
- Miyazaki T, et al. (2006) Disturbance of cerebellar synaptic maturation in mutant mice lacking BSRPs, a novel brain-specific receptor-like protein family. *FEBS Lett* 580(17):4057–4064.
- Watake K, et al. (1998) Motor discoordination and increased susceptibility to cerebellar injury in GLAST mutant mice. *Eur J Neurosci* 10(3):976–988.
- Watanabe M (2008) Molecular mechanisms governing competitive synaptic wiring in cerebellar Purkinje cells. *Tohoku J Exp Med* 214(3):175–190.
- Watanabe F, et al. (2008) Effects of FAK ablation on cerebellar foliation, Bergmann glia positioning and climbing fiber territory on Purkinje cells. *Eur J Neurosci* 27(4):836–854.
- Sivasankaran R, et al. (2004) PKC mediates inhibitory effects of myelin and chondroitin sulfate proteoglycans on axonal regeneration. *Nat Neurosci* 7(3):261–268.
- Kano M, et al. (1995) Impaired synapse elimination during cerebellar development in PKC gamma mutant mice. *Cell* 83(7):1223–1231.
- Maeder CI, Shen K (2011) Genetic dissection of synaptic specificity. *Curr Opin Neurobiol* 21(1):93–99.
- Margate MA, Shen K (2010) Molecular mechanisms of synaptic specificity. *Mol Cell Neurosci* 43(3):261–267.
- O'Connor TP, et al. (2009) Semaphorin 5B mediates synapse elimination in hippocampal neurons. *Neural Dev* 4:18.
- Vanderhaeghen P, Cheng HJ (2010) Guidance molecules in axon pruning and cell death. *Cold Spring Harb Perspect Biol* 2(6):a001859.
- Cesa R, et al. (2011) Eph receptors are involved in the activity-dependent synaptic wiring in the mouse cerebellar cortex. *PLoS ONE* 6(4):e19160.
- Nishida K, Flanagan JG, Nakamoto M (2002) Domain-specific olivocerebellar projection regulated by the EphA-ephrin-A interaction. *Development* 129(24):5647–5658.
- Hashimoto K, Ichikawa R, Kitamura K, Watanabe M, Kano M (2009) Translocation of a "winner" climbing fiber to the Purkinje cell dendrite and subsequent elimination of "losers" from the soma in developing cerebellum. *Neuron* 63(1):106–118.
- Uemura T, et al. (2010) Trans-synaptic interaction of GluRdelta2 and Neurexin through Cbln1 mediates synapse formation in the cerebellum. *Cell* 141(6):1068–1079.
- Santos Da Silva J, Schubert V, Dotti CG (2004) RhoA, Rac1, and cdc42 intracellular distribution shift during hippocampal neuron development. *Mol Cell Neurosci* 27(1):1–7.
- Fischer M, Kaech S, Knutti D, Matus A (1998) Rapid actin-based plasticity in dendritic spines. *Neuron* 20(5):847–854.
- Willi R, Aloy EM, Yee BK, Feldon J, Schwab ME (2009) Behavioral characterization of mice lacking the neurite outgrowth inhibitor Nogo-A. *Genes Brain Behav* 8(2):181–192.

Supporting Information

Petrinovic et al. 10.1073/pnas.1214255110

SI Materials and Methods

Animals. Nogo-A knockout (KO) [pure C57BL/6 background; postnatal day (P) 4–60] and transgenic mice overexpressing Nogo-A exclusively in Purkinje cells (PC) under the L7 promoter (L7–Nogo-A TG) (in FVB/N background; P4–P60) were used in this study. Wild-type (WT) mice of both C57BL/6 and FVB/N strains were used as respective controls. All animal experiments were performed according to the guidelines of the Veterinary Office of the Canton of Zürich, Switzerland, and approved by its Commission for Animal Research. All efforts were made to minimize animal suffering and to reduce the number of animals required.

Nogo-A KO mice were generated by homologous recombination of exons 2 and 3 in the Nogo-A gene as described previously (1). Animals were backcrossed with C57BL/6 WT mice for more than 10 generations resulting in strain purity of > 99.98% (2). The backcrossed heterozygous mice were then bred to get homozygous WT or KO mice. The generation of transgenic mice overexpressing Nogo-A under the cerebellar PC-specific L7 promoter (3, 4) has been previously described (5). In this study we used line 24 in which the rat Nogo-A transgene is expressed in all cerebellar PCs.

Antibodies. For immunohistochemical detection of Nogo-A we used the polyclonal rabbit antibody Rb173A (Laura, 1:200), which recognizes the Nogo-A-specific region (amino acids 174–979) (6, 7). The polyclonal rabbit antibody Rb1 (Bianca) which is specific for the N terminus of Nogo-A and Nogo-B (amino acids 1–172, 1:15,000) (6, 7) was used for immunodetection of these two proteins in cerebellar lysates. Monoclonal antibody 3D11, which recognizes the C-terminal part of a rat but not mouse Nogo-A-specific region (amino acids 910–920, 1:50) (7) was used for the detection of the transgene in L7–Nogo-A TG mice. Polyclonal goat antibody against NgR1 (R&D Systems; 1:500) was used for detection of this Nogo-A receptor and anti-calbindin D-28k (Swant; 1:500) antibody was used for immunohistochemical identification of PCs. Anti-vesicular glutamate transporter 1 (VGluT1) antibody (Synaptic Systems; 1:1,000) and anti-vesicular glutamate transporter 2 (VGluT2) antibody (Synaptic Systems; 1:1,000) were used for immunohistochemical identification of parallel (PF) and climbing fiber (CF) terminals, respectively, as well as for identification of respective proteins in cerebellar tissue lysates. Antibodies against CaMKII (Upstate; 1:1,000), PSD95 (Abcam; 1:1,000), SNAP25 (Chemicon; 1:500), GluR2/3 [gift from P. Streit (Brain Research Institute, University of Zurich, Zurich, Switzerland); 1:500], GluR1 (gift from P. Streit; 1:500), phospho-PKC γ (Abcam; 1:1,000), and Homer (Synaptic Systems; 1:500) were used for detection of these proteins in cerebellar tissue lysates. Monoclonal antiglyceraldehyde-3-phosphate dehydrogenase (GAPDH) antibody served as a protein loading control on Western blots (Abcam; 1:10,000).

The following secondary antibodies were used: horseradish peroxidase (HRP)-conjugated goat anti-mouse IgG (Pierce; 1:15,000), HRP-conjugated donkey anti-rabbit IgG (Pierce; 1:10,000), HRP-conjugated mouse anti-goat IgG (Pierce; 1:10,000), Cy3-coupled goat anti-rabbit IgG (Jackson ImmunoResearch Laboratories; 1:3,000), Cy3-coupled goat anti-mouse IgG (Jackson ImmunoResearch Laboratories; 1:2,000), Cy2-coupled goat anti-mouse IgG (Jackson ImmunoResearch Laboratories; 1:2,000), Cy3-coupled mouse anti-goat IgG (Jackson ImmunoResearch Laboratories; 1:3,000), and DyLight 640 streptavidin (Jackson ImmunoResearch Laboratories; 1:1,000).

Immunoblotting. Mice were killed by cervical dislocation and the cerebella were quickly removed and sectioned into 400- μ m thick sagittal slices using a McIlwain tissue chopper. The slices were then submerged in ice-cold phosphate buffer (pH 7.4), the deep white matter was removed, and the molecular layer was then quickly hand dissected under a dissection microscope (8) and subsequently flash frozen in liquid nitrogen. The tissues were then stored at -80°C until extraction in lysis buffer (50 mM NaH_2PO_4 , 150 mM NaCl, 0.5% CHAPS, pH 8.0) containing protease inhibitors (Complete Mini; Roche Diagnostics). After homogenization, samples were centrifuged for 15 min at $2,000 \times g$ at 4°C , and the protein concentration of the supernatant was determined using NanoDrop ND 1000 (NanoDrop Technologies, ThermoFisher Scientific). Protein samples (30 μ g) were separated by electrophoresis on 4–12% NuPAGE gels (Invitrogen) and electroblotted to polyvinylidene difluoride membranes (Millipore). Membranes were incubated in 3% (wt/vol) Top Block (Lubio Science)/0.1% TBST (0.1 M Tris base, 0.1% Tween 20, pH 7.4) for 1 h at room temperature, followed by incubation with primary antibodies overnight at 4°C . Immunoreactivity was visualized using HRP-conjugated secondary antibodies and a chemiluminescent substrate (SuperSignal West Pico; Pierce). Images were captured with the Stella system (Rytest) and densitometry analysis was performed with ImageJ software (National Institutes of Health, NIH). Quantification was done by normalizing the protein band intensities to GAPDH values.

Immunohistochemistry. Mice were deeply anesthetized with pentobarbital (Nembutal, 75 mg/100 g body weight; Abbott Laboratories) and transcardially perfused with PBS (pH 7.4), followed by 4% (wt/vol) paraformaldehyde (PFA)/0.05% glutaraldehyde solution in PBS. The cerebella were then removed and postfixed in 4% PFA either overnight (P14–P60 mice) or for 2 d (P4–P7 mice). After cryoprotection in 30% (wt/vol) sucrose the cerebella were rapidly frozen on dry ice and stored at -80°C . Forty-micrometer-thick sagittal sections were cut on a cryostat and collected in cold PBS. Tissue sections were stained with Cresyl violet, and images were taken with a Zeiss Axiophot microscope equipped with a cooled CCD camera (CoolSNAP HQ; Photometrics). For immunofluorescence, free floating tissue sections were permeabilized and nonspecific protein interactions were reduced by incubation in a blocking buffer [4% (vol/vol) normal goat serum, 0.3% Triton X-100 in TBS, pH 8.0] for 30 min at room temperature. Primary antibodies were applied overnight at 4°C and after washing with TBS, sections were incubated with the appropriate secondary antibody for 2 h at room temperature. Finally, sections were mounted on Superfrost-Plus slides (Menzel-Gläser) and coverslipped with Mowiol.

Epifluorescence images were acquired with a cooled CCD camera (CoolSNAP HQ; Photometrics) coupled to a Zeiss Axiophot microscope interfaced by the MCID/M2 Imaging System (Imaging Research). A 5 \times objective (PLAN NEOFLUAR, NA 0.15) was used. Confocal imaging was performed by using a Spectral Confocal Microscope TCS SP2 AOBS (Leica) and a 5 \times (HC PL FLUOTAR, NA 0.15), 20 \times (HC PL FLUOTAR, NA 0.50), and a 63 \times oil immersion objective (HCX PL APO Oil, NA 1.32). The pinhole was set at 1 Airy unit. Double-immunofluorescence staining was visualized with sequential acquisition of separate color channels to avoid cross-talk between fluorochromes.

Quantitative Measurements and Data Analysis. As the cerebellar lobules, and even different regions of the same lobule, mature at different time points (9), and as the CF innervation of PCs in the sulcus is different from that in the bank and gyrus subdivisions (10), we analyzed the bank and gyrus regions of the lobules IV/V, VI/VII, and IX in each animal. Quantification was done in a blind manner with respect to the genotypes.

To evaluate quantitative differences in CF extensions between normal and mutant cerebella, we measured the distance from the base of the molecular layer to the most distal tips of continuous VGluT2 immunopositive puncta, which ascended along the dendritic tree of a given PC, relative to the vertical length of the entire molecular layer. Furthermore, to estimate the translocation of CFs from the soma to dendrites of PCs, they were divided into three categories: PCs without VGluT2⁺ CF varicosities on their soma, PCs with one to five VGluT2⁺ CF terminals, and PCs with more than six VGluT2⁺ CF varicosities. The sample size was: WT/BL6 ($n = 120$ cells from six mice), Nogo-A KO ($n = 126$ cells from six mice), WT/FVB ($n = 132$ cells from six mice), and L7–Nogo-A TG ($n = 127$ cells from six mice).

For quantification of VGluT1⁺ and VGluT2⁺ terminals, confocal imaging was performed by using a Spectral Confocal Microscope TCS SP2 AOBS (Leica) and a 63 \times oil immersion objective (HCX PL APO Oil, NA 1.32). Confocal image acquisition consisted of 12 images in the z dimension with a step size of 0.7 μm and image size of 0.36 μm per pixel (1,024 \times 1,024). Double-immunofluorescence staining was visualized with sequential acquisition of separate color channels to avoid cross-talk between fluorochromes. Quantification of VGluT1⁺ and VGluT2⁺ terminals was done by using ImageJ software (NIH). The sample size for VGluT1 was: WT/BL6 ($n = 118$ cells from six mice), Nogo-A KO ($n = 129$ cells from six mice), WT/FVB ($n = 145$ cells from six mice), and L7–Nogo-A TG ($n = 133$ cells from six mice); the sample size for VGluT2 was: WT/BL6 ($n = 105$ cells from six mice), Nogo-A KO ($n = 116$ cells from six mice), WT/FVB ($n = 114$ cells from six mice), and L7–Nogo-A TG ($n = 103$ cells from six mice).

Acute Cerebellar Slices. Acute cerebellar slices were prepared from P28 mice anesthetized with Halothane (Sigma). After decapitation, the vermis was removed and mounted in a chamber filled with cooled (0–3 $^{\circ}\text{C}$) extracellular solution containing the following (mmol): 120 NaCl, 26 NaHCO₃, 2 KCl, 2 CaCl₂, 1.19 MgSO₄, 1.18 NaH₂PO₄, and 11 glucose (osmolality 285–295 mosmol/kg, pH 7.4 when equilibrated with 95% O₂–5% CO₂). The 225- μm -thick slices were cut using a VT1000S slicer (Leica Instruments) and incubated in oxygenated extracellular solution at 32 $^{\circ}\text{C}$ for at least 30 min before they were transferred to the recording chamber mounted on the stage of an upright microscope (Zeiss; Axioskop 2) where they were continuously perfused with oxygenated extracellular solution at room temperature. Midsagittal slices were used for all of the experiments except for those requiring PF stimulation for which horizontal slices were used. For the study of excitatory synaptic transmission, 20 μM picrotoxin (Sigma) was added to the extracellular medium. PCs were visually identified and recorded using the perforated-patch configuration of the patch clamp technique (11).

Electrophysiology. Patch pipettes were made of borosilicate glass (Hilgenberg) with resistances of 2–6 M Ω when filled with the patch pipette solution containing the following (mmol): 80 K₂SO₄, 10 NaCl, 15 glucose, 5 Hepes (osmolality 230 mosmol/kg, pH adjusted to 7.2 with KOH). Recordings were performed for both current- and voltage-clamp modes using an EPC 10 amplifier (HEKA) or an Axopatch 500B (Molecular Devices) with an ITC16 analog-to-digital converter (Instrutech) and an 8-pole analog Bessel low-pass filter (Frequency Devices). All current-clamp recordings were made using the fast current-clamp mode of the

amplifiers. Stimulus generation and data acquisition were made with Pulse 8.65 software (HEKA). Spontaneous and depolarization-evoked potential signals were filtered at 4 kHz and digitally sampled at 20 kHz. Evoked postsynaptic currents were filtered at 2 kHz and digitally sampled at 10 kHz. Evoked postsynaptic potentials (complex spikes) were filtered at 20 kHz and digitally sampled at 100 kHz.

Spontaneous action potential firing frequency was analyzed from current-clamp recordings. Intrinsic excitability was investigated by setting the membrane potential at –80 mV and injecting 1-s steps of depolarizing current (from 0 to 2.5 nA in 50-pA increments). When injected with sufficient depolarizing current, PCs generated repetitive spikes. Action potential frequency was measured as the action potential frequency remains stable for a given injected current intensity. The average frequency over the time of current injection was measured by dividing the number of interspike intervals by the time interval between the first and the last spike. These values were used to construct current–frequency plots. A close-to-linear relationship between frequency and current is observed (12). The slope of the first six points of the current–frequency curve was used as a measure of the intrinsic cell excitability. The sample size was: WT/BL6 ($n = 21$ cells from four mice), Nogo-A KO ($n = 25$ cells from six mice), WT/FVB ($n = 24$ cells from six mice), and L7–Nogo-A TG ($n = 26$ cells from five mice).

Parallel fiber stimulation. For PF stimulation, a patch pipette filled with 0.9% NaCl was placed in the molecular layer at about two-thirds of the distance between the PC layer and the pial surface. The holding potential was set at –90 mV. Negative current pulses ranging from 0 to 8 μA with duration of 150 μs were delivered in ascending order with 1- μA increments at 5-s intervals. These pulses were generated by an Iso-flex stimulus isolation unit (AMPI) driven by a programmable Master 8 Stimulator/Pulse generator (AMPI) synchronized with data acquisition through Pulse software. PF excitatory postsynaptic currents (EPSCs) were identified by their characteristic features (graded response amplitude and paired-pulse facilitation) (13). EPSC amplitude was measured as the difference between the current baseline level before the stimulus artifact and the peak of the EPSC. For each stimulus intensity, a single EPSC value was calculated as the mean of three successive evoked responses. Linear fits were obtained from EPSC slope values in each cell for the first eight points of the stimulus–response curve. Input–output relations measuring EPSC initial slope (pA/ms, output) as a function of PF stimulus intensity (μA , input) were established for each recorded neuron. Because this relation is linear, we used the mean linear slope factor for the first eight points of the stimulus–response curve to compare the synaptic strength of the PF–PC synapse. Paired-pulse facilitation (PPF) was elicited by twin pulses at different time intervals (5–245 ms by 2-ms increments) as previously described (14). A single EPSC value was calculated as the mean of five successive evoked responses. PPF ratio was expressed as the difference between the second and the first EPSC divided by the size of the first EPSC. To elicit CF responses, the stimulating micropipette was placed in the granule cell layer and moved in the vicinity of the recorded PC until the typical response characterized by multiple wavelets (complex spike) was obtained. The membrane potential was set at –90 mV with constant current injection. The sample size was: WT/BL6 ($n = 23$ cells from four mice), Nogo-A KO ($n = 20$ cells from six mice), WT/FVB ($n = 19$ cells from five mice), and L7–Nogo-A TG ($n = 25$ cells from four mice).

Climbing fiber stimulation. PCs were patched with a patch pipette (2–4 M Ω) filled with a solution containing (mmol): 100 CsCl, 35 Cs-sulfonate, 11 Tris-phosphocreatine, 10 Hepes, 4.5 Mg ATP, 0.3 Tris-GTP, (osmolality: 298 mosmol, pH adjusted to 7.25 with NaOH). To inactivate voltage-dependent conductances and to reduce the driving force and current amplitudes, the holding

potential was set at -10 mV. For CF stimulation, a patch pipette (1 M Ω) filled with artificial cerebrospinal fluid (CSF) was placed in the granule cell layer, in the vicinity of the PC, and moved until the CF response could be elicited with a minimal stimulus intensity. Two current pulses (0.1 ms, paired-pulse interval: 100 ms) were applied every 20 s. These pulses were generated by a stable IS4 stimulator (SC Devices). Subsequently, the stimulus intensity was lowered until all synaptic responses disappeared, then increased again and the increase in the synaptic response as a function of the stimulus intensity was analyzed. Only events with a clear threshold and showing paired-pulse depression were counted as CF responses. Cells with a single threshold were classified as monoinnervated, whereas cells with more than one threshold event were classified as polyinnervated. The sample size for P14 was: WT/BL6 ($n = 26$ cells from six mice), Nogo-A KO ($n = 29$ cells from eight mice); and for P28: WT/BL6 ($n = 28$ cells from eight mice) and Nogo-A KO ($n = 30$ cells from seven mice).

Morphological Reconstruction of Single Purkinje Cells. In a separate series of whole-cell recordings used for morphological reconstruction, the intracellular solution contained (mmol): 126 K gluconate, 0.05 CaCl₂, 0.15 BAPTA, 4 NaCl, 1 MgSO₄, 15 glucose, 5 Hepes, 3 Mg ATP, 0.1 GTP (pH adjusted to 7.2 with KOH), and 0.4% biocytin (Sigma). Granule cell migration, which defines the depth of the molecular layer, was always complete. Purkinje cells, situated in the bank and gyrus regions of lobules IV/V, VI/VII, and IX, were filled with biocytin during 15 min and fluorescence was subsequently revealed by cytochemistry. To this end, slices were fixed by immersion in 4% PFA overnight and biocytin was revealed with streptavidin-conjugated fluorescein isothiocyanate (FITC, Jackson Immunoresearch; 1:200). After three rinses in TBS, slices were mounted on coverslips with "Slow Fade Light" (Invitrogen) mounting medium in 50% (vol/vol) glycerol and secured with nail polish. Images of the fluorescent cells were acquired using a LSM 510 META laser scanning confocal system (Zeiss) mounted on an Axiovert 200M inverted microscope (Zeiss) equipped with c-Achroplan NIR 40 \times /0.8 W objective (Zeiss). Images of the dendritic endings were acquired on the same system with a c-Apochromat 63 \times /1.2 W objective (Zeiss). The excitation beam of an Argon laser (488 nm) and band-pass emission filters (500–550 nm) were used for selective detection of the green fluorochrome. Sequential optical sections of 2048 \times 2048 pixels were taken at 1.0- μ m intervals along the z axis to allow 3D reconstruction. Possible distortion caused by the histological processing has been shown to cause less than 5% error on estimated length (15). Data acquisition and analysis were performed in a blind manner with respect to the genotypes. The sample size for quantitative image analysis was: WT/BL6 ($n = 14$ cells from 3 mice), Nogo-A KO ($n = 24$ cells from four mice), WT/FVB ($n = 11$ cells from four mice), L7-Nogo-A TG ($n = 18$ cells from three mice).

Morphometric Analysis of Purkinje Cell Dendrites and Spines. Cellular volumes were computed by evaluating the number of voxels inside the cells. For each cell, the threshold value defining the cell surface was set using the ISODATA algorithm implemented in ImageJ software (NIH). The total number of voxels inside the cell was then evaluated using the VoxelCounter plugin for ImageJ software (NIH) and multiplied by the unitary voxel volume. 2D fractal dimensions were obtained on z -projections with the box counting method using the FracLac 2.3 plugin for ImageJ software (NIH).

Due to the complexity of the PC dendritic tree, the skeletonization algorithms available in existing software (Imaris, NeuroLucida) give unreliable results and do not allow a quantitative analysis of the dendritic structure. Therefore, we have chosen to use the computation of the fractal dimension as a measure of the overall complexity of the object in 2D images obtained by doing

z -projections of the images stacks. Neurons can indeed be represented as fractal or space-filling objects and the fractal dimension represents a very good parameter for the characterization of the dendritic structure (16–20). Furthermore, as shown by Jelinek and Fernandez (19), the shrinkage or expansion of a neuron due to the experimental manipulation will not affect their fractal values as long as the artifact acts equally in all directions and the measured points still lie on the linear segment of the graph. Therefore, fractal dimensions of different neurons that have been processed in different batches or at different laboratories can be compared directly if the same methodology for calculating fractal dimensions is applied.

The average width of distal dendritic segments was evaluated by measuring the apparent area in z -projection. Dendritic spine number per unit length (spine density) was counted on z -projections and divided by the length of the dendrites. The sample size was: WT/BL6 ($n = 14$ cells from 3 mice), Nogo-A KO ($n = 24$ cells from 4 mice), WT/FVB ($n = 11$ cells from four mice), L7-Nogo-A TG ($n = 18$ cells from three mice).

Anterograde Tracing of Climbing Fibers. The anterograde tracing of CFs was performed in P7 and P21 WT/BL6 and Nogo-A KO mice as described previously (21, 22). P7 animals were placed on ice for 4.5 min to induce anesthesia by hypothermia. P21 mice were anesthetized with a s.c. injection of Hypnorm (0.047 mg/100 g, VetaPharma) and Dormicum (1.5 mg/100 g, Roche Diagnostics). Animals were mounted in a rodent stereotaxic frame and the cerebellomedullary cistern was identified by palpation. After opening the skin, muscle layers and connective tissue were opened along the sagittal midline leaving the ligament intact. A 10- μ L NanoFil syringe with a 33 gauge bevelled needle (World Precision Instruments) was aligned to the occipital bone at the cerebellomedullary cistern. The needle was then slowly lowered to a final depth of 2.5–2.7 mm bellow the ligament in P7 animals and to 2.7–3.0 mm in P21 mice. By moving the needle slowly down and constantly observing the skull and the needle shaft we identified the depth of the floor of the occipital bone. The needle was then retracted for 0.3 mm from the ventral surface and 1 μ L of 10% (vol/vol) biotinylated dextran amine (BDA) (Invitrogen) solution was slowly injected (50 nL/s). After being kept in place for additional 2 min, the needle was slowly retracted and the wound was closed with Histoacryl (BBraun). Seven days after the surgery, animals were perfused with 4% (wt/vol) PFA and the brains were collected and processed for immunohistochemistry (as described above). After staining with anticalbindin and anti-VGluT2 antibodies (as described in *Immunohistochemistry*), tissue sections were stained for 30 min with Cy5-conjugated streptavidin to visualize the BDA-labeled CFs. The sample size for quantitative image analysis for P14 was: WT/BL6 ($n = 24$ cells from five mice), Nogo-A KO ($n = 21$ cells from four mice); and for P28: WT/BL6 ($n = 21$ cells from six mice) and Nogo-A KO ($n = 19$ cells from four mice).

Electron Microscopy. Mice were deeply anesthetized with pentobarbital (Nembutal, 75 mg/100 g body weight; Abbott Laboratories) and transcardially perfused with 0.1 M PBS (pH 7.4), followed by 4% (wt/vol) PFA/0.05% glutaraldehyde solution in 0.1 M PBS (pH 7.4). The cerebella were dissected and postfixed in the same solution for 4 h. Forty-micrometer-thick parasagittal sections were cut on a cryostat and postfixed in 2% (wt/vol) OsO₄ at 4 $^{\circ}$ C for 1 h (23). After dehydration in ethanol, the sections were contrasted in 0.5% uranyl acetate in 95% (vol/vol) ethanol for 1 h and embedded in Epon. Ultrathin sections of 80 nm were analyzed in a Zeiss EM10 electron microscope. Excitatory synapses were identified in electron micrographs as mushroom-shaped spines containing a postsynaptic density (PSD) juxtaposed to a presynaptic terminus with associated synaptic vesicles according to previously described criteria (23). PSD length of at

least 70 spines per animal was determined in the upper half of the molecular layer by using ImageJ software (NIH). All measurements were made by an experimenter blinded to the sample identity.

For immunolocalization of Nogo-A and NgR1, 50- μm -thick cerebellar cryosections were treated with freshly made 0.5% NaBH_4 in TBS for 10 min to reduce the background staining. Sections were then rinsed several times in TBS and incubated overnight with the primary antibody (Laura, 1:200; NgR1, 1:500). Sections were subsequently treated with 0.025% 3,3'-diaminobenzidine tetrahydrochloride (DAB) in the presence of 0.006% H_2O_2 for 15 min. DAB staining was subsequently intensified by methanamine silver-gold reaction according to the protocol of

Teclerariam-Mesbah et al. (24). The high electron density of gold-substituted silver grains facilitates ultrastructural recognition of stained structures. Finally, sections were osmicated, embedded in Epon, and ultrathin sections of 100 nm were analyzed in a Zeiss EM10 electron microscope.

Statistical Analysis. All data are shown as mean values \pm SEM and considered significant at a level of $P < 0.05$. Two-way ANOVA test was used for comparison of paired-pulse facilitation data, whereas the significance between groups in all of the other measurements was calculated using Student's t test. Graphs were generated using GraphPad Prism. The levels of significance are indicated as follows: * $P < 0.05$, ** $P < 0.01$, *** $P < 0.001$.

1. Simonen M, et al. (2003) Systemic deletion of the myelin-associated outgrowth inhibitor Nogo-A improves regenerative and plastic responses after spinal cord injury. *Neuron* 38(2):201–211.
2. Dimou L, et al. (2006) Nogo-A-deficient mice reveal strain-dependent differences in axonal regeneration. *J Neurosci* 26(21):5591–5603.
3. Oberdick J, Smeyne RJ, Mann JR, Zackson S, Morgan JI (1990) A promoter that drives transgene expression in cerebellar Purkinje and retinal bipolar neurons. *Science* 248(4952):223–226.
4. Smeyne RJ, et al. (1991) Dynamic organization of developing Purkinje cells revealed by transgene expression. *Science* 254(5032):719–721.
5. Aloy EM, et al. (2006) Synaptic destabilization by neuronal Nogo-A. *Brain Cell Biol* 35(2-3):137–156.
6. Dodd DA, et al. (2005) Nogo-A, -B, and -C are found on the cell surface and interact together in many different cell types. *J Biol Chem* 280(13):12494–12502.
7. Oertle T, et al. (2003) Nogo-A inhibits neurite outgrowth and cell spreading with three discrete regions. *J Neurosci* 23(13):5393–5406.
8. Sandoval ME, Cotman CW (1978) Evaluation of glutamate as a neurotransmitter of cerebellar parallel fibers. *Neuroscience* 3(2):199–206.
9. Altman J (1972) Postnatal development of the cerebellar cortex in the rat. I. The external germinal layer and the transitional molecular layer. *J Comp Neurol* 145(3):353–397.
10. Nishiyama H, Linden DJ (2004) Differential maturation of climbing fiber innervation in cerebellar vermis. *J Neurosci* 24(16):3926–3932.
11. Horn R, Marty A (1988) Muscarinic activation of ionic currents measured by a new whole-cell recording method. *J Gen Physiol* 92(2):145–159.
12. Llinás R, Sugimori M (1979) Calcium conductances in Purkinje cell dendrites: Their role in development and integration. *Prog Brain Res* 51:323–334.
13. Konnerth A, Keller BU, Lev-Tov A (1990) Patch clamp analysis of excitatory synapses in mammalian spinal cord slices. *Pflügers Arch* 417(3):285–290.
14. Sacchetti B, Scelfo B, Tempia F, Strata P (2004) Long-term synaptic changes induced in the cerebellar cortex by fear conditioning. *Neuron* 42(6):973–982.
15. Roth A, Häusser M (2001) Compartmental models of rat cerebellar Purkinje cells based on simultaneous somatic and dendritic patch-clamp recordings. *J Physiol* 535(Pt 2):445–472.
16. Alves SG, Martins ML, Fernandes PA, Pittella JEH (1996) Fractal patterns for dendrites and axon terminals. *Physica A* 232(1-2):51–60.
17. Billeci L, Pioggia G, Vaglini F, Ahluwalia A (2010) Automated extraction and classification of dynamic metrical features of morphological development in dissociated Purkinje neurons. *J Neurosci Methods* 185(2):315–324.
18. Caserta F, et al. (1995) Determination of fractal dimension of physiologically characterized neurons in two and three dimensions. *J Neurosci Methods* 56(2):133–144.
19. Jelinek HF, Fernandez E (1998) Neurons and fractals: How reliable and useful are calculations of fractal dimensions? *J Neurosci Methods* 81(1-2):9–18.
20. Takeda T, Ishikawa A, Ohtomo K, Kobayashi Y, Matsuoka T (1992) Fractal dimension of dendritic tree of cerebellar Purkinje cell during onto- and phylogenetic development. *Neurosci Res* 13(1):19–31.
21. Lorenzetto E, et al. (2009) Genetic perturbation of postsynaptic activity regulates synapse elimination in developing cerebellum. *Proc Natl Acad Sci USA* 106(38):16475–16480.
22. Miyazaki T, Hashimoto K, Shin HS, Kano M, Watanabe M (2004) P/Q-type Ca^{2+} channel $\alpha 1A$ regulates synaptic competition on developing cerebellar Purkinje cells. *J Neurosci* 24(7):1734–1743.
23. Schikorski T, Stevens CF (1997) Quantitative ultrastructural analysis of hippocampal excitatory synapses. *J Neurosci* 17(15):5858–5867.
24. Teclerariam-Mesbah R, Wortel J, Romijn HJ, Buijs RM (1997) A simple silver-gold intensification procedure for double DAB labeling studies in electron microscopy. *J Histochem Cytochem* 45(4):619–621.

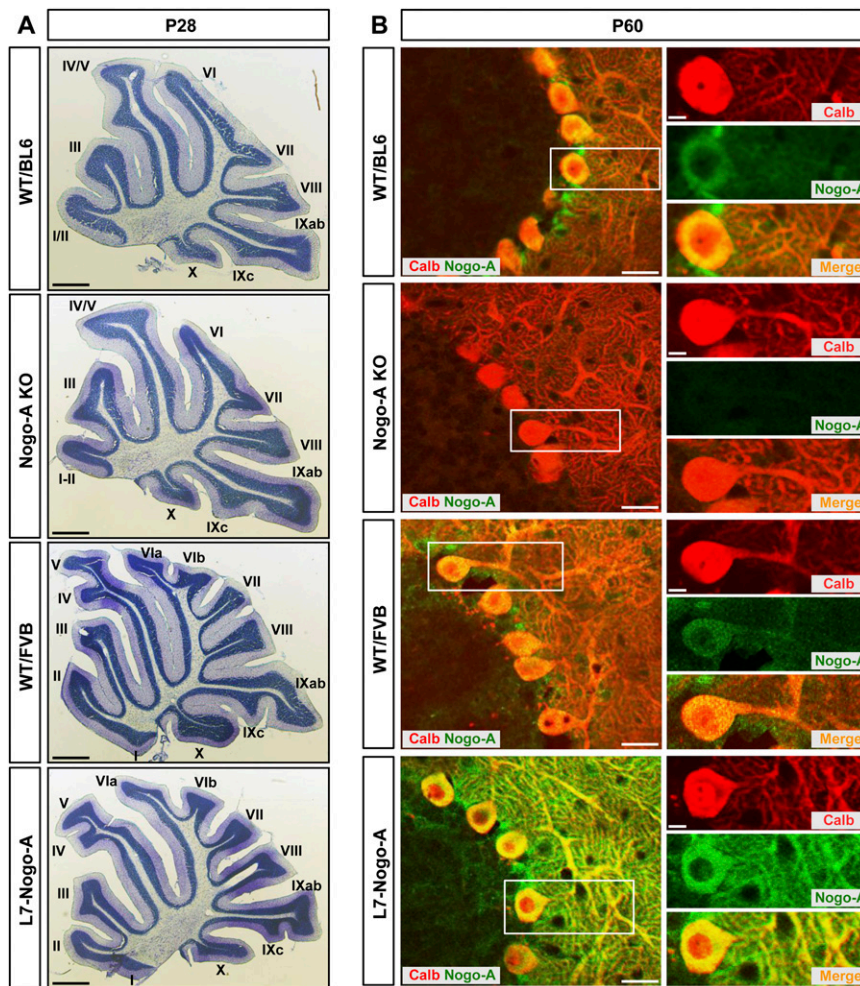


Fig. 51. Histological and immunohistochemical analysis of cerebella of wild-type and mutant mice. (A) Nissl-stained sagittal cerebellar sections from P28 Nogo-A KO, L7-Nogo-A TG, and corresponding WT mice. The lobule number is indicated by the numbers I–X. The cerebella of mutant mice show similar size, foliation, laminar organization, and histology to that of strain-matched control animals. (Scale bars, 300 μm .) (B) Expression of Nogo-A in the cerebellum of WT and mutant mice. Double immunolabeling with anti-calbindin (red) and anti-Nogo-A (green) antibodies revealed the low expression level of Nogo-A in PCs of adult (P60) WT mice of both strains, whereas it was highly expressed in PCs of L7-Nogo-A TG animals. Note the small calbindin⁻ but Nogo-A⁺ cells in the PC layer, which may correspond to candelabrum cells. Nogo-A was not detected in PCs of Nogo-A KO mice. Higher power micrographs correspond to the boxed regions. (Scale bars, 20 μm ; 4 μm in the *Insets*.)

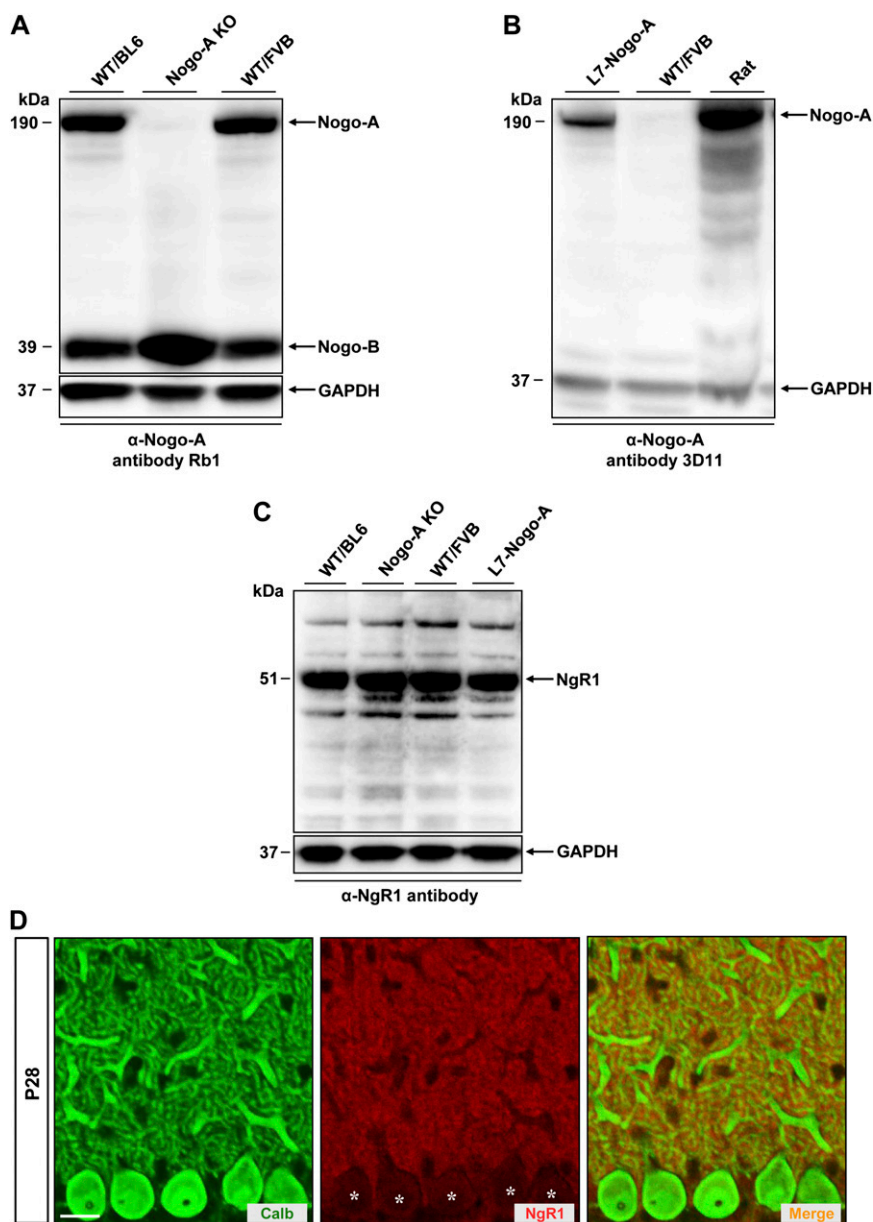


Fig. S2. Western blot analysis of Nogo-A and NgR1 expression in the cerebellar lysates of wild-type and mutant mice. (A) Immunoblotting with affinity-purified anti-Nogo-A antiserum Rb1 (Bianca) showing the expression of both Nogo-A and Nogo-B in the cerebella of P28 WT mice of C57BL/6 and FVB strain. A total of 30 μ g of protein was loaded in each lane. Molecular markers are indicated on the *Left*. No difference in either Nogo-A or Nogo-B expression levels were detected due to the strain differences. This antibody shows no Nogo-A band in the Nogo-A KO cerebellar lysate, thus confirming its specificity. (B) Western blot analysis of a Nogo-A transgene expression in the cerebellar lysates (30 μ g of protein per lane) of a P28 rat, WT/FVB, and L7-Nogo-A TG mice. In addition to confirming the presence of the transgene in the cerebellar lysates of L7-Nogo-A TG mice, the 3D11 antibody, specific for the rat Nogo-A, gave no detectable band in the cerebellar lysate of WT/FVB mice thus confirming its specificity. (C) Immunoblot analysis of NgR1 protein expression in cerebellar molecular layer lysates (30 μ g per lane) of P28 Nogo-A KO, L7-Nogo-A TG, and the corresponding WT mice. No change in the amount of NgR1 protein was detected due to changes in the expression levels of Nogo-A. (D) Expression of NgR1 in the cerebellum of WT mice. Colabeling with anti-calbindin (green) and anti-NgR1 (red) antibodies revealed the high expression of NgR1 in the molecular layer and its very low expression in the PC bodies (stars) of P28 WT/BL6 mice. (Scale bar, 20 μ m.)

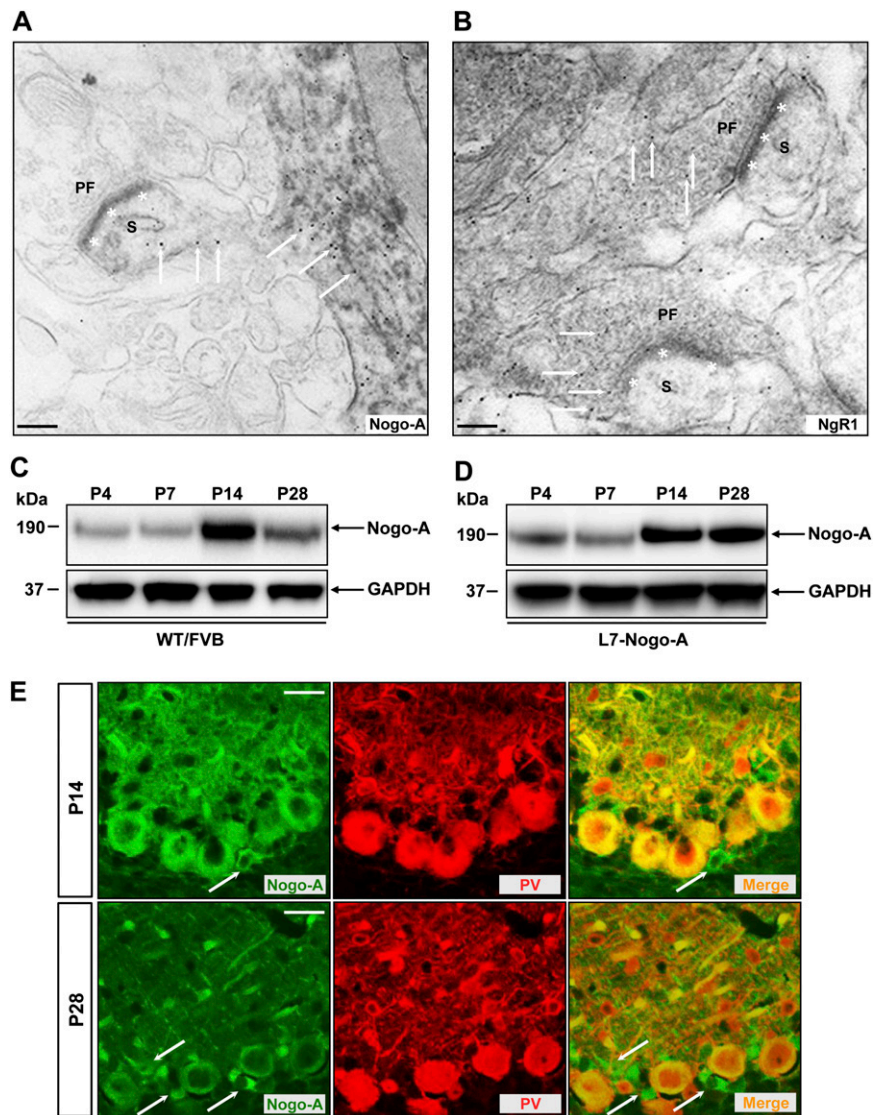


Fig. S3. Distribution of Nogo-A and NgR1 in the cerebellum. (A and B) Immunoelectron microscopic localization of Nogo-A and NgR1 in PF-PC synapses of P28 WT/BL6 mice. DAB staining was intensified with methenamine silver followed by gold substitution. Dark immunopositive staining for Nogo-A, intensified with silver-gold particles (arrows), is present in the postsynaptic PC dendritic spines (S) (A), whereas NgR1 immunolabeling, intensified with silver-gold particles (arrows), is confined to the presynaptic parallel fiber terminals (PF) (B). Stars demarcate postsynaptic densities. (Scale bars, 1 μm .) (C and D) Immunoblot analysis of Nogo-A expression during cerebellar development in WT/FVB and L7-Nogo-A TG mice. Western blot analysis of the cerebellar molecular layer lysates (30 μg of protein per lane) with monoclonal anti-Nogo-A antibody 11C7 shows that, in mice of both genotypes, Nogo-A reaches its peak of expression around P14 (C and D) and is afterward down-regulated in WT/FVB mice (C). In contrast, Nogo-A continues to be highly expressed in the molecular layer of L7-Nogo-A TG mice after P14, thus showing that the overexpression of Nogo-A under the L7 promoter starts only postnatally (D). (E) Expression of Nogo-A in the developing cerebellum of WT/BL6 mice. Double immunolabeling with anti-Nogo-A (green) and anti-parvalbumin (PV) (red) antibodies revealed the developmental down-regulation of Nogo-A protein expression in the PCs of WT/BL6 mice. The small, Nogo-A⁺ cells lined up along the PC-GC layer interface are most likely candelabrum cells, as suggested by their position and the lack of parvalbumin immunoreactivity (1). (Scale bars, 20 μm .)

- Schilling K, Oberdick J, Rossi F, Baader SL (2008) Besides Purkinje cells and granule neurons: an appraisal of the cell biology of the interneurons of the cerebellar cortex. *Histochem Cell Biol* 130(4):601-615.

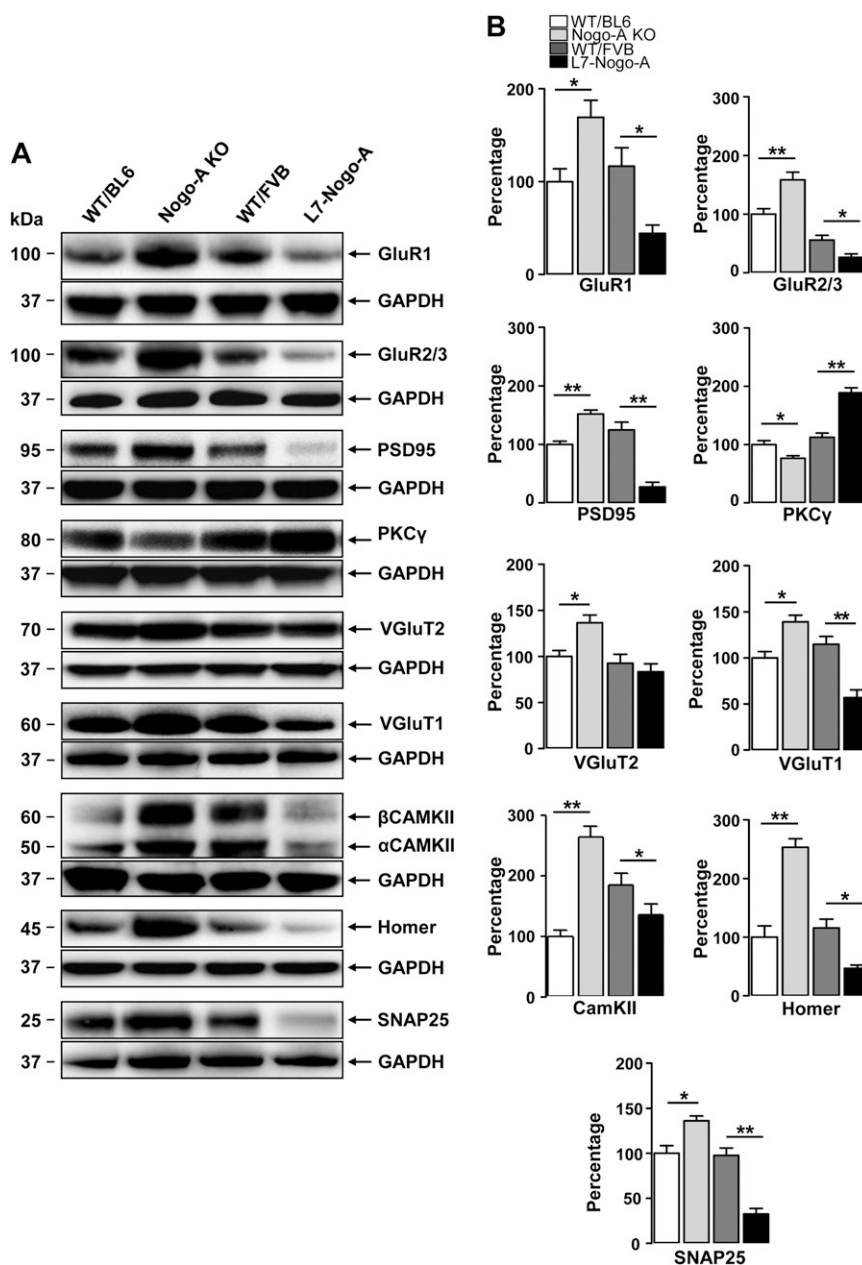


Fig. 54. Western blot analysis of GluR1, GluR2/3, PSD95, PKC γ , VGlut1, VGlut2, CamKII, Homer, and SNAP25 protein expression in the cerebellar lysates of wild-type and mutant mice. (A) Immunoblot analyses of GluR1, GluR2/3, PSD95, PKC γ , VGlut1, VGlut2, CamKII, Homer, and SNAP25 protein expression in the cerebellar molecular layer lysates (30 μ g per lane) of P28 Nogo-A KO, L7-Nogo-A TG, and the corresponding WT mice. (B) The intensity of protein bands was quantified by densitometry and normalized to GAPDH protein used as a loading control, followed by normalization toward WT/BL6. Nogo-A negatively affects the expression levels of GluR1, GluR2/3, PSD95, VGlut1, CamKII β , Homer, and SNAP25, whereas the protein level of PKC γ is positively correlated with the amount of Nogo-A in PCs. Genetic deletion of Nogo-A resulted in an increase in the amount of the VGlut2, whereas overexpression of Nogo-A had no effect on the expression level of this protein. Values represent means \pm SEM of three experiments repeated with three different animals per group; * P < 0.05, ** P < 0.01, Student t test.

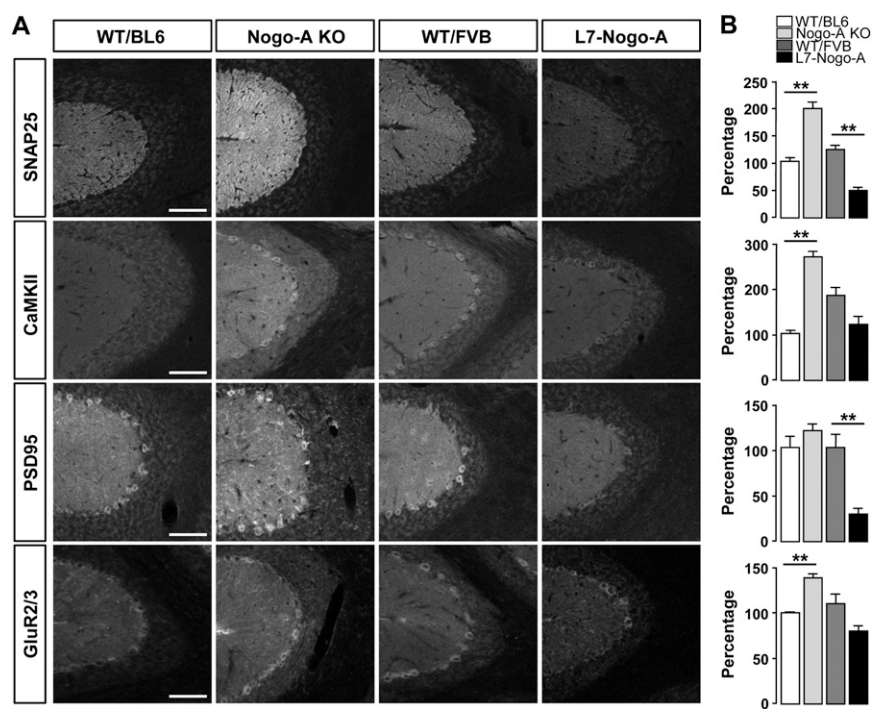


Fig. 55. Immunohistochemical analysis of SNAP25, CamKII, PSD95, and GluR2/3 protein expression in the cerebellar molecular layer of wild-type and mutant mice. (A) Expression pattern of SNAP25, CamKII, PSD95, and GluR2/3 in the cerebellar molecular layer of P28 Nogo-A KO, L7-Nogo-A TG, and corresponding WT mice. (Scale bars, 100 μm .) (B) The intensity of immunolabeling was quantified by densitometry and normalized toward WT/BL6 mice. The expression levels of SNAP25, CamKII, PSD95, and GluR2/3 are negatively correlated with the amount of Nogo-A. Values represent means \pm SEM of three experiments repeated with three different animals per group; **** $P < 0.01$, Student t test.**

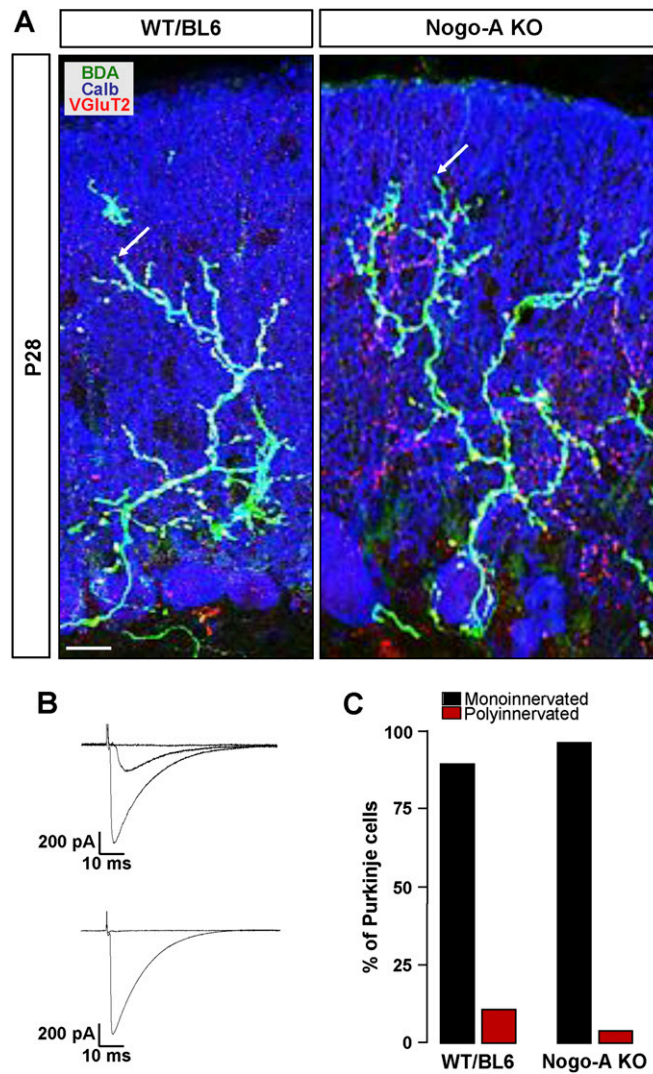


Fig. S6. Innervation pattern of Purkinje cells by climbing fibers at P28. **(A)** CF monoinnervation of Purkinje cells in P28 Nogo-A KO and WT/BL6 mice as revealed by a triple fluorescent labeling for calbindin (blue), BDA (green), and VGLuT2 (red). In both Nogo-A KO ($n = 19$ cells from four mice) and control WT/BL6 ($n = 21$ cells from six mice) mice BDA-labeled CFs completely overlapped with VGLuT2⁺ CF terminals. Note also the increased CF innervation territory in Nogo-A KO mice (arrows). (Scale bar, 20 μ m.) **(B)** Representative traces of EPSCs evoked by stimulation of poly- (*Upper*) and mono-innervated (*Lower*) CFs in the granule cell layer of P28 Nogo-A KO and WT/BL6 mice. Two to three traces are superimposed at each threshold stimulus intensity. Holding potential was -10 mV. **(C)** Summary histogram showing the percentage of mono- and polyinnervated PCs in P28 WT/BL6 ($n = 28$ cells from eight mice) and Nogo-A KO ($n = 30$ cells from seven mice) mice.

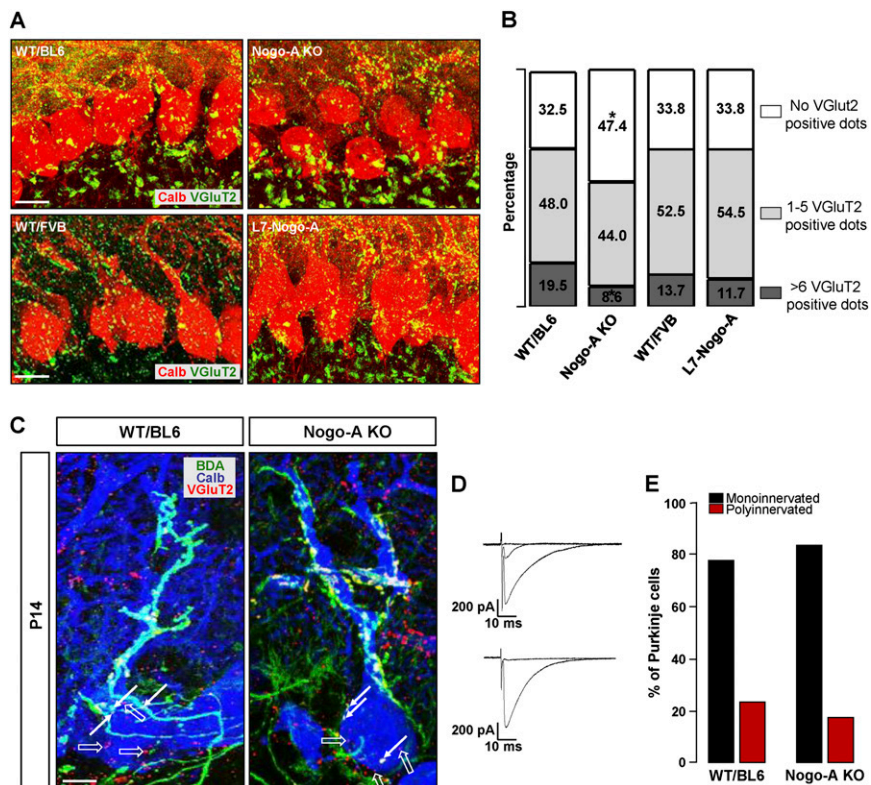


Fig. S7. Genetic deletion of Nogo-A affects the somatodendritic translocation of climbing fiber terminals. (A) Confocal images of VGLuT2-labeled CF terminations (green) on P14 PCs stained for calbindin (red). (Scale bar, 20 μ m.) (B) To estimate the translocation of CFs from the soma to dendrites of PCs, they were divided into three categories: PCs without VGLuT2⁺ CF varicosities on their soma, PCs with one to five VGLuT2⁺ CF terminals, and PCs with more than six VGLuT2⁺ CF varicosities. Genetic deletion of Nogo-A resulted in a faster translocation of CF synapses from PC bodies to their dendrites, whereas overexpression of Nogo-A had no effect on this process. Values represent means \pm SEM of 120–132 cells (sampled from six mice) per genotype; **P* < 0.05, Student *t* test. (C) CF innervation of PCs in P14 Nogo-A KO and WT/BL6 mice as revealed by a triple fluorescent labeling for calbindin (blue), BDA labeling of individual CF axons (green), and VGLuT2 (red). Polyinnervated Nogo-A KO (*n* = 21/102 cells from four mice) and control WT/BL6 (*n* = 24/92 cells from five mice) PCs have comparable numbers of BDA⁺/VGLuT2⁺ (arrows) and BDA⁻/VGLuT2⁺ CF terminals (empty arrows) on their somata. (Scale bar, 5 μ m.) (D) Representative traces of EPSCs evoked by the stimulation of poly- (Upper) and mono-innervated (Lower) CFs in the granule cell layer in WT/BL6 and Nogo-A KO mice at P14. Two to three traces are superimposed at each threshold stimulus intensity. Holding potential was -10 mV. (E) Summary histogram showing the percentage of mono- and polyinnervated PCs in P14 WT/BL6 (*n* = 26 cells from six mice) and Nogo-A KO (*n* = 29 cells from eight mice) mice.

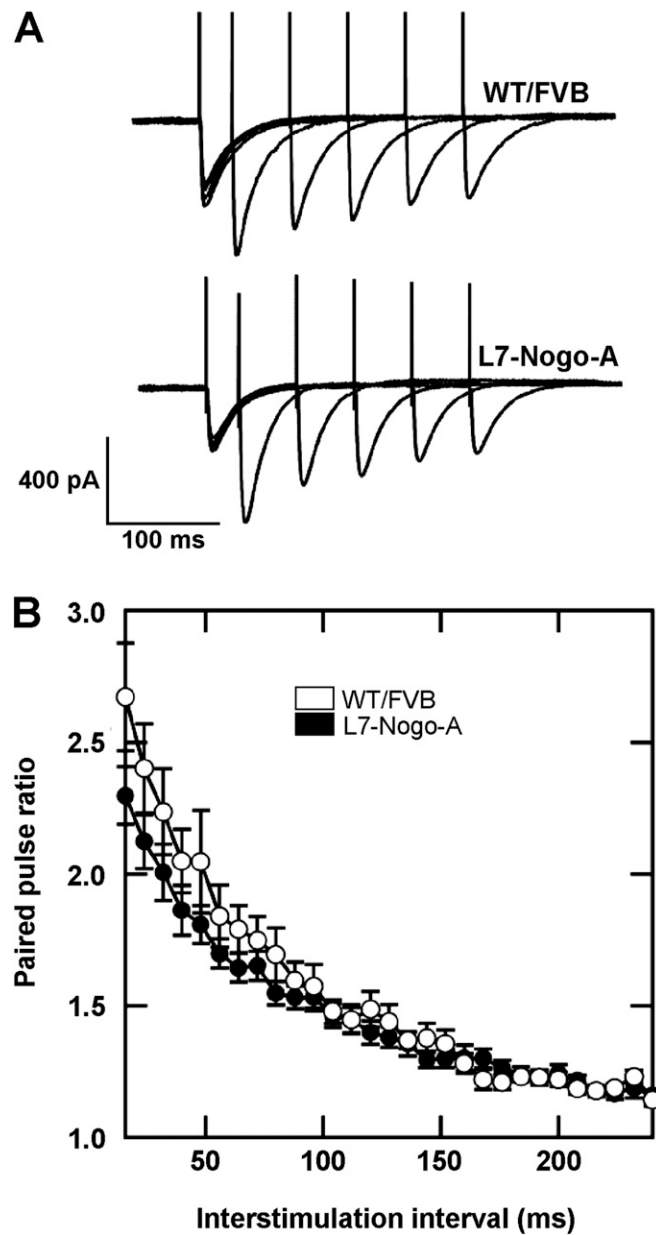


Fig. 58. Paired-pulse facilitation is not affected by Nogo-A overexpression. (A) Typical paired-pulse facilitation traces in L7-Nogo-A TG (P28) mice are indistinguishable from their WT controls. (B) Plotted values of paired-pulse facilitation ratio (the ratio was expressed as the difference between the second and the first EPSC divided by the size of the first EPSC) as a function of twin pulse interval. Overexpression of Nogo-A does not alter the probability of glutamate release from the presynaptic PFs. Values represent means \pm SEM of 19–25 cells (sampled from four to five mice) per genotype; Student *t* test.



Shared Synaptic Pathophysiology in Syndromic and Nonsyndromic Rodent Models of Autism

Stéphane J. Baudouin *et al.*

Science **338**, 128 (2012);

DOI: 10.1126/science.1224159

This copy is for your personal, non-commercial use only.

If you wish to distribute this article to others, you can order high-quality copies for your colleagues, clients, or customers by [clicking here](#).

Permission to republish or repurpose articles or portions of articles can be obtained by following the guidelines [here](#).

The following resources related to this article are available online at www.sciencemag.org (this information is current as of October 4, 2012):

Updated information and services, including high-resolution figures, can be found in the online version of this article at:

<http://www.sciencemag.org/content/338/6103/128.full.html>

Supporting Online Material can be found at:

<http://www.sciencemag.org/content/suppl/2012/09/12/science.1224159.DC1.html>

A list of selected additional articles on the Science Web sites **related to this article** can be found at:

<http://www.sciencemag.org/content/338/6103/128.full.html#related>

This article **cites 27 articles**, 7 of which can be accessed free:

<http://www.sciencemag.org/content/338/6103/128.full.html#ref-list-1>

This article appears in the following **subject collections**:

Neuroscience

<http://www.sciencemag.org/cgi/collection/neuroscience>

HSV-Gadd45g infusion into the NAc of normal mice did not affect the rewarding actions of a moderate dose of morphine (12.5 mg/kg). However, *gadd45g* overexpression in the NAc of mice with local VTA knockdown of TrkB enhanced morphine CPP as compared to HSV-GFP treated mice (Fig. 4K). No changes were observed in baseline levels of place preference.

We observed the opposite effect of BDNF-TrkB signaling in the VTA-NAc on morphine reward to that seen in earlier observations with cocaine and other stimulants. Prior work has shown that knockdown of BDNF from the VTA, or knockdown of BDNF or TrkB from the NAc, antagonizes behavioral responses to cocaine, whereas knockdown of TrkB in the VTA has no effect (3). These findings identified the NAc as the primary site of action of BDNF-TrkB signaling in regulating cocaine reward. In contrast, we show here that the primary site of action of BDNF-TrkB signaling in regulating morphine reward is the VTA, because knockdown of either BDNF or TrkB in the VTA promotes behavioral responses to morphine, whereas knockdown of TrkB in the NAc and BDNF administration into the NAc were without effect. On the other hand, our findings that optical stimulation of VTA DA nerve terminals in the NAc completely reverses the ability of BDNF, acting in the VTA, to impair morphine reward demonstrate that BDNF's influence on VTA DA neuron excitability is responsible for its behavioral effects reported here (fig. S12). These optogenetic experiments also identify the NAc as the key neural site where VTA BDNF's influence on morphine reward is ultimately mediated, and we showed that this occurs via DA activation of D1 receptors on NAc neurons. For this reason, we analyzed morphine-induced changes in gene expression in the NAc as a function of VTA BDNF and demonstrated the importance of two genes, *sox11* and *gadd45g*, among numerous other putative genes regulated in a similar fashion, in behavioral responses to morphine (fig. S12). The results of the present study differ from those in an earlier report (10), which found that exogenous BDNF increases opiate reward in rats by altering GABA_A receptor function in VTA GABAergic neurons (fig. S12). The different findings could be due to the different species, drug treatment regimens, or behavioral models used.

Consistent with the differences in BDNF's influence on cocaine versus morphine action are the very different ways in which the drugs initially affect the VTA-NAc pathway. In addition, although opiate and stimulant drugs of abuse induce many common molecular and cellular adaptations in both the VTA and NAc (38), some notable differences are seen as well with respect to synaptic plasticity (39, 40) and to VTA BDNF expression (fig. S1B). Further studies are now needed to directly investigate whether the opposite interactions between BDNF and stimulants versus opiates are related to these adaptations. Given the substance-specific features of drug addiction syndromes, it will be important to further explore the downstream functional consequences of the

BDNF-stimulant feed-forward loop versus the BDNF-opiate negative feedback loop in addiction and to study how they influence polydrug use.

References and Notes

- H. Thoenen, *Science* **270**, 593 (1995).
- R. C. Pierce, A. A. Bari, *Rev. Neurosci.* **12**, 95 (2001).
- D. L. Graham *et al.*, *Biol. Psychiatry* **65**, 696 (2009).
- F. S. Hall, J. Drgonova, M. Goeb, G. R. Uhl, *Neuropsychopharmacology* **28**, 1485 (2003).
- B. A. Horeger *et al.*, *J. Neurosci.* **19**, 4110 (1999).
- L. Lu, J. Dempsey, S. Y. Liu, J. M. Bossert, Y. Shaham, *J. Neurosci.* **24**, 1604 (2004).
- M. K. Lobo *et al.*, *Science* **330**, 385 (2010).
- D. L. Graham *et al.*, *Nat. Neurosci.* **10**, 1029 (2007).
- S. E. Hyman, R. C. Malenka, E. J. Nestler, *Annu. Rev. Neurosci.* **29**, 565 (2006).
- H. Vargas-Perez *et al.*, *Science* **324**, 1732 (2009).
- N. N. Chu *et al.*, *Addict. Biol.* **13**, 47 (2008).
- S. Numan *et al.*, *J. Neurosci.* **18**, 10700 (1998).
- M. T. Berhow *et al.*, *Neuroscience* **68**, 969 (1995).
- M. S. Mazei-Robison *et al.*, *Neuron* **72**, 977 (2011).
- S. J. Russo *et al.*, *Nat. Neurosci.* **10**, 93 (2007).
- L. Sklair-Tavron *et al.*, *Proc. Natl. Acad. Sci. U.S.A.* **93**, 11202 (1996).
- E. R. Kramer *et al.*, *PLoS Biol.* **5**, e39 (2007).
- C. A. Altar *et al.*, *Nature* **389**, 856 (1997).
- A. A. Grace, S. B. Floresco, Y. Goto, D. J. Lodge, *Trends Neurosci.* **30**, 220 (2007).
- S. B. Floresco, A. R. West, B. Ash, H. Moore, A. A. Grace, *Nat. Neurosci.* **6**, 968 (2003).
- V. Krishnan *et al.*, *Biol. Psychiatry* **64**, 691 (2008).
- E. J. Nestler, M. Alreja, G. K. Aghajanian, *Biol. Psychiatry* **46**, 1131 (1999).
- N. S. Desai, L. C. Rutherford, G. G. Turrigiano, *Learn. Mem.* **6**, 284 (1999).
- H. C. Tsai *et al.*, *Science* **324**, 1080 (2009).
- K. P. Abraham, I. M. Quadros, M. L. Souza-Formigoni, *Int. J. Neuropsychopharmacol.* **14**, 175 (2011).
- G. D. Stuber *et al.*, *Nature* **475**, 377 (2011).
- F. G. Kaddis, N. J. Uretsky, L. J. Wallace, *Brain Res.* **697**, 76 (1995).
- V. Vialou *et al.*, *Nat. Neurosci.* **13**, 745 (2010).
- S. M. Boye, R. J. Grant, P. B. Clarke, *Neuropharmacology* **40**, 792 (2001).
- Y. Goto, A. A. Grace, *Nat. Neurosci.* **8**, 805 (2005).
- M. Korostynski, M. Piechota, D. Kaminska, W. Solecki, R. Przewlocki, *Genome Biol.* **8**, R128 (2007).
- M. Piechota *et al.*, *Genome Biol.* **11**, R48 (2010).
- C. Sanchis-Segura, J. P. Lopez-Atalaya, A. Barco, *Neuropsychopharmacology* **34**, 2642 (2009).
- S. Spijker *et al.*, *FASEB J.* **18**, 848 (2004).
- M. P. Jankowski, P. K. Cornuet, S. McIlwraith, H. R. Koerber, K. M. Albers, *Neuroscience* **143**, 501 (2006).
- C. A. McClung, E. J. Nestler, *Nat. Neurosci.* **6**, 1208 (2003).
- J. Ying *et al.*, *Clin. Cancer Res.* **11**, 6442 (2005).
- E. J. Nestler, *Nat. Neurosci.* **8**, 1445 (2005).
- A. Badiani, D. Belin, D. Epstein, D. Calu, Y. Shaham, *Nat. Rev. Neurosci.* **12**, 685 (2011).
- S. J. Russo *et al.*, *Trends Neurosci.* **33**, 267 (2010).

Acknowledgments: We thank R. E. Burger-Caplan and N. Mensah for excellent technical assistance. This work was supported by grants from the National Institute on Drug Abuse (E.J.N. and M.S.M.-R.) and a Rubicon Grant from the Dutch Scientific Organization (C.S.L.).

Supplementary Materials

www.sciencemag.org/cgi/content/full/338/6103/124/DC1
Materials and Methods
Figs. S1 to S12
Tables S1 to S3
References (41–53)

21 March 2012; accepted 25 July 2012
10.1126/science.1222265

Shared Synaptic Pathophysiology in Syndromic and Nonsyndromic Rodent Models of Autism

Stéphane J. Baudouin,¹ Julien Gaudias,¹ Stefan Gerharz,^{1*} Laetitia Hatstatt,¹ Kuikui Zhou,² Pradeep Punnakkal,¹ Kenji F. Tanaka,^{3,4} Will Spooren,⁵ Rene Hen,³ Chris I. De Zeeuw,^{2,6} Kaspar Vogt,¹ Peter Scheiffele^{1†}

The genetic heterogeneity of autism poses a major challenge for identifying mechanism-based treatments. A number of rare mutations are associated with autism, and it is unclear whether these result in common neuronal alterations. Monogenic syndromes, such as fragile X, include autism as one of their multifaceted symptoms and have revealed specific defects in synaptic plasticity. We discovered an unexpected convergence of synaptic pathophysiology in a nonsyndromic form of autism with those in fragile X syndrome. Neuroligin-3 knockout mice (a model for nonsyndromic autism) exhibited disrupted heterosynaptic competition and perturbed metabotropic glutamate receptor-dependent synaptic plasticity, a hallmark of fragile X. These phenotypes could be rescued by reexpression of neuroligin-3 in juvenile mice, highlighting the possibility of reverting neuronal circuit alterations in autism after the completion of development.

Autism comprises a heterogeneous group of neurodevelopmental disorders characterized by variations in social interactions and communication and the manifestation of ritualistic behaviors (1). A large number of rare high-impact mutations have been identified in autistic patients (2–4). However, most insights into the synaptic pathophysiology of autism are derived from models of monogenic syndromes, such as fragile X syndrome, in which about 25%

of patients meet diagnostic criteria of autism (5). In fragile X, the key defect in synaptic transmission is elevated group I metabotropic glutamate receptor-dependent long-term depression (mGluR-LTD). However, most cases of autism are nonsyndromic, and it is unclear whether these share pathophysiology with fragile X. One class of nonsyndromic forms of autism is associated with mutations in the neuroligin genes (*Nlgn1*, -2, -3, and -4), which encode postsynaptic adhesion molecules

involved in synapse assembly (proteins NL1, -2, -3, and -4) (6–8). For *Nlgn3*, a R451C point mutation (7) and deletions (4, 9) have been identified in several patients with autism. The R451C point mutation results in NL3 trafficking defects (10), whereas the deletions remove the entire *Nlgn3* coding sequence (4, 9). *Nlgn3*^{R451C} knockin and *Nlgn3*^{KO} (KO, knockout) mice exhibit impairments in social interactions, social memory, ultrasonic vocalization, and olfaction [(11, 12) but see (13)]. In *Nlgn3*^{R451C} mice, synaptic transmission is altered in the somatosensory cortex and hippocampus (12, 14). However, the subcellular localization of NL3 protein in vivo and synaptic defects resulting from *Nlgn3* ablation are unclear (15, 16). To understand the pathophysiology of *Nlgn3* deletions, we focused on the synaptic connectivity in the cerebellum, because cerebellar activation is altered in autistic patients (17), and

cerebellar lesions result in behavioral changes reminiscent of autism (18, 19). Using NL3-specific antibodies (16), we detected strong NL3 immune reactivity in the molecular layer and surrounding mossy fiber glomeruli of the inner granular layer (Fig. 1, A and B). Antibody reactivity was largely abolished in mutant mice carrying a STOP cassette inserted after the transcriptional start site (20), which resulted in a complete loss of NL3 expression (*Nlgn3*^{KO}) (Fig. 1A and fig. S1, A and B). In the inner granular layer, NL3 was detected at glutamatergic as well as γ -aminobutyric acid-responsive (GABAergic) synapses, whereas NL3 in the molecular layer was primarily detected at parallel fiber synapses (Fig. 1, C and D). In the same preparations, we detected only little apposition of NL3 immune reactivity with markers of climbing fiber and interneuron synapses (fig. S1C). Similar observations were made in *Nlgn3*^{PC} mice, carrying a knockout allele where NL3 is selectively reexpressed in Purkinje cells (PCs) under the control of the tetracycline transactivator (Fig. 1, A and B, and fig. S1D).

Ultrastructural analysis of parallel fiber synapses in *Nlgn3*^{KO} mice did not reveal a dramatic difference in several morphological parameters (Fig. 2A). Miniature excitatory postsynaptic current (mEPSC) recordings in *Nlgn3*^{KO} PCs identified a small but significant reduction in mEPSC

amplitude (Fig. 2B), whereas paired-pulse facilitation of parallel fiber synapses was not detectably altered (Fig. 2C and fig. S2A). Parallel fiber synapses exhibit a marked LTD that is thought to contribute to forms of cerebellar function and learning [(21) but see (22)]. Simultaneous activation of group I mGluRs and AMPA receptors in the postsynaptic compartment results in protein kinase C activation, AMPA receptor (GluA2 subunit) phosphorylation at serine 880, and subsequent dissociation from the postsynaptic scaffold and endocytosis (21, 23). Given the reduction in mEPSC amplitudes, we tested whether mGluR-dependent LTD was modified in *Nlgn3*^{KO} PCs. In 2- to 3-month-old wild-type mice, application of the group I mGluR agonist DHPG resulted in a persistent reduction of EPSC amplitudes. No depression was observed in *Nlgn3*^{KO} cerebellar slices (Fig. 2D and fig. S2B). This loss in mGluR-LTD may be a consequence of an impaired LTD expression or an occlusion due to constitutive activation. We observed a twofold increase in basal GluA2 phosphorylation at serine 880 in *Nlgn3*^{KO} as compared to the wild-type. Upon DHPG stimulation, phospho-GluA2 levels were increased in wild-type but decreased in *Nlgn3*^{KO} mice, probably due to mGluR-stimulated degradation of the phosphorylated form of GluA2 (Fig. 2E) (24).

¹Biozentrum of the University of Basel, Basel, Switzerland. ²Department of Neuroscience, Erasmus MC, Rotterdam, Netherlands. ³Department of Neuroscience, Columbia University, New York, NY, USA. ⁴Department of Neuropsychiatry, School of Medicine, Keio University, Tokyo, Japan. ⁵Hoffmann-La Roche, Basel, Switzerland. ⁶Netherlands Institute for Neuroscience, Royal Netherlands Academy of Arts and Sciences, Amsterdam, Netherlands. *Deceased. †To whom correspondence should be addressed. E-mail: peter.scheiffele@unibas.ch

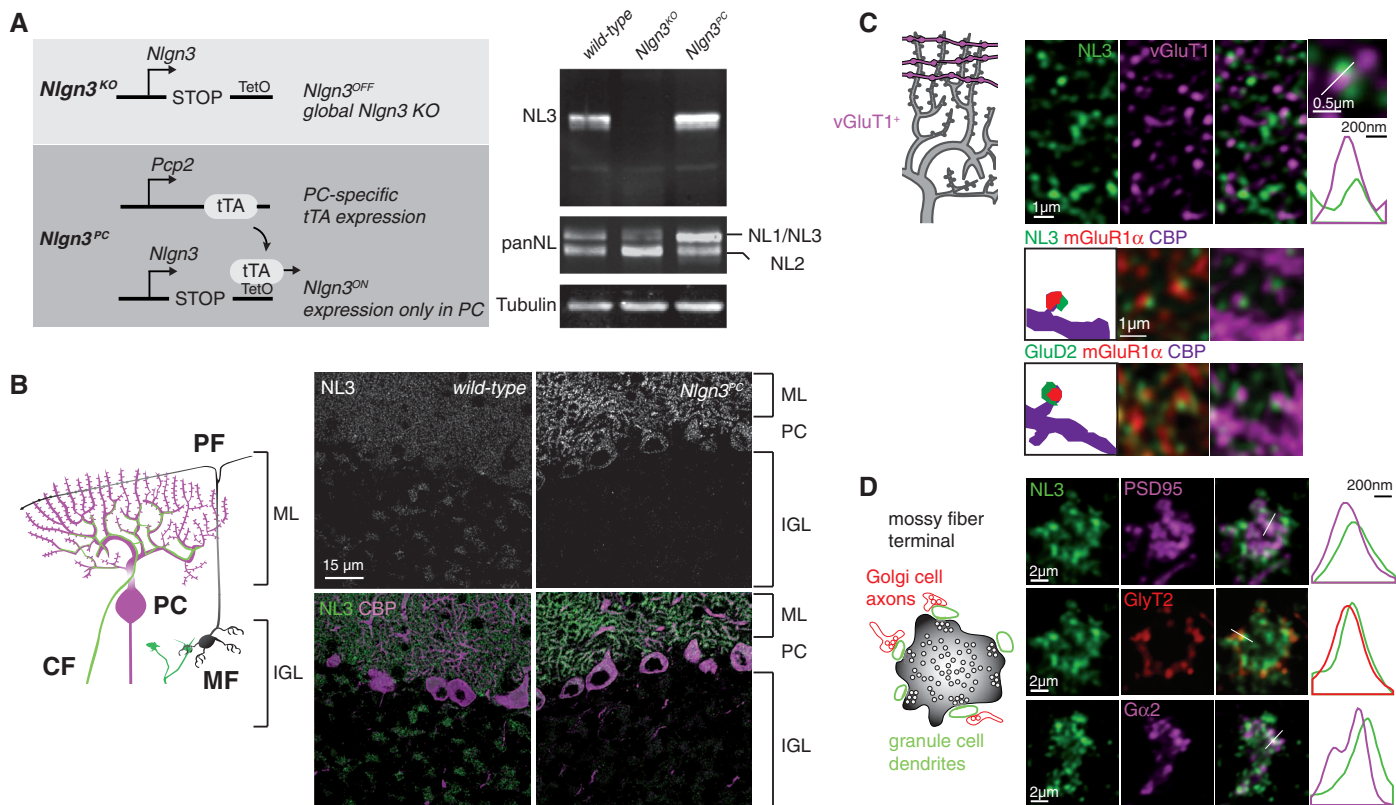


Fig. 1. Cell type-specific synaptic localization of NL3. **(A)** *Nlgn3*^{KO} (*Nlgn3*^{STOP-tetO}) mice lack NL3 protein expression, and *Nlgn3*^{PC} mice (*Nlgn3*^{STOP-tetO::Pcp2}^{tTA}) show reexpression in cerebellar lysates. **(B)** Mossy fiber inputs (MF) in the inner granular layer (IGL) are relayed to PCs via parallel fibers (PF). Climbing fibers (CF) form synapses directly onto the proximal PC dendritic arborization. In

Nlgn3^{PC} mice, NL3 immunoreactivity is increased on PC dendrites (calbindin, CBP) and abolished in the IGL. **(C)** NL3 is apposed to vGluT1⁺ PF boutons and colocalizes with mGluR1 α in CBP⁺ spines, similar to GluD2. **(D)** In glomeruli, NL3 is detected at PSD95⁺ and GABA-A receptor α 2⁺ synapses and colocalizes with GFP⁺ terminals in *GlyT2*^{GFP} transgenic mice.

The constitutive increase in phospho-GluA2 in the *Nlgn3^{KO}* cerebellum indicated a gain of function in the synaptic plasticity pathway. Parallel fiber LTD is regulated by several postsynaptic

receptors, including GluA2, GluD2, and mGluR1 α (21). Using quantitative Western blotting, we discovered a selective increase in the mGluR1 α protein in the *Nlgn3^{KO}* cerebellum, whereas the

mRNA level was unchanged (Fig. 3, A and B, and fig. S3; there is a similar mGluR1 α protein increase in the thalamus). mGluR2 and mGluR7, two additional metabotropic receptors expressed

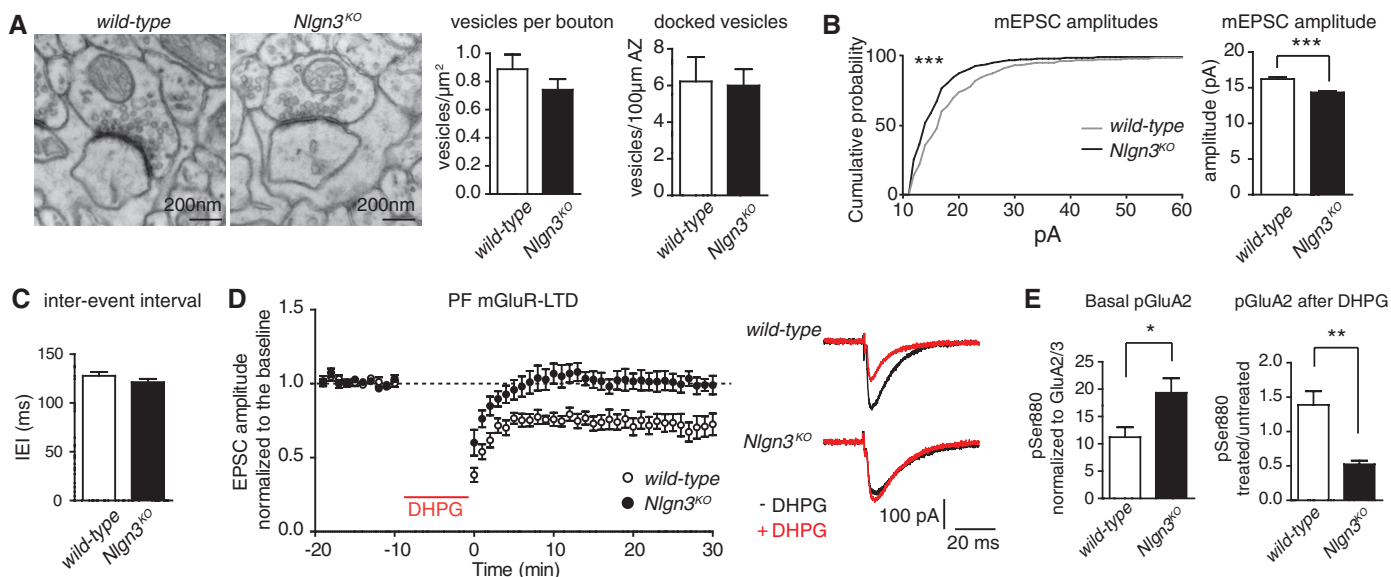


Fig. 2. Occlusion of mGluR-LTD in *Nlgn3^{KO}* mice. (A) PF synaptic ultrastructure in *Nlgn3^{KO}* mice by transmission electron microscopy ($n \geq 4$ animals, 200 synapses per animal). (B) Cumulative distribution of mEPSCs ($***P < 0.001$, Kolmogorov-Smirnov test) and mean amplitude ($n = 9$ cells for wild-type and $n = 21$ cells for *Nlgn3^{KO}* mice; $***P < 0.001$, Mann-Whitney test). (C) mEPSC inter-event intervals, paired pulse ratios ($n = 9$ wild-type and $n = 15$ *Nlgn3^{KO}*

cells). (D) mGluR-LTD induced by 10 min of 50 μM DHPG ($n \geq 8$ cells) and representative traces before (black) and after (red) DHPG stimulation. (E) Quantitative Western blot of basal and DHPG-induced phospho-GluA2 (normalized to GluA2/3 protein level, $n \geq 4$ mice, $*P < 0.03$, t test). DHPG-induced phosphorylation is expressed as the ratio of treated to untreated samples ($n \geq 4$ mice, $**P < 0.01$, t test).

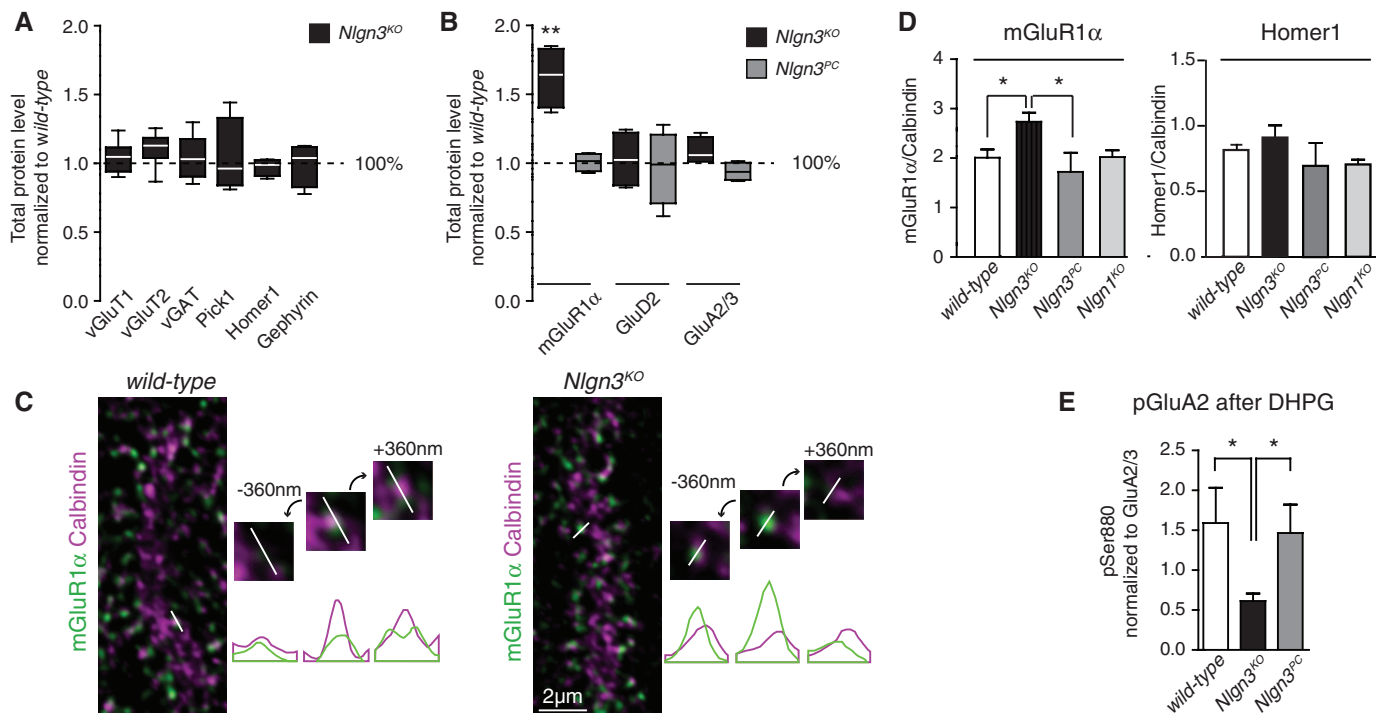


Fig. 3. Elevation of synaptic mGluR1 α levels in *Nlgn3^{KO}* mice. (A) Quantitative Western blot. Protein levels were normalized to tubulin and expressed relative to the wild type. (B) Quantitative Western blot of mGluR1 α , GluD2, and GluA2/3 levels in the cerebellum (normalized to tubulin and expressed relative to the wild type, $n \geq 4$, $**P = 0.002$, t test). (C) Quantitative line scan on cerebellar sections stained with antibodies to mGluR1 α , Homer 1, and calbindin.

(D) Line scan intensity ratios of mGluR1 α /CBP and Homer1/CBP ($n = 6$ mice, 1200 synapses per genotype; mGluR1 α , $*P = 0.04$; Homer, $P = 0.6$; t test). Reexpression of NL3 in PCs restores mGluR1 α level ($n = 4$ mice, $P = 0.4$). There was no difference in *Nlgn1^{KO}* mice ($n = 6$ mice, $P = 0.9$). (E) DHPG-induced phosphorylation of GluA2 expressed as the ratio of treated to untreated samples (normalized to GluA2/3 protein level, $n \geq 5$ mice, $*P < 0.05$, t test).

in the cerebellum, were unaltered (fig. S3B). Endogenous mGluR1 α and NL3 colocalized in the heads of Purkinje dendritic spines (Fig. 1D). In *Nlgn3^{KO}* mice, synaptic mGluR1 α levels were increased but were unaltered in the *Nlgn1^{KO}* cerebellum (Fig. 3, C and D). This mGluR1 α deregulation was a cell-autonomous consequence of NL3 loss of function, because reexpression of NL3 specifically in PCs (*Nlgn3^{PC}*) reduced the mGluR1 α protein level and its synaptic abundance back to the wild-type level (Fig. 3, B and D). Moreover, DHPG-induced phospho-GluA2 signals were returned to wild-type levels in mice that selectively reexpressed NL3 protein in PCs (*Nlgn3^{PC}*, Fig. 3E).

We next examined whether the loss of NL3 results in wiring alterations in the cerebellar network. In the mature cerebellum, each PC is innervated by a single climbing fiber, and synaptic competition between parallel fiber and climbing fiber inputs excludes climbing fiber inputs from

the PC distal dendrites (21, 25). In *Nlgn3^{KO}* cerebella, we observed a significant invasion of vGluT2⁺ terminals into the distal molecular layer (Fig. 4, A and B, and fig. S4A). Ectopic climbing fiber synapses were not observed in *Nlgn1^{KO}* cerebella, and the expression of *Nlgn3* exclusively in PCs was sufficient to suppress ectopic synapse formation in *Nlgn3^{PC}* mice. Synapse density along the entire length of the overshooting climbing fibers was unaltered, resulting in an increased total number of climbing fiber synapses (Fig. 4, A and B, and fig. S4A). Consistent with this observation, evoked climbing fiber transmission was elevated in the *Nlgn3^{KO}* mice (Fig. 4C; there is a normal regression of multi-innervation, fig. S4B).

We used the Erasmus ladder (26) to explore motor coordination in *Nlgn3^{KO}* mice. In this behavioral assay, mice cross a ladder consisting of pressure sensors that measure motor output. Wild-type and *Nlgn3^{KO}* mice completed the same num-

ber of valid runs on the ladder. Step times for *Nlgn3^{KO}* mice were significantly elevated, indicating a perturbation of motor coordination (Fig. 4D). The occurrence of missteps during ladder crossing was unaltered in the *Nlgn3^{KO}* mice and declined similarly as for wild-type mice over several days of training. NL3 expression specifically in PCs rescued the elevated step times progressively after several training days (Fig. 4D). *Nlgn3^{PC}* mice did exhibit a higher number of missteps (Fig. 4D), most likely because the reexpression in PCs exceeds the endogenous NL3 level and results in a gain-of-function phenotype.

The extensive ectopic synapse formation in *Nlgn3^{KO}* mice raises the question of whether such structural defects can be corrected after the completion of development. We used the tetracycline transactivator to temporally control the reexpression of NL3 in PCs of *Nlgn3^{PC}* mice (Fig. 4E). *Nlgn3^{PC}* mice were raised in the presence of doxycycline [transactivator inactive, NL3 expres-

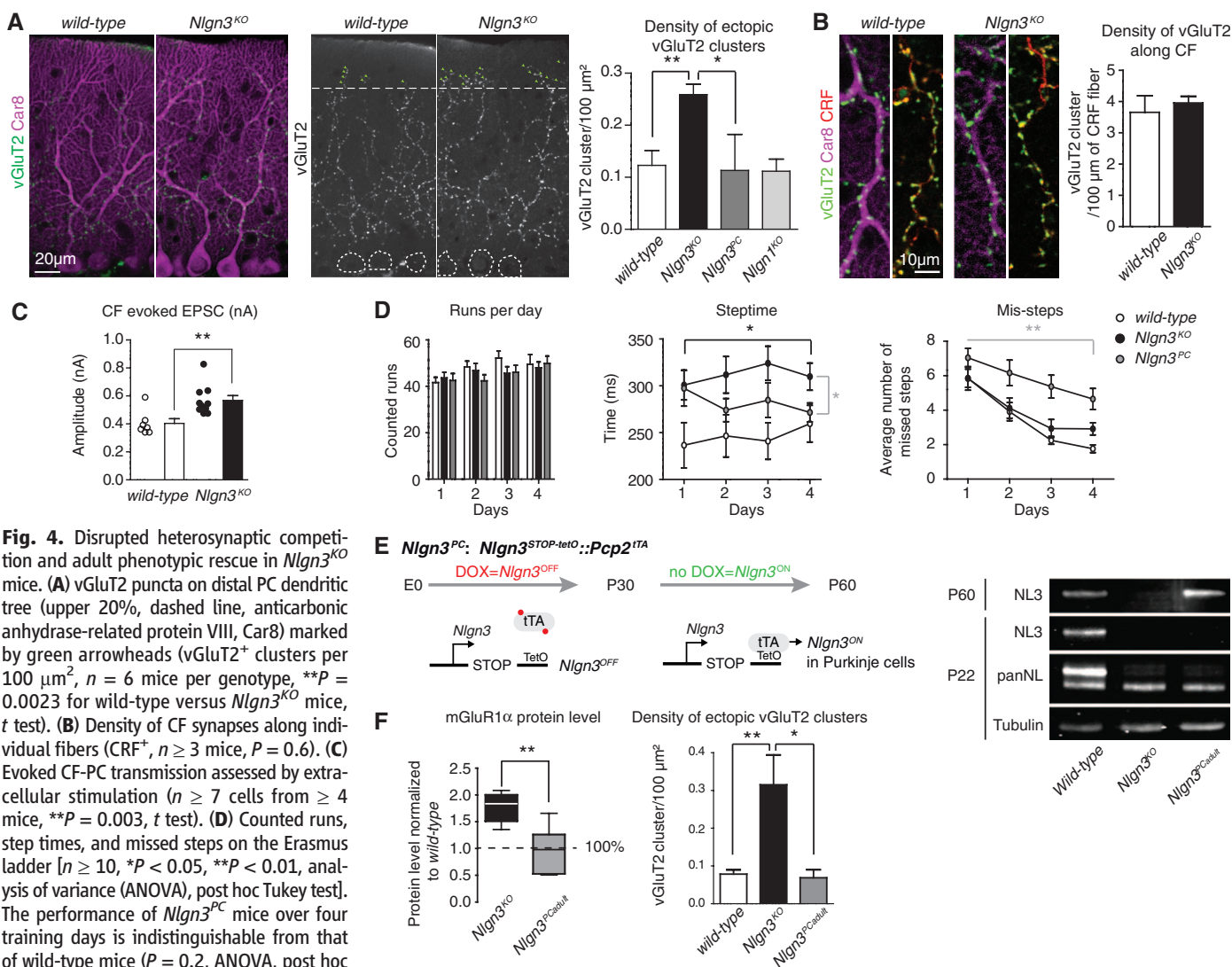


Fig. 4. Disrupted heterosynaptic competition and adult phenotypic rescue in *Nlgn3^{KO}* mice. **(A)** vGluT2 puncta on distal PC dendritic tree (upper 20%, dashed line, anticonic anhydrase-related protein VIII, Car8) marked by green arrowheads (vGluT2⁺ clusters per 100 μ m², $n = 6$ mice per genotype, $**P = 0.0023$ for wild-type versus *Nlgn3^{KO}* mice, t test). **(B)** Density of CF synapses along individual fibers (CRF⁺, $n \geq 3$ mice, $P = 0.6$). **(C)** Evoked CF-PC transmission assessed by extracellular stimulation ($n \geq 7$ cells from ≥ 4 mice, $**P = 0.003$, t test). **(D)** Counted runs, step times, and missed steps on the Erasmus ladder [$n \geq 10$, $*P < 0.05$, $**P < 0.01$, analysis of variance (ANOVA), post hoc Tukey test]. The performance of *Nlgn3^{PC}* mice over four training days is indistinguishable from that of wild-type mice ($P = 0.2$, ANOVA, post hoc Tukey test). **(E)** Adult reexpression of NL3. Doxycycline (100 μ g/ml from embryonic day 0) was removed at P30, and mice were killed at P60. **(F)** (Left) Quantitative Western blot of mGluR1 α in *Nlgn3^{PCadult}* mice (at P60, $n \geq 5$ mice, $**P = 0.004$). (Right) Quantification of vGluT2 ectopic puncta (at P60, $n \geq 3$ mice, $**P = 0.003$, $*P = 0.03$).

sion off (Fig. 4E)]. At 30 days after birth (P30), doxycycline was removed, permitting the reexpression of NL3 selectively in PCs. Reexpression restored wild-type mGluR1 α protein levels and resulted in the removal of ectopic synapses from the distal PC dendritic tree (Fig. 4F and fig. S4, C and D). Therefore, neurodevelopmental phenotypes and ectopic synapse formation arising from *Nlgn3* deletion can be corrected in the mature cerebellar system.

Our results provide insight into the synaptic pathophysiology of a model of nonsyndromic autism. Phenotypes observed in *Nlgn3*^{KO} mice represent a surprising parallel to the synaptic pathophysiology in *Fmr1* and *Tsc2* mutant mice (27). Like these syndromic autism models, *Nlgn3*^{KO} mice exhibit a deregulation of mGluR-LTD. In the *Fmr1*^{KO} mice, mGluR-LTD in the forebrain and cerebellar neurons is increased, and this phenotype can be suppressed by reduction of group I mGluR activity (5, 28, 29). *Nlgn3*^{KO} mice exhibit an occlusion in mGluR-LTD due to increased mGluR1 α expression, indicating a common core pathway of synaptic dysfunction. mGluR5 antagonists can revert cellular phenotypes in *Fmr1*^{KO} mice and may show therapeutic benefit in some fragile X patients (5, 30). Our work indicates that group I mGluR antagonists hold promise for designing treatment strategies for nonsyndromic autism. Our genetic experiments in *Nlgn3*^{KO} mice reveal that not only functional alterations but also ectopic synapse formation can be reversed, high-

lighting the fact that structural neurodevelopmental phenotypes can be rescued by intervention after the completion of development.

References and Notes

- American Psychiatric Association Task Force On DSM-IV, *Diagnostic and Statistical Manual of Mental Disorders: DSM-IVTR* (American Psychiatric Association, Arlington, VA, 2000).
- R. Toro *et al.*, *Trends Genet.* **26**, 363 (2010).
- D. Levy *et al.*, *Neuron* **70**, 886 (2011).
- S. J. Sanders *et al.*, *Neuron* **70**, 863 (2011).
- H. Y. Zoghbi, M. F. Bear, *Cold Spring Harb. Perspect. Biol.* **4**, a009886 (2012).
- T. C. Südhof, *Nature* **455**, 903 (2008).
- S. Jamain *et al.*; Paris Autism Research International Sibpair Study, *Nat. Genet.* **34**, 27 (2003).
- B. Chih, H. Engelman, P. Scheiffele, *Science* **307**, 1324 (2005).
- S. R. Gilman *et al.*, *Neuron* **70**, 898 (2011).
- B. Chih, S. K. Afridi, L. Clark, P. Scheiffele, *Hum. Mol. Genet.* **13**, 1471 (2004).
- K. Radyushkin *et al.*, *Genes Brain Behav.* **8**, 416 (2009).
- K. Tabuchi *et al.*, *Science* **318**, 71 (2007).
- K. K. Chadman *et al.*, *Autism Res.* **1**, 147 (2008).
- M. Etherton *et al.*, *Proc. Natl. Acad. Sci. U.S.A.* **108**, 13764 (2011).
- F. Varoqueaux *et al.*, *Neuron* **51**, 741 (2006).
- E. C. Budreck, P. Scheiffele, *Eur. J. Neurosci.* **26**, 1738 (2007).
- S. H. Mostofsky *et al.*, *Brain* **132**, 2413 (2009).
- J. D. Schmahmann, J. B. Weilburg, J. C. Sherman, *Cerebellum* **6**, 254 (2007).
- P. T. Tsai *et al.*, *Nature* **488**, 647 (2012).
- K. F. Tanaka *et al.*, *Biol. Psychiatry* **67**, 770 (2010).
- M. Kano, K. Hashimoto, T. Tabata, *Philos. Trans. R. Soc. Lond.* **363**, 2173 (2008).
- M. Schonewille *et al.*, *Neuron* **70**, 43 (2011).
- J. P. Steinberg *et al.*, *Neuron* **49**, 845 (2006).
- A. M. Mabb, M. D. Ehlers, *Annu. Rev. Cell Dev. Biol.* **26**, 179 (2010).
- R. Cesa, P. Strata, *Neuroscience* **162**, 624 (2009).
- R. S. Van Der Giessen *et al.*, *Neuron* **58**, 599 (2008).
- B. D. Auerbach, E. K. Osterweil, M. F. Bear, *Nature* **480**, 63 (2011).
- S. K. Koekkoek *et al.*, *Neuron* **47**, 339 (2005).
- C. Lüscher, K. M. Huber, *Neuron* **65**, 445 (2010).
- S. Jacquemont *et al.*, *Sci. Transl. Med.* **3**, 64ra1 (2011).

Acknowledgments: We are grateful to our colleagues Arber, Barde, Gosh, Sylwestrak, Witte, and Xiao for comments on the manuscript; to Ponti, Genoud, Sauder, Ahrné, Ehrenfeuchter, and Stiefvater for technical help; and Zeilhofer, Fritschy, Brose, and Sans for sharing reagents. C.D.Z. was supported by the Dutch Organization for Medical Sciences (ZonMw); Life Sciences (ALW); Senter (NeuroBasic); Prinses Beatrix Fonds; and the European Research Council—advanced, CEREBNET, and C7 programs (European Community). This work was supported by a SystemsX grant (P.S. and W.S.); by EU-AIMS (European Autism Interventions), which receives support from the Innovative Medicines Initiative Joint Undertaking under grant agreement no. 115300, the resources of which are composed of financial contributions from the European Union's Seventh Framework Programme (grant FP7/2007-2013), from the European Federation of Pharmaceutical Industries and Associations companies' in-kind contributions, and from Autism Speaks, resulting in a total of €29.6 million; by NCCR *Synapsy*; the Swiss National Science Foundation; and Kanton Basel-Stadt.

Supplementary Materials

www.sciencemag.org/cgi/content/full/science.1224159/DC1
Materials and Methods
Figs. S1 to S4
References

2 May 2012; accepted 17 August 2012
Published online 13 September 2012;
10.1126/science.1224159

In Monkeys Making Value-Based Decisions, LIP Neurons Encode Cue Salience and Not Action Value

Marvin L. Leathers^{1,2*} and Carl R. Olson^{1,2}

In monkeys deciding between alternative saccadic eye movements, lateral intraparietal (LIP) neurons representing each saccade fire at a rate proportional to the value of the reward expected upon its completion. This observation has been interpreted as indicating that LIP neurons encode saccadic value and that they mediate value-based decisions between saccades. Here, we show that LIP neurons representing a given saccade fire strongly not only if it will yield a large reward but also if it will incur a large penalty. This finding indicates that LIP neurons are sensitive to the motivational salience of cues. It is compatible neither with the idea that LIP neurons represent action value nor with the idea that value-based decisions take place in LIP neurons.

Each of us makes hundreds of value-based decisions every day. Deciding whether to take a drink of juice or a sip of coffee at breakfast is a process driven by the subjective value of each outcome. So is deciding whether

to go to graduate school or medical school. There has been debate in recent years concerning the neural mechanisms of such decisions. This debate has pitted a goods-based account against an action-based account. The goods-based account holds that limbic areas such as orbitofrontal cortex mediate a choice between goods (juice or coffee) on the basis of their respective values and that the choice is translated into an appropriate motor command (reach for the glass or the cup) in parietal and dorsal frontal cortex (1–3). The action-based account holds that the values of

juice and coffee are computed in orbitofrontal cortex and transmitted to parietal and dorsal frontal cortex, where neurons involved in planning to reach for the glass and the cup become active in proportion to the values of juice and coffee. The decision then evolves through competition between neuronal populations representing the opposed action plans (4–9). The goods-based model is intuitive and fits with the assumption underlying classic behavioral economics that decisions concern anticipated outcomes as distinct from motor plans. However, the action-based model has received apparent support from single-neuron recording studies of the lateral intraparietal area (LIP). In monkeys making value-based decisions between saccade targets, LIP neurons representing each saccade fire early in the trial at a rate proportional to the reward expected upon its completion (10–14). This observation is compatible with the idea that LIP neurons represent action value in the service of an action-based decision process. However, there is another possible interpretation. Emotionally potent stimuli are salient in the sense that they automatically capture attention (15, 16). This is true in particular of stimuli associated with rewards and penalties (17–19). LIP neurons fire at an enhanced rate when attention is directed into their response fields (20). Thus, LIP neurons might fire strongly when a valued target is in the response field simply because the target is motivationally salient (21, 22).

¹Center for the Neural Basis of Cognition, Carnegie Mellon University, Mellon Institute, Room 115, 4400 Fifth Avenue, Pittsburgh, PA 15213, USA. ²Department of Neuroscience, University of Pittsburgh, Pittsburgh, PA 15260, USA.

*To whom correspondence should be addressed. E-mail: mleathers@cnbc.cmu.edu

List of abbreviations:

ACSF = artificial cerebrospinal fluid
ASD = autism spectrum disorder
AMPA = α -amino-3-hydroxy-5-methyl-4-isoxazolepropionic acid receptor
AP = action potential
bAP = backpropagating Action potentials
BDNF = brain derived neurotrophic factor
CB1 = cannabinoid receptor 1
Cf = critical frequency
CF = climbing fiber
CNS = central nervous system
DHPG = 3,5-dihydroxyphenylglycine
EPSP = excitatory post synaptic potential
GABA = γ -aminobutyric acid
GABA_AR = GABA_A receptor
GAD65/67 = L-glutamic acid decarboxylase
GC = granule cell
GluA2 = subunit AMPA R 2
KO = knock-out
LTD = long-term depression
LTP = long-term potentiation
MF = mossy fiber
mGluR1 = metabotropic glutamate receptor 1
NgR1 = Nogo receptor 1
nlgn = neuroligin (protein)
NL = neuroligin (gene)
NMDA = N-Methyl-D-Aspartat
PC = Purkinje cell
PF = parallel fiber
PV = parvalbumin
S1 = primary somatosensory cortex
SEM = standard error of the mean
STDP = spike-timing dependent plasticity
V1 = primary visual cortex
VGCC = voltage-gated calcium channel
WT = wild type

Acknowledgements

I would like to thank Prof. Kaspar Vogt, for the opportunity to work with him, and also for his constant support, help, enthusiasm and endless patience to answer all my questions. These 4.5 years in the lab were really enjoyable, scientifically as well as personally.

I also want to thank Marija Petrinovic, Stephane Baudouin and Prof. Peter Scheiffele for the opportunity to be a part of these very successful collaborations.

I want to thank all the people from our lab and the Biozentrum. Silvia for the endless argumentation about music, Lydia because we suffered together as PhD students, Rosie for all the stainings and the continuous poking about my incompetence in German, Mathieu for the daily combo coffee/gossips, Marco for the whine/cheese evenings, Markus for the weekly chat about bike and heavy metal, Jan for showing me around the old Rhein and Marktkauf, Martijn for making me buy a race bike and the suffering over mountain passes, Nico and Enrique for the fondue evenings... All the 'french mafia' also, as some people refers to: Valerie, Chantal, Anne-Sophie, H el ene... and I probably forget a lot of people. I'll finish with Stephan, who couldn't stay with us as long as we all wished but was a great friend and a really nice colleague.

I want to thank my girlfriend Sandrine for her continuous support and motivation. This is also true for my parents (and my brother), for their continuous support over so many years, despite they have no idea about what I do in the lab. And a last word for all my friends back in Strasbourg, Emilie, Anne-H el ene, Nath and all the others, who were always there, whenever I decided to come back there.

Many thanks to all of you!!!

Curriculum Vitae

Personal data

Date of birth: 8th October 1983, in Strasbourg (France)

Nationality: French

Diploma & Education

University of Basel (Switzerland) – Biozentrum, Neurobiology Department

- PhD Student, group of Prof. Kaspar Vogt (2009 – present)

Louis Pasteur University (Strasbourg, France) – Life Science Faculty

- Master of Neurosciences, cellular and integrative neurosciences (2008)
- Licence of Biology, cellular biology and physiology (2006)
- DEUG Sciences & Technologies, Biology (2005)

High School Diploma, scientific (2001) Lycée Kléber (Strasbourg, France)

Scientific training

2009 - Present: PhD student: University of Basel, Biozentrum, Department of Neurobiology, group of Prof. K. Vogt.

2007 - 2008: Master training: Louis Pasteur University (Strasbourg, France), INSERM U666, Clinical and experimental physiopathology of schizophrenia, group of Prof. D. Pinault.

Scientific communications

Scientific publications

- Variations of action potentials backpropagation and spike-timing dependent plasticity in the mouse primary visual cortex, during the critical period. Gaudias J, Vogt K., *in preparation*.

- Opposite effects of ketamine and deep brain stimulation on thalamocortical information processing in rats. Kulikova S. P., Tolmacheva E.A., Anderson P., Gaudias J, Adams B.E., Zheng T., Pinault D., **European Journal of Neuroscience** 2012

- Shared synaptic pathophysiology in syndromic and non-syndromic rodent models of autism. Baudouin S.J., Gaudias J., Gerharz S., Hatstatt L., Zhou K., Punnakkal P., Tanaka K.F., Spooren W., Hen R., DeZeeuw C., Vogt K., Scheiffele P., **Science** 2012
- Neuronal Nogo-A negatively regulates dendritic morphology and synaptic transmission in the cerebellum. Petrinovic M.M., Hourez R., Aloy E.M., Dewarrat G., Gall D., Weinmann O., Gaudias J., Bachmann L., Schiffmann S.N., Vogt K., Schwab M.E., **PNAS** 2013
- NMDA receptor hypofunction leads to generalized and persistent aberrant gamma oscillations independent of hyperlocomotion and the state of consciousness. Hakami T., Jones N.C., Tolmacheva E.A., Gaudias J., Chaumont J., Salzberg M., O'Brien T.J., Pinault D., **PLoS ONE** 2009

Poster presentations

- Maturation of the inhibitory system in the primary visual cortex. Gaudias J., Deogracias R., Sütterlin R., Vogt K., SfN Annual Meeting 2012, New Orleans, USA.
- Opposite effects of ketamine on spontaneous and sensory-evoked γ oscillations in the thalamocortical system. Kulikova S.P., Tolmacheva E.A., Anderson P., Gaudias J., Adams B.E., Zheng T.W., Pinault D., Neurex Annual Meeting 2012, Strasbourg, France.
- Maturation of the inhibitory system in the primary visual cortex. Gaudias J., Deogracias R., Vogt K., Swiss Society of Toxicology and Pharmacology Annual Meeting 2011, Zürich, Switzerland.
- Maturation of the inhibitory system in the primary visual cortex. Gaudias J., Deogracias R., Vogt K., 13th International Neuroscience Winter Conference 2011, Sölden, Austria.
- Maturation of the inhibitory system in the primary visual cortex. Gaudias J., Vogt K., Biovalley/MipTech Annual Congress 2010, Basel, Switzerland.
- Disruption of the thalamocortical signal-to-noise ratio in the pathogenesis of psychoses. Pinault D., Kulikova S., Tolmacheva E.A., Gaudias J., Adams B.E., Zheng T., SfN Annual Meeting 2011, Washington, USA.
- Non-competitive NMDAr antagonist ketamine disrupts the state and function of the somatosensory thalamocortical system. Pinault D., Tolmacheva E.A., Gaudias J., Zheng T., Ordikhani-Seyedlar M., Kulikova S., Guy J., Adams B.E., FENS meeting 2010, Amsterdam, the Netherlands.
- Ketamine and MK-801 produce generalized aberrant γ (30-80Hz) oscillations in rodent corticothalamic systems: EEG, network and cellular features. Pinault D., Chaumont J., Gaudias J., SfN Annual Meeting 2009, Chicago, USA.
- NMDAr Hypofunction leads to generalized persistent and aberrant γ (30-80Hz) oscillations independent of hyperlocomotion and the state of consciousness. Jones N.C., Hakami T., Tolmacheva E.A., Gaudias J., Chaumont J., Salzberg M., O'Brien T.J., Pinault D., SfN Annual Meeting 2009, Chicago, USA.